

See discussions, stats, and author profiles for this publication at: <https://www.researchgate.net/publication/275045967>

Optical Properties of Secondary Organic Aerosols and Their Changes by Chemical Processes

ARTICLE *in* CHEMICAL REVIEWS · APRIL 2015

Impact Factor: 46.57 · DOI: 10.1021/cr5005259 · Source: PubMed

CITATIONS

7

READS

29

3 AUTHORS:



Tamar Moise

Copiah-Lincoln Community College

18 PUBLICATIONS 664 CITATIONS

[SEE PROFILE](#)



Michel Flores

Weizmann Institute of Science

21 PUBLICATIONS 193 CITATIONS

[SEE PROFILE](#)



Yinon Rudich

Weizmann Institute of Science

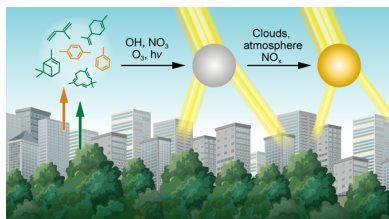
206 PUBLICATIONS 8,340 CITATIONS

[SEE PROFILE](#)

Optical Properties of Secondary Organic Aerosols and Their Changes by Chemical Processes

Tamar Moise, J. Michel Flores, and Yinon Rudich*

Department of Earth and Planetary Sciences, Weizmann Institute, Rehovot 76100, Israel



CONTENTS

1. Introduction	
1.1. Motivation and Scope	
1.2. Overview	
2. Optical Parameters and Instrumentation	
2.1. Measured and Derived Optical Parameters	
2.2. Instrumentation	
2.2.1. Instrumentation for Extinction Measurements	
2.2.2. Instrumentation for Scattering Measurements	
2.2.3. Instrumentation for Absorption Measurements	
2.2.4. Combined Instruments for Simultaneous Measurements	
2.2.5. Single-Particle Techniques	
3. Scattering by Secondary Organic Aerosol	
3.1. Secondary Organic Aerosol Generation	
3.2. Measured Values of Real Part of Refractive Index (m_r)	
3.3. Real Part of Refractive Index (m_r) as a Function of Oxidation Pathway, Precursor, and Reaction Duration	
3.3.1. Spectral Dependence of m_r	
3.3.2. Dependence of m_r on Precursor and Oxidation Pathway	
3.3.3. Changes in m_r with Oxidation Time	
3.4. Compositional and Volatility Changes as Secondary Organic Aerosols Evolve and Effect on m_r	
3.4.1. Linking Particle Oxidative State to Refractive Index	
3.5. Similarities between Ambient and Smog Chamber Secondary Organic Aerosol Composition	
3.6. Predictive Tools for Refractive Index of Secondary Organic Aerosol	
4. Optical Absorption by Secondary Organic Aerosol	
4.1. Reaction Pathways for Formation of Secondary Brown Carbon	

A	4.2. Optical Absorption of Secondary Organic Aerosol Formed via In Situ Oxidation Studies	U
B	4.2.1. Influence of Chemical Structure	V
C	4.3. Aging of Secondary Organic Aerosols with Reduced Nitrogen Compounds [$\text{NH}_{3(g)}$, NH_4^+ , and Amino Acids]	X
D	4.3.1. Aqueous and Heterogeneous Reactions with Dicarbonyls: Glyoxal and Methylglyoxal	X
D	4.3.2. Aqueous and Heterogeneous Reactions with Mono- and Sesquiterpenes	Z
G	4.4. Acid-Catalyzed Aldol Condensation	AA
G	4.5. Comparison of Mass Absorption Cross Section and Imaginary Part of Refractive Index between Studies, Compounds, and Laboratory and Ambient Measurements	AB
G	5. Absorption by Internally Mixed Organic Matter/Black Carbon Aerosol	AD
H	5.1. Absorption Amplification in Core–Shell Aerosol	AD
H	5.2. Deriving Absorption Contributions of Black Carbon, Brown Carbon, and Internally Mixed Brown–Black Carbon Aerosol Fractions via Multispectral Analysis	AD
I	6. Summary and Prospects	AE
K	6.1. Recommendations for Future Directions	AF
K	Author Information	AH
L	Corresponding Author	AH
L	Notes	AH
L	Biographies	AH
M	Acknowledgments	AH
M	Abbreviations	AH
M	References	AI
O		
O		
R		
S		
S		
S		

1. INTRODUCTION

Atmospheric aerosols play a key role in the Earth's atmosphere. Aerosols influence cloud formation and their lifetime, they affect the distribution and amount of trace gases, and they influence the radiative balance by scattering and absorbing solar and terrestrial radiation.¹ Atmospheric aerosols are formed from a variety of natural and anthropogenic sources. They can be directly emitted to the atmosphere (primary particles) by volcanic eruptions, biomass burning, combustion processes, and wind-driven processes (e.g., mineral dust, sea spray, plant debris, and pollen dispersion) or they can be directly formed in

Special Issue: 2015 Chemistry in Climate

Received: September 16, 2014

the atmosphere (secondary particles) by gas-to-particle conversions (e.g., nucleation, condensation) and heterogeneous and multiphase chemical reactions. The direct radiative impact of aerosols depends on their abundance and distribution within the atmospheric column, their hygroscopicity, and on their intrinsic optical properties, namely, how they scatter and absorb radiation. Light-absorbing particles (e.g., black carbon, brown carbon, and mineral dust) are still one of the major uncertainties in the evaluation of Earth's radiative budget. It is now well established that black carbon (BC) is the strongest aerosol absorber of solar radiation in the atmosphere,² dominating absorption of light at wavelengths in the visible and near-infrared region, 400–700 nm.^{3,4} The Intergovernmental Panel on Climate Change (IPCC) Fifth Assessment Report estimates the radiative forcing (RF) by BC as approximately +0.6 W·m⁻².¹ In a recent study, Wang et al.⁵ estimate a lower RF of +0.21 W·m⁻², arguing that previous models upon which the IPCC estimate is based^{1,4,6} overestimate the RF of BC, due to too high an estimate of BC lifetimes and incorrect attribution of brown carbon (BrC) absorption to BC. The term atmospheric BrC refers to light-absorbing organic particulate matter,⁷ for which the absorbance is strongly wavelength-dependent, with higher absorption at near-ultraviolet and blue wavelengths.^{8–10} Large uncertainties still exist with regard to the contribution of brown carbon to radiative forcing. BrC has been estimated to account for 15–50% of total light absorption in the atmosphere, snow, and sea ice.^{4,9,11–13} Light-absorbing organic aerosols are a significant constituent of particulate matter originating from low-temperature combustion sources such as vehicle emissions and residential coal burning^{3,7,14,15} and biomass burning emissions.^{12,16–18} Additional sources of organic carbon (OC), such as humic substances from soils, plant debris, and bioaerosols (e.g., fungi) may also be a source of primary BrC particles.^{7,18,19} In situ atmospheric chemical processes have also been shown to form light-absorbing secondary organic aerosol (SOA), following gas to particle conversion^{15,20} and secondary organic pathways such as aqueous and particle-phase reactions.⁷ Field measurements have shown BrC to track water-soluble organic carbon (WSOC) and to be associated with the specifically identified SOA component of WSOC,^{14,21} indicating a strong association between BrC and SOA. As SOA undergoes further oxidation and ages, the aerosol may become more absorbing, especially in the UV.^{22–25} Recent altitude-resolved measurements of BrC show its prevalence throughout the tropospheric column, with increased concentrations relative to BC at higher altitude (Figure 1). This may be explained as possible in situ production of BrC, possibly through SOA formation,⁹ or by injections of biomass burning aerosol into the free troposphere, where removal processes are slower due to lower concentrations of oxidants.

Radiative forcing estimates due to concentration changes during the industrial era are shown in Figure 2 according to precursor or aerosol type.²⁶ The organic carbon sources considered are biomass burning and fossil and biofuel. SOA is not included due to the many uncertainties associated with SOA, among them its source inventory. The estimates of global annual SOA production formed from the oxidation products of volatile organic compounds (VOC) vary from 12 to 1820 Tg (SOA)·year⁻¹,^{27–31} and even though key precursors for SOA formation have been identified, the relative contributions from anthropogenic and biogenic emissions and biomass burning sources are still poorly constrained. Some estimations suggest

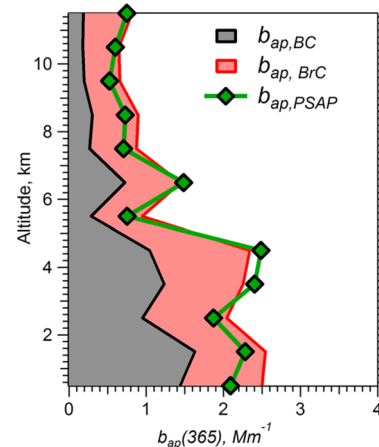


Figure 1. Vertical profiles of estimated black carbon (BC) and brown carbon (BrC) absorption coefficients, along with the inferred ambient aerosol observed total absorption (particle soot absorption photometer, PSAP), all at 365 nm. Uncertainty associated with each parameter was 45% for $b_{ap,BrC(365)}$; 22% for $b_{ap,BC(365)}$; and 29% for $b_{ap,PSAP(365)}$. Reprinted with permission from ref 9. Copyright 2014 John Wiley & Sons, Inc.

that, globally, SOA is dominated by biogenic volatile organic compound (BVOC) precursors, resulting in 90% biogenic secondary organic aerosol (BSOA) and 10% anthropogenic secondary organic aerosol (ASOA).²⁸ However, in many case studies, observations of SOA can be explained only by assuming enhancement of SOA production by anthropogenic influences.^{31–33} Furthermore, it has been shown that interaction between biogenic volatile organic compounds and anthropogenic volatile organic compounds (AVOCs) can significantly affect the properties of SOA.^{31,34–38} Recent studies show that the secondary organic aerosol derived from mixtures of AVOC and BVOC (ABSOA) can be treated as an ideal mixture,³⁹ so that the SOA yields and oxidation levels can be described as linear combinations of the corresponding properties of pure biogenic and anthropogenic systems (however, the aerosol volatility, characterized by the volume fraction remaining, cannot)³⁵ and that the yields can be parametrized by assuming a common organic phase for partitioning.³⁹

Aerosol-phase and aqueous-phase processing is a complementary SOA formation pathway alongside gas–particle partitioning of semivolatile and low-volatility gases. Known pathways for SOA formation following heterogeneous and aqueous-phase oxidation of biogenic and anthropogenic precursors and aging of primary organic aerosol, speciation of SOA chemistry, and SOA yields are detailed in a number of papers.^{40–50}

While in the atmosphere, organic aerosols dynamically change. We use the term “atmospheric aging” to describe an array of processes by which an aerosol particle evolves during its atmospheric lifetime in chemical composition and in physical properties due to condensation, oxidation reactions, etc. Aerosol aging has been discussed in more detail in Rudich et al.⁵¹

1.1. Motivation and Scope

The contribution of SOA to the lower troposphere organic aerosol mass load is estimated at 70–90%,^{28,31,52} such that it is necessary to have more precise spectral information on their intrinsic optical properties to improve the accuracy of direct radiative forcing assessments. Among the 31 global chemistry/

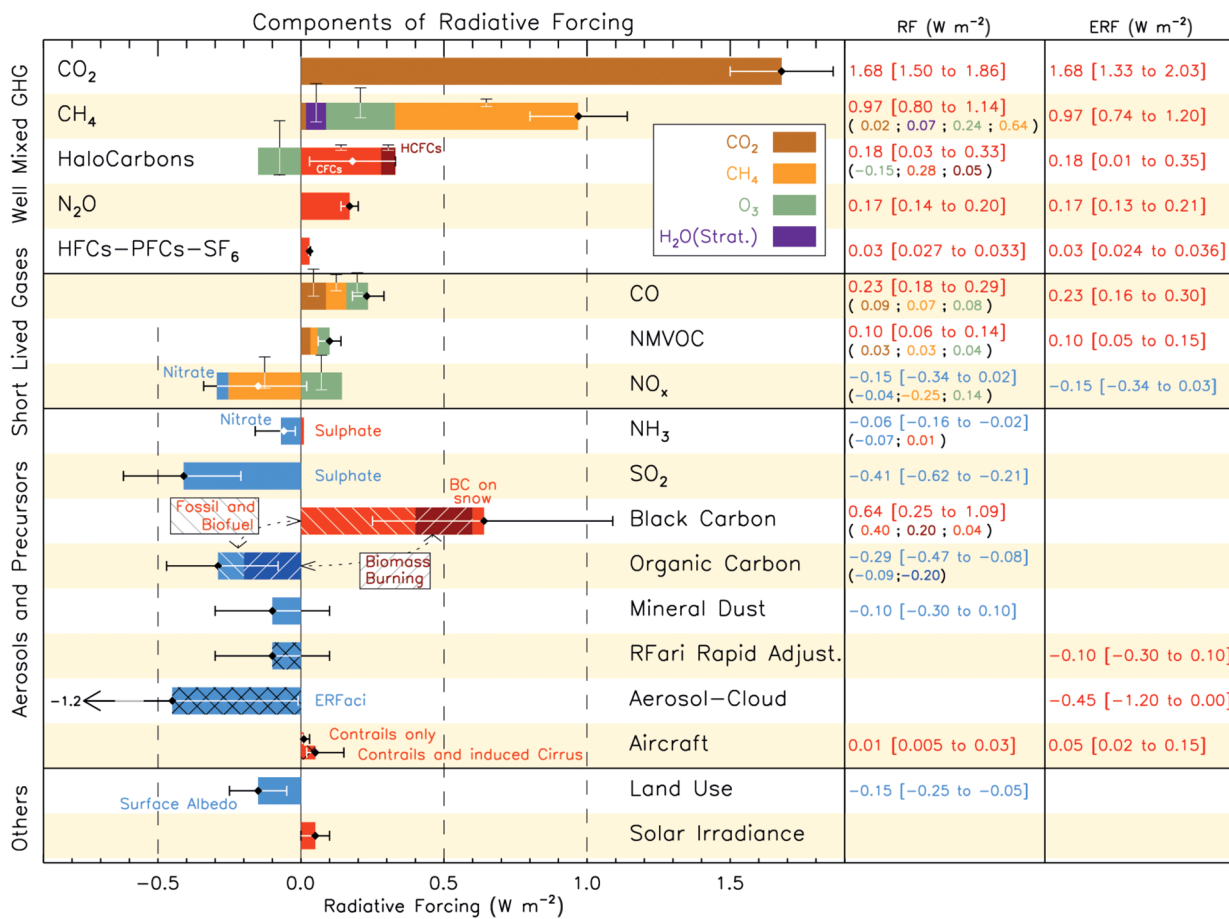


Figure 2. Radiative forcing (RF) of climate change during the industrial era, shown by emitted components from 1750 to 2011. Horizontal bars indicate the overall uncertainty, while the vertical bars are for individual components (vertical bar lengths are proportional to relative uncertainty, with a total length equal to the bar width for $\pm 50\%$ uncertainty). Best estimates for the totals and individual components (from left to right) of the response are given in the right column. Values are RF except for the effective radiative forcing (ERF) due to aerosol–cloud interactions (ERFaci) and rapid adjustment associated with the RF due to aerosol–radiation interaction (RFaci Rapid Adjust.). Secondary organic aerosol has not been included since the formation depends on a variety of factors not currently sufficiently quantified. HFCs, hydrofluorocarbons; PFCs, perfluorcarbons; NMVOC, non-methane volatile organic compounds. Reprinted with permission from ref 26. Copyright 2013 Cambridge University Press.

transport and general circulation models participating in the AeroCom II intercomparison, about half include semivolatile SOA formation, and four also account for multiphase SOA chemistry.⁵³ The already mentioned uncertainties in SOA sources and formation pathways and the different microphysical and chemical representation of SOA in the models lead to large differences in the modeled SOA yields and lifetimes. The radiative impact of SOA, if included, is likewise represented differently between models.⁶ The spectral dependency of BrC means that its greatest impact on radiative forcing is in the UV. However, as UV radiation encompasses only 10% of the total solar irradiance, its contribution to direct radiative forcing is often ignored in climate modeling,⁵⁴ though weak SOA absorption at shorter wavelengths is included in the CAM5.1 model.⁶ Beyond the direct effect of radiative absorbance by BrC, this additional UV absorption can affect photochemical O₃ and OH production,^{15,55} possibly leading to changes in aerosol formation pathways and further inducing radiative changes.⁵⁶

In Figure 3 from the IPCC Working Group I Fifth Assessment Report,¹ estimates of RF from aerosol–radiation interactions are shown, and the contribution from SOA can be compared to that of other atmospheric aerosol constituents. Included are the RF estimates from the AeroCom intercomparison by Myhre et al.⁶ together with the IPCC representation

that includes evaluations also from later studies (such as Shindell et al.⁵⁷) and displays the large uncertainties in the RF_{SOA} estimates, -0.03 (-0.27 to $+0.20$) $\text{W}\cdot\text{m}^{-2}$. Although climate models now include more cloud and aerosol processes and their interaction, there remains low confidence in the representation and quantification of these processes in models.²⁶

The complexity of SOA and BrC formation and aging pathways, chemical composition, and mixing state contribute to the poor constraints on BrC and SOA's contribution to radiative forcing. The strong dependence of light absorption and scattering on aerosol composition and aging has directed more recent studies to focus on understanding the relationship between these optical properties and the aerosol source, chemical composition, physical structure and aging processes. This knowledge, when quantified and parametrized, will enable a better representation of SOA in climate models.

1.2. Overview

Studies that focus on instrumentation and measurement techniques are a large fraction of the recent literature relating to aerosol optical properties, as in situ techniques are being continuously optimized to enable the accuracy and resolution needed for the weakly absorbing BrC aerosol and to resolve

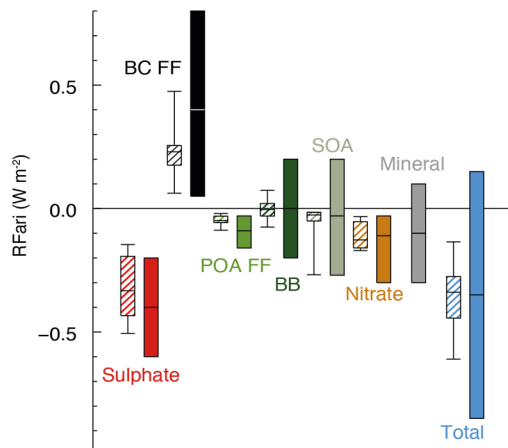


Figure 3. Annual mean top of the atmosphere radiative forcing due to aerosol–radiation interactions (RFari, watts per square meter) due to different anthropogenic aerosol types, for the 1750–2010 period. Hatched whisker boxes show median (line), 5th–95th percentile ranges (box), and min/max values (whiskers) from AeroCom II models⁶ corrected for the 1750–2010 period. Solid colored boxes show the best estimates and 90% uncertainty ranges from the Fifth Assessment Report of the Intergovernmental Panel on Climate Change. BC FF is for black carbon from fossil fuel and biofuel, POA FF is for primary organic aerosol from fossil fuel and biofuel, BB is for biomass burning aerosols, and SOA is for secondary organic aerosols. Reprinted with permission from ref 1. Copyright 2013 Cambridge University Press.

structural and phase characterization of primary, secondary, and aged aerosol. Earlier *in situ* methods to measure absorption suffered from significant uncertainties.⁵⁸ In this review we do not detail the technical side of the many advances in instrumentation since the review paper of Moosmüller et al.,⁵⁸ but rather we point out progress in capabilities of the new generation of instrumentation and focus on their application and on the simultaneous application of multiple instruments to maximize the information derived. Together with the absorbing properties of BrC and SOA, scattering and extinction studies have also been at the forefront of recent studies on SOA,^{55,59–65} similarly addressing the link between particle composition, chemical aging, and the variations in scattering by SOAs. Highly resolved spectral dependence of scattering by organic aerosol has also been investigated,^{55,59,61} and multispectral measurements have been used to understand the effect of organic coatings (weakly absorbing or purely scattering) on an absorbing aerosol core and how these effects change with varying internal composition mixtures and structures.^{66–70}

The sections of this review are as follows:

Section 2 first gives a brief review of aerosol optical parameters measured in laboratory and field studies, followed by advances in instrumentation that enable better-resolved and multiwavelength spectral measurements both in the laboratory and in field campaigns.

Section 3 summarizes the scattering properties of anthropogenic and biogenic secondary organic aerosol formed in laboratory simulation experiments via ozonolysis, OH oxidation, and photo-oxidation under varied NO_x conditions. Results from controlled laboratory and smog chamber experiments are summarized with respect to aerosol precursors, oxidation pathway, H:C and O:C ratios and molecular fragments of the SOA (as measured by aerosol mass spectrometry, AMS), and the densities and volatility of the organic compounds.

Section 4 focuses on optical absorption by “fresh” SOA formed following gas-to-particle conversion and aging of SOA by various chemical pathways: heterogeneous OH chemistry and multiphase or aqueous-phase reactions with NH₃ (ammonia), NH₄⁺ (ammonium), and amino acids. The extent of absorbance is analyzed in the context of average composition and functional group content and, more importantly, as dependent on the molecular structure of the organic aerosol constituents. Values of the mass absorption coefficient (MAC) and the imaginary part of the refractive index (*k*) of different precursor SOAs and BrC sources, from both laboratory and ambient measurements, will be compared.

In section 5 we demonstrate how multispectral absorption measurements, from which the absorption Ångström exponent (AAE) is determined, together with complementary chemical analyses can provide information on ambient aerosol sources and enable assessment of the relative contributions of BrC, BC, and mixed BrC–BC aerosol fractions to total light absorption. The effects of the mixing state of aerosol, especially coatings of brown or nonabsorbing carbon around black carbon cores, on absorption enhancement and AAE values will be reviewed.

Finally, in section 6, we summarize the current findings with regard to scattering and absorbing properties of fresh and aged SOA. We then propose directions for future studies that will advance the body of knowledge on quantification of the optical properties of organic aerosols from varied sources and how they change as a result of atmospheric processes and aging and will advance the integration of this knowledge into quantitative models.

2. OPTICAL PARAMETERS AND INSTRUMENTATION

2.1. Measured and Derived Optical Parameters

Different theories, depending on the size and the shape of the particle, have been developed from solutions to Maxwell's equations to calculate various optical properties. For example, Rayleigh's theory properly models the optical properties of particles that are much smaller than the incident wavelength. For the visible range, this implies aerosol below about 20 nm. Mie theory is often used when particles have approximately the same size as the incident wavelength, and if the particles have a much larger diameter than the wavelength, then classical laws of reflection, refraction, and diffraction can be used for description of the optical properties (geometrical optics). A detailed mathematical description of the different theories is beyond the scope of this work (see for example Kerker,⁷¹ Bohren and Huffman,⁷² Hinds,⁷³ and Redmond et al.⁷⁴); only a brief description of commonly measured and used optical properties will be given here.

The combined effects of absorption and elastic scattering cause a net loss of energy from an incident light beam of irradiance I_0 (in units of watts per square meter), referred to as extinction. Aerosol optical extinction is thus the sum of the effects of absorption and scattering. The total energy removed from an incident beam by a single particle can be expressed as

$$I_{\text{ext}} = I_0 \sigma_{\text{ext}} \quad (1)$$

where σ_{ext} is the optical extinction cross section (normally expressed in square meters) and is defined as

$$\sigma_{\text{ext}} = \sigma_{\text{abs}} + \sigma_{\text{sca}} \quad (2)$$

where σ_{abs} and σ_{sca} represent the optical absorption and scattering cross sections, respectively.

Table 1. Instrumentation Used for In Situ Optical Measurements (Extinction, Scattering, and Absorption) of Atmospheric Aerosol

Method	Instrument	Light source	Principle & Parameters measured	Wavelength (nm)	Selected Studies
EXTINCTION					
CRD	Pulsed Nd:YAG laser	Continuous wave (cw) laser diodes	Difference in ring down time (decay of transmitted light) between sample and background air, β_{ext} , RI	355,405,532 662, 1064	Smith and Atkinson ⁹³ , Langridge et al. ⁹² , Baynard et al. ⁵⁰ , Riziq et al. ⁷⁹ , Freedman et al. ⁸² , Miles et al. ⁹⁴ , Lu et al. ¹⁶⁷ , Trainic et al. ⁹⁵ , Zarzana et al. ⁶⁵
	Nd:YAG laser pumped Optical Parametric Oscillator laser, Pulsed Nd:Yag laser			355,532, 690, 1520	Strawa et al. ⁸⁸ , Lang-Yona et al. ⁹⁶ , Lang-Yona et al. ⁶⁶ , Mellon et al. ⁹⁷
	Cavity Attenuated Phase Shift particle light extinction monitor (CAPS PM _{ex})	Light emitting diode (LED)	Measures distortion in the square wave caused by the effective optical path length within the ~2 km light path cavity as a phase shift in the signal, β_{ext}	450,530,630, 680, 780	Kebabian et al. ¹⁰⁰ , Massoli et al. ¹⁰¹ , Yu et al. ¹⁰² , Petzold et al. ¹⁰³
Broadband	Broadband Cavity Enhanced Spectrometry (BBCES)	LED + collimating lens	The change in the time integrated signal intensity of the transmitted light between background and sample air β_{ext} , RI	360-420 (0.5 nm res.)	Washenfelder et al. ¹⁰⁴ , Flores et al. ^{61,105}
	Xenon arc lamp		The change in the time integrated signal intensity of the transmitted light between background and sample air, β_{ext}	320-410	Wilson et al. ¹⁰⁶
			The change in the fractional absorption of the O ₂ B-band between background and sample air, β_{ext} , RI	687	Varma et al. ¹⁰⁷
	Cavity Enhanced Differential Optical Absorption Spectroscopy (CE-DOAS)	Xenon lamp	Time integrated signal intensity of the transmitted light between background and sample air, Validated for polystyrene latex spheres β_{ext} , RI	220-1050 (0.5 nm res.)	Chartier and Greenslade ¹⁰⁸
	Aerosol Extinction (AE) DOAS	LED	Open path DOAS β_{ext} , RI	673-677 (1.06 nm res.)	Varma et al. ¹⁰⁷
	Broadband CRD	Pulsed broadband dye laser	Time-resolved ring-down signal of aerosol sample β_{ext}	655-665	Varma et al. ¹⁰⁷
SCATTERING					
Polar Nephelometer	IW 532 nm Intelite Inc. [®] Laser		Angular scattering from parallel and perpendicular polarized light β_{sca} , n (RI real)	670, 532	Barkey et al. ¹⁰⁹ , Kim et al. ^{60,110-111} , Kim and Paulson ⁶²
	TSI 3563 [®] integrating nephelometer 3 wavelength	Broadband light source with three optical filters	Back scattered light, (7°-170°) m _r (RI real)	450,550,700	Nakayama et al. ⁹⁹ Commonly used in field studies e.g., Schnaiter et al. ¹¹² , Fischer et al. ¹¹³
Broadband reflected light	Variable angle spectroscopic ellipsometer	Broadband light source	Amplitude ratio and phase shift of reflected parallel, p and perpendicular, s polarized light from the surface for each $\theta-\lambda$ pair, Thin films of deposited SOA RI retrieval	200-1200 (5-10 nm res.)	Liu et al. ^{55,59}
ABSORPTION					
Photoacoustic Spectroscopy (PAS)	Nd:YAG pumped solid-state laser, cw laser diode		Sound pressure produced in an acoustic resonator, the proportionality factor between the photoacoustic signal and the aerosol optical absorption coefficient is calibrated by gas phase measurements β_{abs}	532,685	Arnott et al. ¹¹⁴ , Lu et al. ⁶⁷
	Multi-wavelength PAS	Nd:YAG disc laser	Four detection cells operated independently and in parallel β_{abs} , AAE, (MAC)	266,355,532, 1064	Ajtai et al. ¹¹⁵ , Utry et al. ¹⁹

Table 1. continued

Method	Instrument	Light source	Principle & Parameters measured	Wavelength (nm)	Selected Studies
UV-Vis spectrometer + integrating sphere	Perkin Elmer lambda 35	Aerosol collected on filter substrate , UV visible Spectrophotometer equipped with a Labsphere RSA-PE-20 diffuse reflectance accessory.	Transmittance mode (TUV-IS) and reflective mode (RUV-IS) β_{abs} , MAC, k	280- 800 (1 nm res.)	Zhong and Jang ¹¹⁶
COMBINED INSTRUMENTATION					
ABSORPTION and EXTINCTION					
PAS + CRD	Diode lasers for each wavelength and each cell	Absorption and extinction measurements in different cells with parallel air samples β_{ext} , β_{abs} , SSA	405, 532, 659	Massoli et al. ¹¹⁷ , Cappa et al. ¹¹⁸ , Lack et al. ⁸⁰ , Lambe et al. ⁶³	
ABSORPTION and SCATTERING					
Single, dual and multi-wavelength photoacoustic signal + reciprocal nephelometer. (PASS, PASS-3 and PAX by DMT Inc. [©])	Individual diode lasers for each wavelength	Integrating reciprocal nephelometer within the photoacoustic resonator, At each λ , simultaneous absorption and scattering coefficients for same sample volume using same laser beam β_{sca} , β_{abs} , SSA, AAE	355, 405, 780, 532, 870, 1047	Lewis et al. ¹¹⁹ , Chakrabarty et al. ¹⁷ , Gyawali et al. ¹²⁰ , Nakayama et al. ^{64,121} Commonly used in field studies e.g., Gyawali et al. ¹²² , Flowers et al. ¹²³ , Chan et al. ¹²⁴ , Wang et al. ¹²⁵	
Photoacoustic + nephelometry	Super continuum SC400 (Fianium Inc.) Laser (400-2200)	PAS and nephelometer cells in series, Absorption and scattering measured sequentially at each wavelength band, β_{sca} , β_{abs} , SSA, AAE Instrumentation validated for soot and salt aerosol	Selected : 417, 475, 542, 607, 675	Sharma et al. ¹²⁶	
EXTINCTION + SCATTERING					
CRD and reciprocal nephelometer	Nd:YAG laser	Simultaneous measurement of extinction and scattering, in the same cavity, on the same air sample β_{sca} , β_{abs} , SSA	355 and 532	Dial et al. ¹²⁷ , Ma and Thompson ⁸³ ; Qian et al. ¹²⁸ , Thompson et al. ⁸⁹	
CRD + nephelometer	Pulsed laser (CRD) Broadband light + filters (nephelometer)	Extinction and scattering measurement in different cells β_{sca} , β_{ext} , SSA		Massoli et al. ¹¹⁷	
Broadband	Incoherent Broadband Cavity-Enhanced Absorption Spectrometer (IBBCEAS) + Integrating sphere	Blue LED (445-480)	Simultaneous measurement of scattering and extinction on same aerosol volume β_{sca} , β_{ext} , RI, SSA	β_{sca} from single channel PMT at 465-474	Zhao et al. ¹²⁹

Optical cross sections are defined as

$$\sigma_{\text{ext/abs/sca}} = Q_{\text{ext/abs/sca}} \sigma_{\text{geometric}} \quad (3)$$

where $\sigma_{\text{geometric}}$ is the geometric cross section (for spherical particles $\sigma_{\text{geometric}} = \pi r^2$), r is the particle radius, and the Q terms are the extinction, absorption, or scattering efficiencies. Q is a measure of the dimensional relationship of the optical cross section to the geometrical cross section.

For a collection of particles the extinction (β_{ext}), absorption (β_{abs}), and scattering (β_{sca}) coefficients (normally given in units of $\text{Mm}^{-1} = 10^6 \text{ m}^{-1}$) describe the amount of light removed, absorbed, and scattered, respectively. For the same type of particle, the coefficient can be expressed as the product of the optical cross section and the particle number concentration N :

$$\beta_{\text{ext/abs/sca}} = N \sigma_{\text{ext/abs/sca}} \quad (4)$$

For an ensemble of different types of particles, the optical coefficients are expressed as the sum of the individual optical cross sections of each substance divided by the total volume (V) occupied by this population.

The single scattering albedo (SSA), ω , is defined as the ratio of the scattering coefficient to the extinction coefficient:

$$\omega = \frac{\beta_{\text{sca}}}{\beta_{\text{ext}}} = \frac{\beta_{\text{sca}}}{\beta_{\text{sca}} + \beta_{\text{abs}}} \quad (5)$$

For a single particle, SSA is defined as the ratio of the scattering cross section to the extinction cross section. SSA values range between $0 \leq \omega \leq 1$. A value of 1 represents a purely scattering particle (or population), and 0 represents a purely absorbing one.

All of the optical properties stated above (σ , Q , β , and ω) depend on the wavelength of incident light, size of the particle, and spatial complex refractive index distribution of the surrounding medium in conjunction with the complex refractive index (RI) of the particle, which describes how light interacts with the particular material. In practically all atmospheric applications, the complex refractive index of the surrounding medium can be assumed to be 1. The refractive index (m) is expressed as a complex number: $m = m_r + ik$, where m_r is the real part and k is the imaginary part of the refractive index. Real and imaginary parts express the extent of scattering and absorption, respectively. The complex refractive index is the only intrinsic optical property of a particle (where size is the intrinsic physical property); therefore, knowing the

value of m is highly important to accurately model the optical properties of aerosol.

For particles of the same shape and refractive index, the interaction of a beam of light of a particular wavelength with a particle of a certain size is scale-invariant (i.e., micrometer waves interact with micrometer particles in the same way that nanometer waves interact with nanometer particles); therefore, particle sizes are presented as the particle size parameter (x). For spherical particles, the particle size parameter is given as the ratio of the particle's circumference to the wavelength (λ) of incident light:

$$x = \frac{2\pi r}{\lambda} \quad (6)$$

where r is the radius of the particle.

In many applications, it is often necessary to normalize the extinction, scattering, and absorption cross sections by the mass of the particles (or to normalize the extinction, scattering, and absorption coefficients by the particle density); for example, the mass absorption cross section (MAC, square meters per gram), as pointed out by Bond and Bergstrom,³ is a convenient proxy for the relationship between radiative transfer and aerosol mass represented in models. For small particles (i.e., $x < 1$), MAC is defined as⁷²

$$\text{MAC} = \frac{6\pi}{\rho\lambda} \text{Im} \left[\frac{m^2 - 1}{m^2 + 2} \right] \quad (7)$$

where ρ is the density of the particles. Equation 7 is often assumed to be constant, but this is true only for particles in the Rayleigh regime. For particles larger than about 150–200 nm, MAC is size-dependent (see, for example, Figures 4 and 5 of Bond and Bergstrom³ or Figure 1 of Moosmüller et al.⁵⁸).

In liquid solution measurements, if the density of the dissolved material is known, the bulk absorption coefficient ($\beta_{\text{abs_bulk}}$) can be derived:¹⁰

$$\frac{\beta_{\text{abs_bulk}}(\lambda)}{\rho} = \frac{A(\lambda) \ln(10)}{CL} \quad (8)$$

where $A(\lambda)$ is the base-10 absorbance measurement (unitless), C is the concentration of the liquid solution (grams per cubic meter), and L is the sample path length (meters). Furthermore, since $\beta_{\text{abs_bulk}}$ is directly proportional to the imaginary part of the complex refractive index, $\beta_{\text{abs_bulk}} = 4\pi k/\lambda$, eq 8 can be used to derive k . The ratio $\beta_{\text{abs_bulk}}/\rho$ is often referred to as the mass absorption coefficient and is also abbreviated as MAC. Even though eq 8 has the same units as the mass absorption cross section, they should not be confused. As Sun et al.¹⁰ showed, they can be compared only after eq 8 is multiplied by the “particulate effect” (ξ ; see section 2 of Sun et al.¹⁰):

$$\xi = \frac{9n}{(n^2 - k^2 + 2)^2 + 4n^2k^2} \quad (9)$$

Use of MAC allows us to differentiate between greater absorption resulting from a higher mass loading or from specific functional groups or compounds.

2.2. Instrumentation

The instrumentation to measure optical properties is extensive. The instruments used for measurements presented in this review are listed in Table 1.

2.2.1. Instrumentation for Extinction Measurements.

At the forefront of the new and established instrumentation to

measure in situ aerosol optical extinction are the high-finesse optical cavities consisting of two highly reflective mirrors ($R > 99.9\%$). These optical cavities with optical path lengths of several kilometers provide the sensitivity and low detection levels ($\beta_{\text{ext}} < 1 \text{ Mm}^{-1}$) needed for ambient aerosol samples.⁵⁸ Cavity ring-down spectroscopy (CRDS) has been at the forefront of such high-finesse aerosol extinction measurements and has been used by several groups for laboratory,^{23,63,66,75–87} field,^{88–90} and airborne studies.^{80,91,92} Both pulsed and continuous wave laser sources have been used, with the latter having superior sensitivity but requiring a more complex experimental design than the pulsed counterpart.^{66,87,96,130} Reviews on different CRDS applications can be found in the works of Scherer et al.,¹³¹ Wheeler et al.,¹³² Busch and Busch,¹³³ Berden et al.,¹³⁴ Brown,¹³⁵ and Mazurenka et al.¹³⁰

Cavity-attenuated phase shift (CAPS) spectroscopy determines the particle extinction coefficient from changes in the phase shift of the distorted waveform of a square-wave modulated light-emitting diode (LED) that is transmitted through an optical cavity cell. Though not as widely used as CRDS, it has also been used in laboratory^{103,136} field,^{137–141} and aircraft¹⁰² measurements. CAPS is a lightweight, compact instrument, making it easy to use outside the laboratory environment, and its performance has been validated for both laboratory and field measurements of ambient aerosol.^{101,103}

The need for fully resolved spectral information has promoted the development of optical instrumentation with broadband LED light sources and a monochromator, currently at the forefront of state-of-the-art aerosol optical measurements.^{61,104–108,129,142,143} Cavity-enhanced spectroscopy that combines high-intensity, broadband light sources coupled to a monochromator with optical cavities has had the greatest advancement and has allowed sensitive measurements of optical extinction as a function of wavelength. The availability of inexpensive light sources (i.e., LEDs) and highly reflective mirrors at short visible and ultraviolet wavelengths has enabled measurements at these shorter wavelengths. The broadband spectrum is advantageous in that it enables measurements of multiple gas-phase absorbers whose absorption can be identified and quantified simultaneously. The most significant gas-phase interferences in the UV are ozone, NO₂, SO₂, and water.¹⁰⁸ This is especially pertinent for field measurements and when conducting “online” chemical reactions.

The technique was initially used for gas-phase absorption measurements and referred to as incoherent broadband cavity-enhanced absorption spectroscopy (IBBCEAS or BBCEAS)¹⁴⁴ or alternatively as cavity-enhanced differential optical absorption spectroscopy (CE-DOAS).¹⁴² In this paper we will refer to the method by the more general name of broadband cavity-enhanced spectroscopy (BBCES), as the measurements discussed here are of optical extinction and not only absorption.

In BBCES, the optical output from the cavity is resolved with a spectrometer and recorded by use of a multichannel detector. By measuring the change in light intensity of a filled cavity relative to a particle-free cavity, and taking into account the mirror reflectivity and Rayleigh scattering of the carrier gas, the extinction coefficient of the aerosol is determined.

The BBCES technique has been recently used to retrieve the complex refractive index of aerosol as a function of wavelength in laboratory^{104,105} and chamber^{61,107} studies, for concurrent measurement of NO₂ concentration and β_{ext} in a polluted urban environment,¹⁴³ and for β_{ext} measurements of SOA formed by the photolysis of nitroaromatic compounds¹⁰⁶ and NO₃

oxidation of β -pinene.¹⁰⁷ It was also shown that, for aerosols whose RI has minimal spectral dependence, the selection and measurement of a single particle diameter over the spectral range allows retrieval of the complex refractive index, enabling a faster procedure for RI retrieval.¹⁰⁴

Another instrument that has been recently extended to measure aerosol extinction is the multipass aerosol extinction differential optical absorption spectroscopy (AE-DOAS).¹⁰⁸ The instrument covers the full solar spectrum from 220 to 1050 nm with 0.5 nm resolution. The continuous-duty xenon lamp is fiber-optically coupled to a White-type multipass gas cell, with an adjustable path length of up to approximately 20 m, and then to a single-beam UV-vis spectrometer. The AE-DOAS has been used for extinction measurements of standard aerosol particles and gas-phase absorption.¹⁰⁸

An intercomparison study of three broadband instruments, BBCRDS (broadband cavity ring-down spectroscopy), CEDOAS, and BBCES, was conducted at the SAPHIR atmosphere simulation chamber.¹⁰⁷ Extinction coefficients from the three instruments, measured at around 670 nm, agreed to within 10% and 4% of their mean for dry and wet conditions, respectively. If 10% uncertainty in the mean extinction coefficient is assumed (which is representative of the agreement between instruments and of their stated uncertainties), then the uncertainty attributed to the derived real part of the refractive index was ± 0.03 ($m_r = 1.61 \pm 0.03$).

For all the extinction measurements, if the cavity contains monodisperse homogeneous spherical particles of a known size (within the accumulation mode size range, 0.1–2 μm , for which $x \approx 1$), and the particle's number density is measured, then the measured β_{ext} may be related to the extinction efficiency (Q_{ext}) of the particles in the cavity (see eqs 3 and 4) at the specific wavelength being used. Comparing Q_{ext} as a function of size parameter for a fixed wavelength with the extinction efficiency calculated from a Mie scattering subroutine enables the retrieval of complex RI of the particles^{79,145} (see, for example, Riziq et al.⁷⁹ regarding the technique for fitting to Mie theory). Some limitations on this retrieval procedure can be found in recent studies.^{86,146,147} For mixed composition and nonspherical particles and aggregates, additional theoretical approaches for modeling the optical extinction of aerosol, such as effective medium approximations, extended effective medium approximations, multilayer concentric sphere models, Rayleigh–Debye–Gans theory, the T matrix method, and the discrete dipole approximation are often applied.^{148–150}

2.2.2. Instrumentation for Scattering Measurements.

The integrating nephelometer, first developed by Beuttell and Brewer,¹⁵¹ performs a geometrical integration of the angular distribution of scattering intensity to derive the scattering coefficient of aerosol. Commercial instruments that measure at multiple wavelengths (TSI and Ecotech) are now readily available, and in addition to total scatter they can have additional shutters that are used to retrieve the backscattering coefficient.^{152,153} This provides additional information on phase scattering and the asymmetry parameter.

The polar nephelometer measures light intensities scattered at 21 discrete angles by a stream of aerosol intersecting a single-wavelength laser beam. A 1/2 wave plate is used to rotate the polarization plane of the incident light to be either parallel or perpendicular to the scattering measurement plane. The RI is retrieved via a genetic algorithm approach using Mie–Lorenz scattering theory and the measured particle size distributions.^{60,62,110,111} The instrumentation used in the studies

presented in this review is “second generation” and improved from earlier models¹⁵⁴ as described in Barkey et al.¹⁰⁹ Reliable retrievals are possible for mass concentrations above 5–20 $\mu\text{g}\cdot\text{m}^{-3}$ depending on particle size,¹¹¹ which in the cited studies were between 100 and 300 nm diameters.^{60,62,111} The RI derived from the scattering retrievals is the real part of the refractive index (m_r) only.

Another instrument that has been used to obtain complex refractive indices over a wide spectral range is a variable-angle spectroscopic ellipsometer, covering wavelengths 200–1200 nm.^{55,59} The aerosols are deposited as a thin uniform film on a silicon substrate by use of an electrostatic precipitator and then mounted onto the electrode. Accurate ellipsometry measurements necessitate films of high uniformity and low surface roughness. This can be verified by optical and atomic force microscopy. Silicon was chosen as a substrate, as its conductivity ensured efficient collection by electrostatic precipitation and its high refractive index, significantly different from that of the overlying SOA film, improved ellipsometric characterization of the SOA. The instrumentation has been used for optical measurements of a variety of biogenic and anthropogenic SOA, both those formed via gas-to-particle conversion and also for model compounds of humic substances produced in the atmosphere by aqueous-phase chemistry.^{55,59}

2.2.3. Instrumentation for Absorption Measurements.

The photoacoustic spectrometer (PAS) has been used for direct measurements of aerosol absorption for many years.^{155–157} Since its further development by Arnott et al.,¹¹⁴ attaining higher sensitivity and enabling measurements of aerosol at atmospheric concentrations, the PAS has been increasingly used in both laboratory^{19,58,64,67,119,158–161} and ambient^{58,69,80,120,123,162,163} settings for in situ aerosol measurements. The basic principle of a PAS is that when a pulse of light is absorbed by a particle, the temperature of the particle increases and the heat in the particle is then transferred by conduction to the surrounding air, causing the air to expand. Consequently, a pressure disturbance, or in other words a sound wave, is generated. The acoustic waves have a relatively small amplitude; hence, acoustic resonators are used. A sensitive microphone is placed, in general, at the center of the acoustic resonator, and the signal of the microphone is related to β_{abs} . The theoretical description of the generation of a photoacoustic signal in a resonant cell is complex and beyond the scope of this review (see Meyer and Sigrist,¹⁶⁴ Schäfer et al.,¹⁶⁵ and Miklós et al.¹⁶⁶).

In principle, PAS avoids the fundamental difficulties and errors associated with filter-based absorption measurements^{58,80,158,167} and in situ measurements that derive absorption from the difference between extinction and scattering, which can have high errors for weakly absorbing particles resulting from the propagation of errors through the difference of the two quantities. However, PAS requires calibration by accurate measurement of an absorbing gas such as ozone or NO_2 , which can lead to errors due to photodissociation (NO_2) and contamination (ozone). Aerosol light absorption measurements typically show larger and more poorly understood uncertainties than extinction and scattering measurements.¹⁵⁸ The overall PAS accuracy, with respect to aerosol absorption, has been estimated at about 5%.⁸⁰ Potential biases in PAS are evaporation of volatiles (including water) and energy relaxation kinetics of large particles that might be slow relative to the acoustic period within the PAS.¹⁶⁸ Water evaporation from the heated aerosol consumes energy as latent

heat that would otherwise have contributed to the generation of sound. The evaporation of water thus changes the heat transfer and acoustic signal. A theoretical framework was developed to estimate the magnitude of bias by solving coupled heat and mass transfer equations in the transition-flow regime,¹⁶⁹ and it indicated that absorption measurements at high relative humidity (RH) may not be significantly biased by evaporation effects if the absolute (as opposed to relative) humidity is kept sufficiently low. However, a follow-up and in-depth study in which these corrections were incorporated into PAS measurements, concluded that, in order to minimize RH-related errors in PAS measurements, the RH operational range should be between 10% and 30%.^{81,92}

Another method used for direct absorption coefficient measurements of SOA is a conventional UV-visible spectrometer equipped with an integrating sphere covering wavelengths 280–800 nm.¹¹⁶ The measurements are for SOA collected on a filter such that it is still necessary to correct for the multiple scattering that arises from the filter fibers. However, the method has the advantages that there is no need for solvent extraction of the SOA, the absorption coefficient is measured over a range of wavelengths, and the correction factor is experiment-specific. The integrating sphere is able to collect most of the reflected and scattered light from the filter sample, and the reflective mode (RUV-IS) is used to calculate the absorption coefficient of SOA.

Concurrent multiwavelength extinction^{76,98} and absorption^{80,115,162} studies have been conducted by use of multiple laser wavelengths and channels, in which the aerosol flow is diverted to different cells and the extinction and or absorption is measured in parallel at each wavelength. The light source for each wavelength may be a single laser source with frequency doubling (implying similar fluctuations and stability at different wavelengths) or separate light sources for each wavelength and cell.

2.2.4. Combined Instruments for Simultaneous Measurements. Development of instrumentation that simultaneously measures two of the three optical properties monitored (scattering, absorption, and extinction) on the same aerosol sample can potentially improve the accuracy of measured scattering and absorption parameters, and hence the SSA.⁷⁸ Cavity ring-down (CRD) spectroscopy has been widely used in recent years in combination with direct absorption and scattering measurements of the same aerosol sample. CRD extinction and PAS absorption measurements can be conducted at the same wavelengths, where the experimental configuration is such that the absorption and extinction measurements are conducted in different cells. The CRD, as part of the same system, can be used to calibrate the PAS.^{63,80,117,118}

An improved extinction-minus-scattering technique for sensitive measurement of ambient aerosol light absorption and SSA is the combined CRD and reciprocal nephelometer that measures both extinction and scattering simultaneously on the same aerosol sample. The scattering coefficient is determined through collection of light scattered from the CRD beam.^{83,89,127} As the ratio of scattering to extinction gives the single scattering albedo, the instrument is referred to as the albedometer. Measuring the optical parameters on the same aerosol sample, especially when taking measurements at low number densities, improves the precision of an albedo measurement.

Zhao et al.¹²⁹ combined their BBCES (445–480 nm) with an integrating sphere (IS) for simultaneous in situ measurements

of aerosol scattering and extinction coefficients in the same sample volume. The albedometer measures the scattering signal with a single-channel photomultiplier tube (PMT), providing an integrated value over a narrow bandwidth in the spectral region 465–474 nm. The small truncation angle (0–1.29°) of their system dramatically reduced truncation errors for large particles when compared with the TSI 3563 nephelometer, reducing measurement uncertainties from 6.4% to 0.22%. The broadband albedometer enables accurate, high-sensitivity, and high-precision measurement of ambient aerosol scattering and extinction coefficients, and hence SSA determination. Broadband wavelength-resolved scattering coefficients could be determined by replacing the single-channel PMT with a multichannel PMT or a high-sensitivity spectrometer.¹²⁹

CAPS has recently been integrated with an inverse nephelometer in the same measurement volume to derive SSA directly within a single commercial instrument.¹⁷⁰ Truncation errors are minimal up to a diameter of ~500 nm. At present, the available wavelength band for the SSA monitor is restricted to the 400–700 nm region. The upper value is limited by the availability of suitable PMT photocathodes and the lower limit by the availability of high-quality high-reflectivity mirrors.

An instrument for simultaneous measurement of both absorption and scattering combines photoacoustic spectroscopy with a reciprocal nephelometer within the same cavity.^{17,119,122,123} Commercial extensions (Droplet Measurement Technologies, Inc., Boulder, CO) to this instrumentation are the single-wavelength and multiwavelength PASS and PASS-3 that have been used in several laboratory and field studies,^{64,123} and the newer photoacoustic extintiometer, PAX, that is smaller and lighter, and hence more portable.

Sharma et al.¹²⁶ measure absorption and scattering in sequential cells at multiple wavelength bands, one at a time. Their instrument uses a super continuum light source (ranging from 400–2200 nm,) and wavelength bands are selected by using a set of optical interference filters. The instrument was validated for absorbing (kerosene soot) and purely scattering (NaCl) particles.

An intercomparison between instruments was conducted for slightly absorbing particles by Massoli et al.,¹¹⁷ in which they report uncertainty in SSA values derived from measurements that combine CRD extinction measurements with either nephelometry or photoacoustic spectroscopy. The authors conclude that CRD + TSI nephelometer results in an uncertainty in albedo of roughly 3–5% when $\omega > 0.8$, as is typically encountered in the ambient atmosphere. In comparison, they report an uncertainty of <2% for this same range when photoacoustic absorption measurements are combined with CRD. Propagation of relative uncertainty to SSA from the standard deviation of replicate β_{ext} and β_{sca} measurements measured with the albedometer indicate that $\beta_{\text{ext}} \geq 60 \text{ Mm}^{-1}$ is required to achieve <10% relative uncertainty for single-point measurements of SSA.⁸³

2.2.5. Single-Particle Techniques. The above-mentioned techniques all measure ensembles of particles. Single-particle techniques, in which large (micrometer-size) particles are held in electrodynamic, optical, and acoustic traps, have been used to study aerosol processes and properties¹⁷¹ and have recently been applied also for the measurement of optical extinction, scattering, and absorption.^{171–175} In the optical tweezers technique, a vertically polarized light from a continuous-wave laser is used both for particle trapping and for simultaneous

Table 2. Real Parts of Refractive Index for Secondary Organic Aerosol As Measured in Various Studies^a

Precursor	Reaction	References	Technique	Wavelength	O/C	HC/NO _x or NO _x (ppb)	m_r
α -pinene	ozonolysis	Nakayama et al. ⁹⁹	CRD & Integrating nephelometer, 6m ³ smog chamber	355 532			1.458(^{+0.018} _{-0.018}) 1.411 (± 0.021)
α -pinene	ozonolysis	Nakayama et al. ¹²¹		405 532 781	0.43-0.45		1.463(± 0.019)-1.475(± 0.022) 1.466(± 0.019)-1.475(± 0.022) 1.400(^{+0.027} _{-0.032})- 1.410(^{+0.027} _{-0.028})
α -pinene	Photooxidation UV/NO _x	Nakayama et al. ¹²¹	CRD & PASS-3 6m ³ smog chamber	405 532 781	0.47	180 ppbv NO _x	1.498(± 0.030) 1.458 (± 0.020) 1.422(^{+0.025} _{-0.023})
Toluene	Photooxidation UV/NO _x	Nakayama et al. ⁹⁹	CRD & Integrating nephelometer, 6m ³ smog chamber	355 532		500 ppbv NO _x	1.632(^{+0.038} _{-0.035}) 1.483(^{+0.032} _{-0.036})
Toluene	Photooxidation UV/NO _x	Nakayama et al. ⁶⁴	CRD & PASS-3 6 m ³ smog chamber	405 532 781	0.64-0.73 0.64-0.73 0.64-0.73	109 \rightarrow 571 ppbv NO _x	1.449(± 0.030) - 1.567(^{+0.042} _{-0.042}) 1.431(^{+0.025} _{-0.026}) - 1.498(^{+0.025} _{-0.025}) 1.389(^{+0.053} _{-0.056}) - 1.452(^{+0.31} _{-0.030})
1,3,5-trimethylbenzene	Photooxidation UV/NO _x	Nakayama et al. ⁶⁴		405 532 781	0.49	571 ppbv NO _x	1.485(^{+0.062} _{-0.054}) 1.459(^{+0.028} _{-0.029}) 1.423(^{+0.028} _{-0.027})
α -pinene and β -pinene	ozonolysis	Kim et al. ¹¹⁰	Polar and integrating nephelometer, 24m ³ chamber	670			1.4-1.5
β -pinene	photooxidation UV/NO _x	Kim et al. ¹¹⁰		670			1.38-1.53
α -pinene	photooxidation UV/NO _x	Kim et al. ¹¹⁰		670			1.4-1.53
Limonene	ozonolysis	Kim and Paulson ⁶²	Polar and integrating nephelometer, 24m ³ chamber	532			1.4-1.51
α -pinene	ozonolysis	Kim and Paulson ⁶²		532			1.4-1.56
α -pinene	photooxidation UV/NO _x	Kim et al. ¹¹¹ , Kim and Paulson ⁶²		532		3 HC/NO _x regimes are defined high \rightarrow low HC/NO _x 20-33, 13-19, 6.3-11	1.36-1.52
Limonene	photooxidation UV/NO _x	Kim et al. ¹¹¹ , Kim and Paulson ⁶²		532			1.34-1.56
Toluene	UV/NO _x	Kim and Paulson ⁶²		532			1.35-1.6
α -pinene, β -pinene and limonene	Ozonolysis and photooxidation (low NO _x)	Kim et al. ¹¹¹ , Kim and Paulson ⁶²	Polar and integrating nephelometer 24m ³ chamber	532		high HC/NO _x : 28-33	1.44 ^a
Toluene and phenol	photooxidation UV/NO _x	Kim et al. ¹¹¹ , Kim and Paulson ⁶²		532		HC/NO _x Toluene: 15-33 Phenol: 35-41	1.55 ^b 1.5 1.6
α -pinene	ozonolysis	Redmond and Thompson ¹⁸⁷	Albedometer, 0.9m ³ smog chamber	532			1.49 (± 0.029)- 1.51(± 0.040)
Toluene	ozonolysis	Liu et al. ⁵⁹		405 200-1200 (360-420)	<0.03		1.49 (± 0.040) -1.50 (± 0.038)
α -pinene	ozonolysis	Liu et al. ⁵⁹	Spectroscopic ellipsometry and UV-Vis ellipsometry, oxidation flow reactor	405 200-1200 (360-420)	<0.03		1.511 (± 0.003) 1.579 – 1.491 (1.516 – 1.509)
Limonene	ozonolysis	Liu et al. ⁵⁹		405 200-1200 (360-420)			1.514 (± 0.003) 1.590 – 1.492 (1.520 – 1.512)
Toluene	Photooxidation UV/NO _x	Liu et al. ⁵⁵		320 405			1.567 \pm (0.008)- 1.591 \pm (0.009) 1.546 \pm (0.004)-1.571 \pm (0.005)
<i>m</i> -Xylene	Photooxidation UV/NO _x	Liu et al. ⁵⁵		320 405		0-10 ppm NO ₀	1.554 \pm (0.011) - 1.589 \pm (0.008) 1.531 \pm (0.006) - 1.565 \pm (0.007)
α -pinene	ozonolysis	Flores et al. ¹⁰⁵	BBCES, 1 m ³ oxidation bulb, 3 m ³ reaction flow tube	360-420			1.489(± 0.022) – 1.460(± 0.031)
Limonene	ozonolysis	Flores et al. ¹⁰⁵					1.567(± 0.022) – 1.516(± 0.031)
α -humulene							1.481(± 0.022) – 1.447(± 0.031)

Table 2. continued

Precursor	Reaction	References	Technique	Wavelength	O/C	HC/NOx or NOx(ppb)	m_r
α -pinene + limonene	ozonolysis and OH oxidation	Flores et al. ⁶¹	BBCES, SAPHIR chamber 270 m ³	405	0.37-0.38	1.50 (± 0.01)–1.49 (± 0.01)	
α -pinene + limonene + p-xylene-d ₁₀	ozonolysis and OH oxidation	Flores et al. ⁶¹		405	0.35–0.42	1.46 (± 0.01)–1.51 (± 0.01)	
α -pinene + limonene + p-xylene-d ₁₀ ^c	ozonolysis and OH oxidation	Flores et al. ⁶¹		405 (360–420)	0.39–0.44	1.46 (± 0.01)–1.50 (± 0.02)	
α -pinene	OH oxidation	Lambe et al. ⁶³	CRD-PAS, PAM reactor	405 532	0.42–0.93	1.51(± 0.02)-1.45(± 0.04) 1.48-1.41	
Guaiacol (surrogate for BB)	OH oxidation	Lambe et al. ⁶³	CRD-PAS, PAM reactor	405	0.70–1.14	1.55(± 0.01) - 1.53(± 0.01)	
Naphthalene	OH oxidation	Lambe et al. ⁶³	CRD-PAS, PAM reactor	405	0.52–1.29	1.66(± 0.04) - 1.58(± 0.06)	
α -pinene	ozonolysis	Ma and Thompson ⁸³	CRD & Nephelometer	355		1.45(± 0.02)	
α -pinene	photooxidation	Yu et al. ¹⁷⁸	Nephelometer, 100 m ³ chamber	450 550 700		1.56(± 0.04) 1.51(± 0.03) 1.46(± 0.03)	
Holm Oak Emissions (98% monoterpenes)	photooxidation	Lang-Yona et al. ¹⁷⁶	CRD JPAC chamber, 145 m ³	532		1.53(± 0.08)	
β -pinene	NO ₃ oxidation	Varma et al. ¹⁰⁷	IBBCEAS BBCRDS CE-DOAS	655–687		1.61 (± 0.03)	
Azelaic acid (surrogate for oxidized organic aerosol)			CRD, Flow reactor		0.44–0.75	1.48 (± 0.02) - 1.55(± 0.02)	
Squalane (surrogate for primary organic)	OH oxidation	Cappa et al. ²³		532	0–0.35	1.49(± 0.02) - 1.54(± 0.02)	

^aSuggested representative RI value for biogenic SOA by Kim and Paulson⁶² was taken as median RI value of biogenic SOA produced by both ozonolysis and photooxidation under low NO_x conditions. ^bSuggested representative RI value for anthropogenic SOA by Kim and Paulson.⁶² Figure 6 of that paper would suggest the median m_r for toluene is 1.5 and that for phenol is 1.6. ^cp-Xylene-d₁₀ was added 5 h after the BVOC. Note that AVOC sources are shown in boldface type in the table.

measurement of droplet size and optical extinction. Both are retrieved from the unique solution to the Mie scattering fitting of the whispering gallery modes that appear in the cavity-enhanced Raman spectrum. The real part of the refractive index is retrieved with an uncertainty of ± 0.0012 (better than $\pm 0.11\%$), while the size of the micrometer-sized liquid droplet is simultaneously measured with a precision of better than 1 nm ($<\pm 0.05\%$ error). Modulating the power of a second illuminating laser leads to perturbation to the droplet size, and by measuring induced size changes of <1 nm, the imaginary part of the refractive index can be retrieved even when $k < 1 \times 10^{-8}$ with an accuracy of better than 0.5×10^{-9} .¹⁷⁴ Combined, the complex refractive index of nonabsorbing or slightly absorbing particles is retrieved with high accuracy, with the possibility of making extremely sensitive optical absorption measurements on weakly absorbing aerosol samples. The technique is currently limited to droplets $>1 \mu\text{m}$.^{94,172,173} Extinction cross sections of smaller levitated individual aerosol droplets (<500 nm radius) have also been demonstrated by using a Bessel beam optical trap combined with CRD spectroscopy, with potential for further reducing the droplet size.¹⁷⁵

3. SCATTERING BY SECONDARY ORGANIC AEROSOL

We first focus on studies that investigated the light scattering properties of secondary organic aerosol (SOA) generated following controlled oxidation experiments of biogenic and anthropogenic VOC, using either flow reactors or atmospheric

photochemical chambers.^{59–64,99,105,107,110,112,176–178} Results from controlled laboratory and smog chamber experiments are summarized with respect to aerosol precursors, oxidation pathway, H:C and O:C ratios and molecular fragments of SOA (as measured by aerosol mass spectrometry, AMS), and densities and volatility of organic compounds.

3.1. Secondary Organic Aerosol Generation

SOA composition is expected to depend on the parent hydrocarbon, oxidation chemistry, particle mass concentration, size, temperature, relative humidity, and under longer time scales, potentially in-particle reactions and heterogeneous chemical processes (“aging”).^{28,51,111} In the experiments, SOA are formed from oxidation of parent hydrocarbons initiated in the dark (NO₃, O₃) or light (O₃, OH), with or without NO_x. For dark ozone reactions of unsaturated hydrocarbons, conditions can be adjusted so that organics can react either solely with O₃ or with both O₃ and OH radicals formed from ozonolysis of VOC.¹⁷⁹

Parent hydrocarbons used in laboratory studies are chosen to represent typical groups of sources and compounds: anthropogenic, biogenic, and biomass burning. α -Pinene and limonene are commonly treated as representative biogenic hydrocarbons, as they account for approximately 50%¹⁸⁰ and 16%,³⁰ respectively, of global monoterpene (C₁₀H₁₆) emissions, which themselves comprise approximately 15% of global biogenic emissions.¹⁸¹ Additional BVOCs commonly chosen as model SOA precursor compounds are β -pinene, sesquiter-

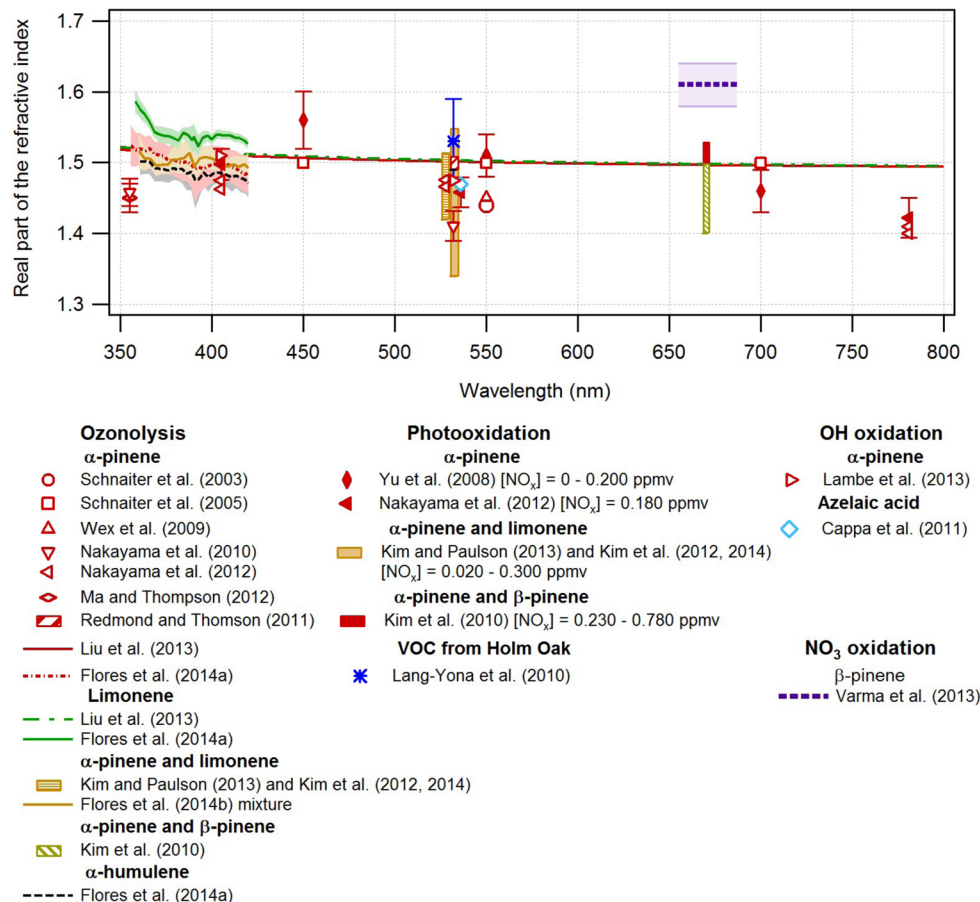


Figure 4. Compilation of the real part of RI (m_r) for biogenic precursor SOAs as measured in various studies. The legend specifies the precursor type and oxidation pathway as well as the reference.

penes ($C_{15}H_{24}$) such as α -humulene, and direct emissions from plants such as Holm oak and species of boreal forest trees that are dominantly monoterpenes.^{176,182–185}

Typical anthropogenic SOA precursors are aromatic hydrocarbons such as toluene, benzene, and *p/m*-xylene that are commonly used as model precursor compounds for urban SOAs in laboratory studies.^{35,186} Toluene is the most abundant aromatic compound emitted globally,³⁰ although benzene and *m*-xylene SOA yields can be comparable.¹⁸⁶

3.2. Measured Values of Real Part of Refractive Index (m_r)

In Table 2 we present a compilation of real parts of refractive indices derived for biogenic and anthropogenic SOA generated in various experiments and experimental setups. These measurements span wavelengths from 220 to 1200 nm and include various oxidation pathways: OH, ozonolysis, and photo-oxidation in the presence or absence of NO_x .

First, we discuss studies of biogenic SOA. It was found that nearly all SOA formed from terpene precursors (α -pinene, β -pinene, α -humulene, limonene, and Holm oak emissions) do not absorb in the solar wavelength range.^{61,99,111,176,187,188} Some of the instrumentation measures scattering only (such as the integrating nephelometer) and attributes RI on the basis of the assumption that the aerosols are nonabsorbing.^{60,62,110,111,177} Studies of biogenic SOA that measure total extinction and scattering (CRD + nephelometer) show similar extinction and scattering cross sections, indistinguishable from each other within the errors, implying that biogenic SOA do not absorb in the visible range.^{83,99} Also the RIs (derived from

Mie retrieval that allows for an absorption component) display no significant absorption,¹⁷⁶ even at shorter wavelengths (360–420 nm).^{61,105} Direct absorption measurements using PASS-3 at 405 nm, as well as simultaneous extinction measurements with CRD, also show no absorption for α -pinene SOA.¹²¹ The few measurements that display a non-negligible but still small absorption component for biogenic SOA, as well as measurements from anthropogenic SOA that display a slightly higher-absorbing component than the biogenic SOA, are detailed in section 4.

The real parts of the refractive index for SOA span quite a wide range, from 1.35 to 1.6, and are depicted graphically in Figure 4 for biogenic SOA and in Figure 5 for anthropogenic SOA, as well as their tabulation in Table 2.

3.3. Real Part of Refractive Index (m_r) as a Function of Oxidation Pathway, Precursor, and Reaction Duration

The spread of experimentally determined values for the real part of RI (m_r), even of SOA generated from the same precursor VOC compounds, necessitates careful analysis prior to the proposition of recommended values for implementation into coupled climate models. The array of measurements shown in Figures 4 and 5 includes different precursor concentrations, oxidation mechanisms, and exposure times, stages of aerosol growth, and aging as well as different instrumentation. In this section, we summarize the observed trends in m_r as a function of oxidation pathway, precursor, and reaction duration, and in the following section we explain how

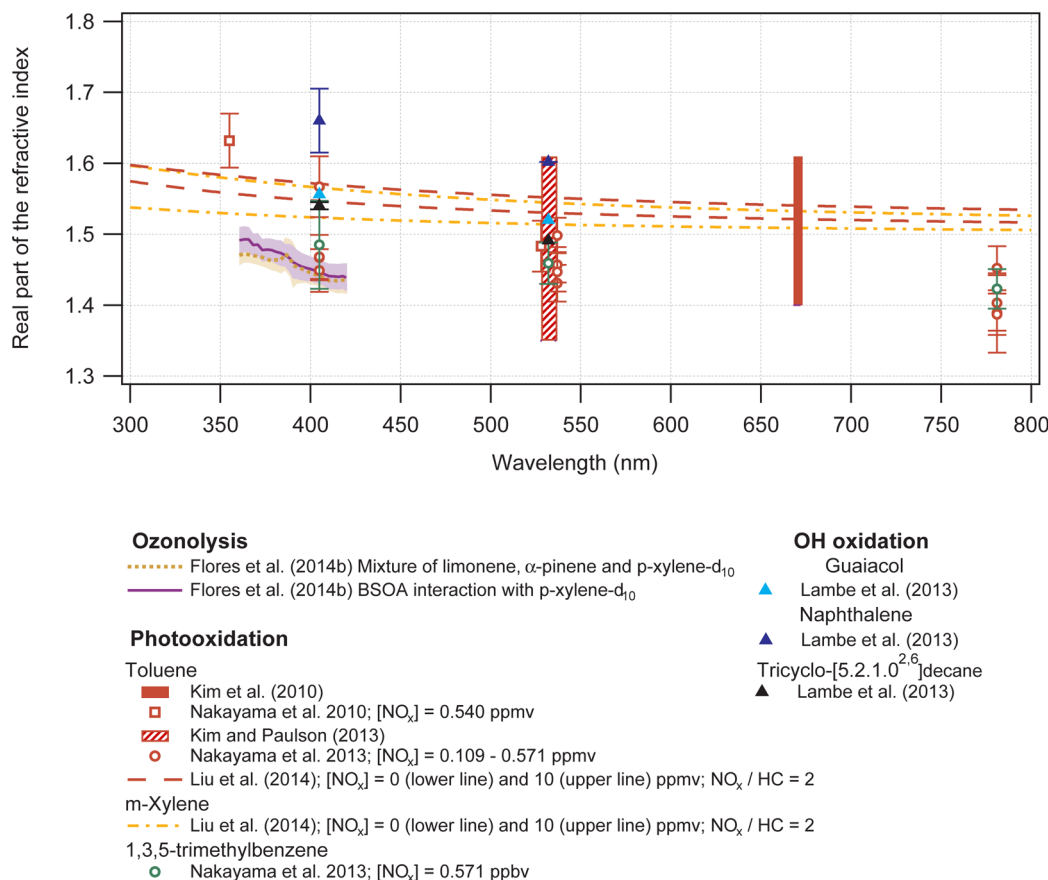


Figure 5. Compilation of the real part of RI for anthropogenic and mixed biogenic/anthropogenic precursor SOAs as measured in various studies. The legend specifies the precursor type and oxidation pathway as well as the reference.

these three parameters govern the differences in the evolving chemistry and chemical composition of SOA.

3.3.1. Spectral Dependence of m_r . The measurements shown in Figures 4 and 5 have been conducted over the near-UV and visible spectrum. The more recent spectrally resolved studies by Florès et al.¹⁰⁵ and Liu et al.^{55,59} in which the RI is retrieved at 0.5 nm and 5–10 nm increments, respectively, show that m_r increases at shorter wavelengths. These measurements portray the earlier indication from multi-wavelength measurements by Nakayama et al.^{64,121} and by Yu et al.¹⁷⁸ for BSOA derived from both α -pinene ozonolysis and photo-oxidation and also ASOA derived from toluene, in which a clear spectral dependence was observed.

3.3.2. Dependence of m_r on Precursor and Oxidation Pathway.

In Figure 6 we show a compilation of measurements of the real part of RI at $\lambda = 532$ and 405 nm for biogenic and anthropogenic precursors together, according to different oxidation pathways. At the mid-visible wavelengths ($\lambda = 532$ nm), the common biogenic and anthropogenic precursor SOAs (alkenes, toluene, and 1,3,5 methylbenzene) have m_r values in the same range, between 1.4 and 1.5. A number of other anthropogenic SOA precursors such as naphthalene and phenol have higher m_r than SOA formed from biogenic precursors when measured with the same instrumentation and under similar conditions, with m_r ranging from 1.58 (± 0.06) to 1.66 (± 0.04) at $\lambda = 405$ nm⁶³ and $m_r = 1.6 (\pm 0.05)$ at $\lambda = 532$ nm,⁶² respectively. The ellipsometry measurements of Liu et al.⁵⁵ show that, within the measurement uncertainties, the m_r values for SOAs derived at the same initial NO concentrations

from the two aromatic precursors, toluene and *m*-xylene, do not differ and are slightly higher than the m_r values they measure for limonene and α -pinene.⁵⁹

Within the general spread of m_r values, SOA formed by ozonolysis and OH oxidation pathways display similar values. At $\lambda = 532$ nm, m_r values of toluene following photooxidation in the presence of NO_x display values in the same range as the other oxidation pathways for both low and high NO_x conditions. However, a spectral dependence is apparent and at shorter wavelengths, $\lambda = 405$ and 355 nm, SOA from toluene displays higher m_r at the higher NO_x concentrations (571 and 500 ppbv), $m_r = 1.567 (\pm 0.042)$ and $m_r = 1.632 (\pm 0.038)$ respectively.^{64,99} As can be seen in Table 2, m_r for toluene is higher at the higher NO_x concentrations (lower HC/ NO_x) at all wavelengths in the study of Nakayama et al.⁶⁴ In toluene SOA, Kim and Paulson⁶² did not observe a higher real part of the refractive index, though the HC/ NO_x ratios (15 and 32) lie within the range of those in the study of Nakayama et al.⁶⁴ (HC/ NO_x from 7 to 36).

The oxidation state, yield, and volatility of SOA vary depending on the branching of RO_2 reactions with HO_2/RO_2 versus NO , which is in turn controlled by the HC/ NO_x ratio.^{185,189,190} While the reaction of RO_2 with HO_2 and NO_2 produces low-volatile species, the $RO_2 + NO$ reaction generates volatile species via fragmentation of the resultant RO radical.^{190,191} SOA formation in the presence of NO_x is thus determined by further reactions of RO. In the high- NO_x regime, nucleation can be suppressed (through NO reactions

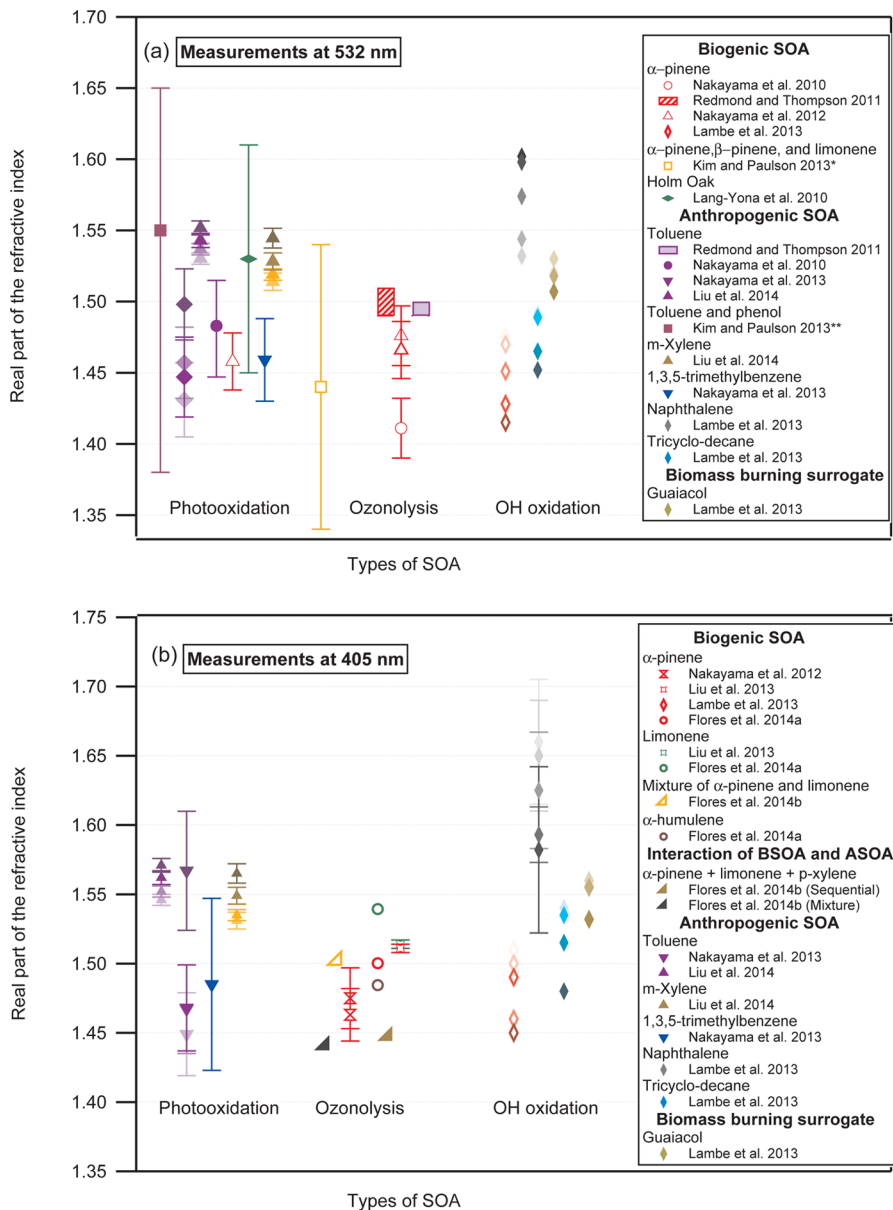


Figure 6. Comparisons of the real part of RI (m_r) for SOA measured in various studies, as dependent on precursor and oxidation pathway at (a) 532 nm and (b) 405 nm. Shading of the markers from light to dark in the study of Lambe et al.⁶³ portrays increasing [OH] exposures and O:C ratios, and in the studies of Nakayama et al.⁶⁴ and Liu et al.⁵⁵ the shading portrays increasing NO_x concentrations. The measurements of Kim and Paulson⁶² are their median m_r for separate measurements of α -pinene and limonene SOA for low NO_x conditions (*) and their median m_r of separately measured toluene and phenol (**). The full ranges of values for both are depicted by the vertical lines from the median value.

with higher generation peroxy-radical-like intermediates), leading to formation of larger particles.¹⁸⁵

The results of optical studies that specifically investigated the effect of HC/NO_x ratios on m_r of biogenic SOA are ambiguous. Kim et al.¹¹¹ show that limonene and α -pinene SOA formed under low HC/NO_x ratios (6.3–9.6) have lower aerosol yields, evolve into larger particles, and have higher m_r values than similar reactions occurring at high HC/NO_x ratios (30–33). The trend is more apparent for limonene SOA, where the m_r range is larger (e.g., for limonene SOA at HC/NO_x = 6.3, m_r at $\lambda = 532$ nm averaged over an experiment = 1.54, whereas at HC/NO_x = 19, m_r at $\lambda = 532$ nm averaged over an experiment = 1.41). However, in later studies under similar HC/NO_x conditions, these trends are not observed.^{60,62} Although Kim et al.⁶⁰ suggest that this may be the result of lower temperatures

(16–29 vs 31–39 °C) and insolation that change the balance between the RO₂/HO₂ and RO₂/NO reactions, one of these latter studies⁶² was also conducted at higher temperatures (28–39 °C). In the study of Liu et al.,⁵⁵ a shift in m_r of +0.02 is observed for both toluene- and *m*-xylene-derived SOAs for an increase in the initial NO concentration from 0 to 10 ppm. The high m_r value of 1.61(±0.03) at $\lambda = 655$ –687 nm in the study of Varma et al.¹⁰⁷ following primarily NO₃ oxidation of β -terpene is significantly larger than m_r values observed following OH- and ozone-initiated terpene oxidation. This has been attributed to the low HC/NO_x ratio in the experiments of Varma et al.¹⁰⁷ (2 vs the lowest HC/NO_x ratio of 6.3 in the study of Kim et al.¹¹¹) and the high proportion (up to 45%) of organic nitrates in the particle phase.¹⁰⁷

For SOA of α -pinene following ozonolysis, lower oxidation temperatures (in the range of \sim 14–19 vs 24–26 °C) possibly affect the refractive index values, lowering m_r by \sim 0.05.⁶⁰

3.3.3. Changes in m_r with Oxidation Time. Changes in extinction, scattering, and m_r of newly formed SOA are manifested as the particles evolve during the oxidation reaction and have been monitored (a) directly as a function of time following the mixing of a gas-phase oxidant and VOC,^{61,64,192} (b) as a function of the number of oxidation lifetimes determined from the measured cumulative OH exposures,²³ and (c) as a function of the particle diameter as the reaction proceeds.⁶⁰ Kim et al.^{60,62,111} assumed that the growth in particle diameter axis is equivalent to a reaction time axis, as particle diameter continuously increases throughout each experiment, and is used to visualize the initial growth phase.

The large spread in RI values (Figure 5) of Kim et al.^{60,62,110,111} may result from the relatively large number of experimental runs, which were conducted at different temperatures with different precursor and reactant concentrations, and also from changes in m_r over time. In many cases, the freshest, smallest size particles have the lowest m_r , which increases with particle diameter but then decreases again (slightly) above a certain size. This pattern is observed for β -pinene¹¹⁰ and α -pinene and toluene^{62,110,111} SOA following photo-oxidation and for limonene SOA from both photo-oxidation and ozonolysis,^{62,111} although the pattern is not always consistent.^{62,60} The decrease in m_r above a certain size is more frequently observed and more pronounced at low HC/NO_x concentrations.⁶²

Changes in m_r with particle growth (as an equivalent measure of reaction progress) are from 1.35 to 1.61 for toluene SOA (diameter change from \sim 180 to 360 nm), from 1.43 to 1.54 for α -pinene SOA (diameter change from \sim 190 to 350 nm), from 1.43 to 1.54 for limonene SOA (diameter change from \sim 210 to 300 nm), and for limonene ozonolysis from 1.39 to 1.52 (diameter change from \sim 100 to 200 nm).⁶² These changes occur over a couple of hours. The refractive index changes only slowly after the initial growth.^{62,110,111} For reactions of α -pinene and limonene SOA from photo-oxidation, m_r is either constant or decreases respectively when the measurements took place at around 300 nm.⁶² It is not always apparent from other optical studies at what stage of aerosol growth the reported measurements are taken, but it seems that many reported values are from aerosol that are no longer in the rapid “initial growth stage” as termed by Paulson and co-workers. For example, in Varma et al.,¹⁰⁷ the RI is an averaged value around the extinction maximum, which is just after the mass concentration has reached its peak and particles are still growing from around 200 to 250 nm diameter, and in Nakayama et al.⁶⁴ the RI is derived from measurements at near-stable (and maximal) mass concentrations and particle growth.⁶⁴ To the best of our knowledge, only two studies have specifically monitored how RI changes with aging of these SOA, via in-particle reactions and heterogeneous chemical processes following their initial formation and rapid growth stage, and have monitored RI as it changes over a longer duration upon continuing oxidation.^{23,61}

Cappa et al.²³ observed an increase in the extinction cross section of model organic aerosol as they undergo an increasing number of OH heterogeneous oxidation lifetimes. The m_r at $\lambda = 532$ nm increases from 1.49 (± 0.02) to 1.54 (± 0.02) and from 1.48 (± 0.02) to 1.55 (± 0.02) following continuous oxidation of squalane (as a surrogate for primary organic

aerosol) and azelaic acid (a surrogate for oxidized organic aerosol), respectively. A similar increase in m_r of 0.05 was observed for aging SOA by Flores et al.⁶¹ for SOA mixtures of BVOC and AVOC over a diurnal cycle, with m_r at $\lambda = 405$ nm increasing from 1.46 (± 0.01) to 1.51 (± 0.01) after 29 h of aging. In that study, an additional experiment was conducted in which the AVOC was added to the reaction chamber after the initial BVOC particle nucleation has taken place. In this case, the change in RI with aging is diminished at shorter wavelengths ($\lambda < 385$ nm), whereas for the mixed-composition precursors (AVOC and BVOC nucleating together), RI increases across the full spectral window monitored (360–420 nm) as the SOA ages, with the RI also at $\lambda = 365$ nm increasing from 1.49 to 1.56 after 29 h (see Figure 3 in Flores et al.⁶¹). These (limited) results suggest that that the interaction of BVOCs and AVOCs could generate aerosols with higher value for m_r , which is significant as there are many regions where anthropogenic and biogenic emissions regularly mix (which may also lead to some enhancement in BSOA yields^{37,50}). To date, this is the only laboratory study to investigate the optical trends of SOA formed from interaction of anthropogenic and biogenic emissions.

The change in m_r with SOA aging in the studies of Cappa et al.²³ and Flores et al.⁶¹ is similar (Δm_r between 0.05 and 0.08) and is somewhat smaller than the changes observed in the studies of Kim et al.^{60,62,111} during the initial aerosol growth stage and are within the same range of variance in m_r values between different studies as seen in Figure 6.

3.4. Compositional and Volatility Changes as Secondary Organic Aerosols Evolve and Effect on m_r

SOA formation is accompanied by formation of polar functional groups, which often decreases the volatility of the product SOA.³⁰ Volatility and O:C ratio are generally inversely correlated.¹⁹³ The opening of cyclic rings usually leads to products with the same carbon number as the precursor (thus increasing O:C and decreasing H:C ratios). The first-generation oxidation products generally contain two (or more) polar functional groups such that the oxidation of cyclic compounds leads to low-volatility products.²⁸ SOA properties dynamically evolve in the atmosphere with aging,¹⁹³ and further oxidation can change the dominant pathway from functionalization to fragmentation or/and oligomerization. These transformations of SOA are commonly described in terms of the carbon oxidation state and volatility.^{193–195} Partitioning of the semivolatile oxygenated organics between gas and particle phases is described by theories first developed by Pankow¹⁹⁶ and later extended by Odum et al.,¹⁹⁷ Chan et al.,¹⁹⁸ and others. More recent oxidation studies of terpenes have also shown significant mass yields of highly oxygenated, extremely low volatility compounds (ELVOCs), which have a saturation concentration (C^*) $< 3 \times 10^{-4} \mu\text{g}\cdot\text{m}^{-3}$ ¹⁹⁹ and are expected to condense irreversibly onto aerosol surfaces to produce SOA and to contribute significantly to atmospheric SOA mass.^{180,200} The processing of aerosol by oxidants can lead, however, to release of volatile compounds as well, and the overall aerosol growth is a balance between growth and evaporation.^{193–195,201,202}

3.4.1. Linking Particle Oxidative State to Refractive Index. The O:C and H:C ratios are useful metrics to measure the oxidative state and compositional changes of SOA. The O:C and H:C space, in the form of the van Krevelen diagram, has been utilized to depict compositional changes of organic

compounds as they evolve²⁰³ and to illustrate how reactions involving the addition of specific functional groups are traced in this space along a line of a particular slope.^{29,204} Chemical composition and mass size distribution of SOA components are commonly measured in real time on the Aerodyne high-resolution time-of-flight aerosol mass spectrometer (HR-ToF-AMS; Aerodyne, Billerica, MA),^{29,44,195,205,206} from which the elemental O:C and H:C ratios can be calculated by the method outlined by Aiken et al.^{207,208}

The AMS measurements enable us to map the SOA composition evolution both in the form of a van Krevelen diagram and as a plot that depicts the f_{44} versus f_{43} mass fraction (defined as the fractions of the signal at $m/z = 44$ and 43 of the total organics measured by AMS). The m/z 44 fragment ion has been related to the CO_2^+ ion,²⁰⁹ and the m/z 43 ion corresponds mainly to the $\text{C}_2\text{H}_3\text{O}^+$ and C_3H_7^+ fragments from both saturated hydrocarbons and oxidized species such as aldehydes and ketones. Ng et al.²⁰⁶ suggested that the degree of oxidation and volatility of oxygenated organic aerosol (OOA) components can be estimated from the f_{44}/f_{43} ratio; they defined the more oxidized (higher f_{44}) as low-volatility OOA and the less oxidized components (lower f_{44}) as semivolatile OOA. In other words, a higher f_{44}/f_{43} value indicates lower volatility OOA, and a low f_{44}/f_{43} value can be used as an indication of semivolatile OOA. In Figure 7 we show the area

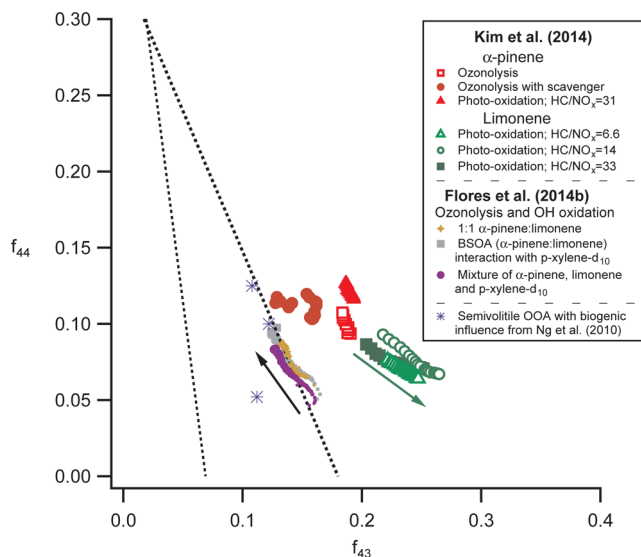


Figure 7. Time evolution of f_{44} vs f_{43} mass fractions for SOA in the studies of Flores et al.⁶¹ and Kim et al.⁶⁰ Change in the size of the markers for the study of Flores et al.⁶¹ depicts time; smaller markers refer to the beginning of the experiment and larger markers to the end. Arrows also show the direction of change over time for both studies. Dotted lines show the triangular area that represents the common values of ambient oxygenated organic aerosol components. Adapted with permission from ref 206. Copyright 2010 Copernicus Publications.

proposed by Ng et al.²⁰⁶ (commonly referred to as “triangle plot”), which encompasses the majority of OOA measured in ambient samples. Previous studies have utilized O:C ratios,^{23,64} van Krevelen diagrams,^{61,63} and “triangle plot” and volatility measurements^{60,61} to relate the time-resolved RI to the evolving aerosol composition.

In Figure 8 we show a compilation of the real part of the refractive index at $\lambda = 405$ nm (only the data from Kim et al.⁶⁰

are at $\lambda = 532$ nm) plotted against measured O:C ratios (values of which are also detailed in Table 2). Some studies display a positive correlation between increasing RI and increasing O:C ratio. For heterogeneous OH oxidation of squalane, the O:C ratio ranged from 0 to 0.35 and m_r changed from 1.47 to 1.52, and for azelaic acid the O:C ratio ranged from 0.44 to 0.75 and m_r changed from 1.47 to 1.52. The O:C ratio range following photo-oxidation aging of mixed BVOC and AVOC⁶¹ was 0.39–0.44 and 0.35–0.42 for two different mixing conditions, with comparable changes in m_r of 1.46–1.50 and 1.46–1.51, respectively. For mixed BVOC compounds in the same study, reliable measurements could be retrieved only over a shorter time span such that both O:C ratio and m_r barely changed (0.37–0.38 and 1.51, respectively).

The O:C ratios measured in the toluene photo-oxidation study⁶⁴ are a result of different initial NO_x concentrations (100–570 ppbv) rather than progression of the reaction with time. The real part of RI is higher for higher NO_x concentration and O:C ratio, although the increase in m_r is slight for intermediate NO_x concentrations whereas the O:C ratio increases gradually with increasing NO_x (see Figure 8). Overall, the O:C range is small, 0.64–0.73, and m_r increased from 1.43 to 1.5 at $\lambda = 532$ nm and from 1.45 to 1.57 at $\lambda = 405$ nm. Two studies found an opposite trend with respect to the O:C ratio: namely, m_r decreased as O:C increased. In the study of Lambe et al.,⁶³ the increase in O:C ratio was much greater, ranging from 0.42 to 0.93 and from 0.52 to 1.29 for the OH oxidation of α -pinene and naphthalene, respectively, with a corresponding decrease in m_r at $\lambda = 405$ nm from 1.51 (± 0.02) to 1.45 (± 0.04) for α -pinene and from 1.66 (± 0.04) to 1.58 (± 0.06) for naphthalene. As for the study of Nakayama et al.,⁶⁴ the compositional change and increase in O:C reflected an increase in the initial oxidant (OH) concentration. Kim et al.⁶⁰ also observed a decrease in m_r as O:C increased for SOA formed from photo-oxidation of limonene at low HC/NO_x ratios. For limonene SOA formed at high HC/NO_x ratios, the O:C ratio first decreased and then increased, though m_r increased continuously.

As seen in Figure 8, m_r values cannot be predicted by O:C ratios alone. Additional information on the chemical speciation of SOA derived from van Krevelen diagrams, f_{44} , f_{43} , and additional mass fragments and volatility measurements can provide further insight on the relationship between m_r and composition.

In the study of Kim et al.,⁶⁰ initial nucleation and growth begins with the most highly oxygenated (high O:C) and least volatile species, and these are later diluted in the particle phase by the continuing condensation of less oxygenated semivolatile species, accompanied by continuous increases in the refractive index, H:C, and f_{43} and rapid decrease in O:C and f_{44} . In some cases, late in the experiments, O:C trends upward again as additional oxidation processes overtake partitioning of semivolatile species, leading to an increase in the oxidation state of SOA.²⁰⁴ Thermodenuder measurements by Kim and Paulson⁶² also corroborate that the compounds that condense on the particle during the reaction and lead to particle growth have higher volatility than the SOA of the initial nucleation stage. An outcome of these studies is that Paulson and co-workers⁶⁰ differentiate between an early stage of growth and compositional changes due to condensational growth of more-volatile species, in which they observe higher m_r , and a later aging or oxidation stage (in which O:C increases), in which the condensing species become more oxidized and m_r either

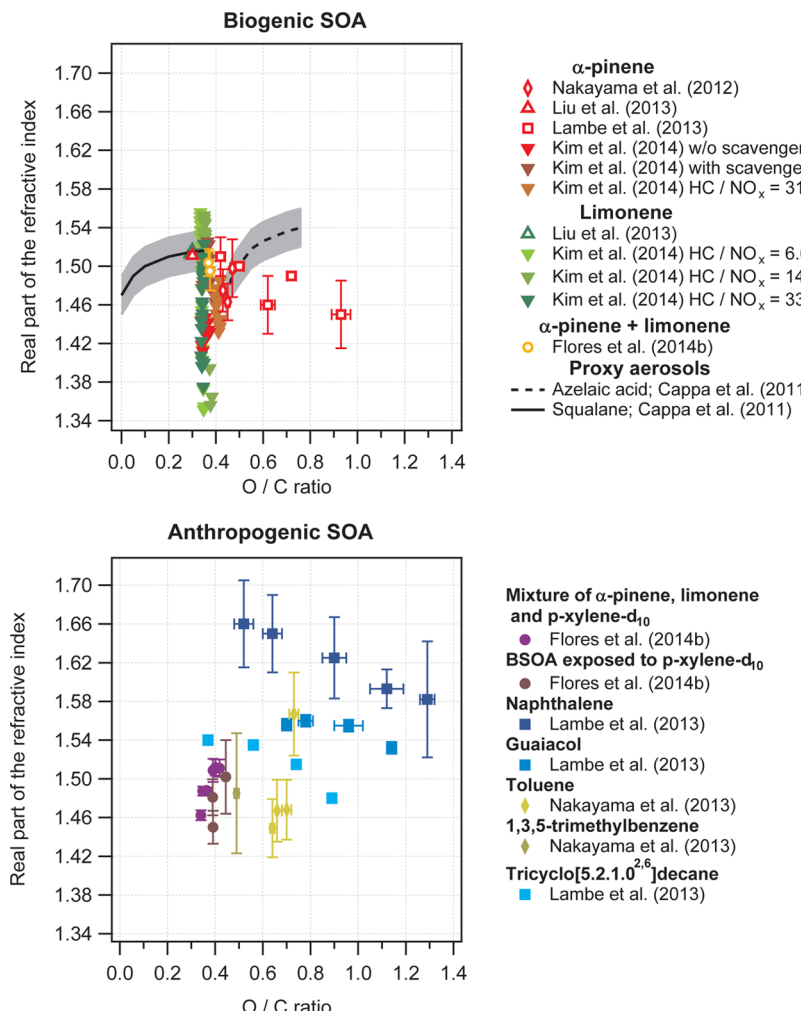


Figure 8. Real part of the refractive index at $\lambda = 405$ nm (data from Kim et al.⁶⁰ are at $\lambda = 532$ nm) plotted against measured O:C ratios for oxygenated organic aerosol from various studies. RI displays both positive and negative trends with increasing O:C ratios, depending on the study.

decreases slightly (i.e., for limonene photo-oxidation SOA) or may increase (i.e., for α -pinene ozonolysis SOA). It seems that the direction of change in the values of m_r as O:C increases with aging is closely linked to whether the SOA changing composition is dominated by condensational growth of semivolatile OOA or by oxidative aging of the particles. Even when the O:C ratio increases during the limonene reaction, H:C continues to increase, implying continued partitioning of semivolatile species but that either condensing species are more oxygenated or species already incorporated in the particles are becoming oxidized.⁶⁰ The H:C ratio and mass fragments of $m/z = 43$ and 55 ($C_2H_3O^+$, $C_4H_7^+$) correlated best with m_r for all aerosol types investigated.

In the study of Flores et al.,⁶¹ the aerosol becomes less volatile as the reaction progresses (increase in f_{44} and O:C and decrease in H:C and f_{43}). The study of Cappa et al.²³ focuses on oxidative aging rather than condensational growth. In both studies, oxidative aging leads to transformation of the SOA composition to higher density species that display an increase in m_r as oxidation progresses. In experiments with a mixture of α -pinene, limonene, and *p*-xylene- d_{10} , an initial increase in H:C ratio also indicates an early phase of vigorous chemistry and particle growth for which m_r also increases, similarly to its continued increase at the later photochemical aging stage, at which the chamber is depleted in semivolatiles and the VOC

and SOA were converted to higher oxidized generations by OH reactions.⁶¹ Time-resolved volatility measurements of ABSOA by Flores et al.⁶¹ confirm that as the ABSOA age and oxidation progressed (over a 30 h aging period), their volatility decreased and was inversely correlated to the increase in m_r .

In the study of Lambe et al.,⁶³ the composition of SOA formed in the potential aerosol mass (PAM) reactor at lower OH concentrations, with lower O:C ratios, higher (or near unchanged) H:C ratios, and higher f_{43} signal than at higher [OH] exposures, is indicative of a greater fraction of hydrocarbon-like semivolatile species. These have higher m_r values than the more highly oxidized SOA that prominently show an increase in the f_{44} signal. Although the different [OH] exposures in the PAM represent extended atmospheric aging of 2–14 days, the measured optical and chemical properties of the SOA do not monitor a progressive change in time. This may imply a different chemistry between the progressively aged SOA^{23,61} and highly oxidized precursor VOC that condense directly from low-volatility species and may involve different second- and third-generation products.

It is possible that the highly oxidized SOA are perhaps in a third, other regime (following condensational growth and functionalization due to aging) with competing effects of fragmentation versus functionalization that may lead to different trends in m_r . Fragmentation (C–C cleavage) increases

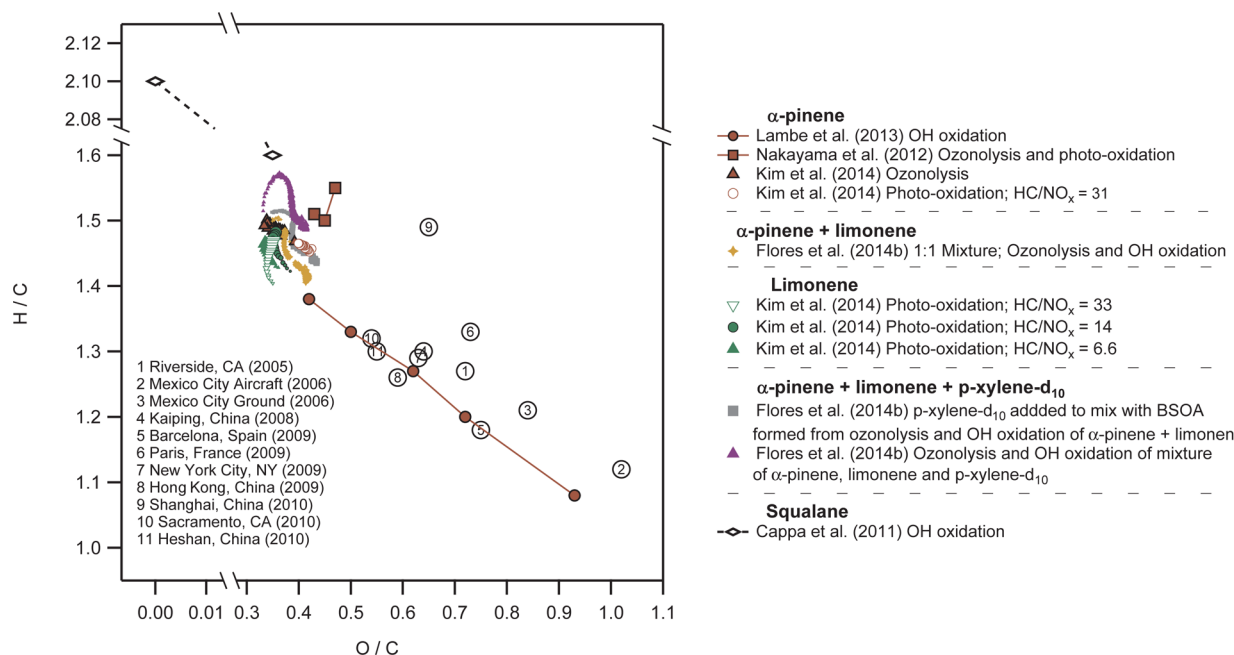


Figure 9. Van Krevelen diagram showing the ratio of H:C to O:C measured from various studies. The change in marker size depicts time; smaller markers refer to the beginning of the experiment and larger markers to the end. Results are compared to low-volatility oxygenated organic aerosol factors from HR-AMS field campaigns (numbered circles, adopted from Daumit et al.²⁹³). Adapted with permission from ref 61. Copyright 2014 Copernicus Publications.

dramatically as O:C rises¹⁹⁵ and generates products over a wide volatility range. Some products are radicals that immediately functionalize to form more oxygenated, stable products and can be less volatile than the precursor. In addition, fragments can also functionalize in a subsequent oxidation step.²¹⁰ Organic fragmentation products can therefore have a low carbon number (with high O:C and H:C values) while remaining in the condensed phase.²¹¹ Tkacik et al.²¹² attributed the decrease in SOA yields at high OH exposures in the PAM to fragmentation-dominated mechanisms rather than functionalization. The PAM-produced SOA might represent a mixture of highly oxidized species from gas-phase reactions and condensation and of heterogeneous oxidation (i.e., “aging”) and it may be that lower molecular weight fragments may account for the lower m_r values. The connection between PAM and real atmospheric oxidation processes remains to be studied.

Significant uncertainties still remain as to the interplay between fragmentation, oligomerization, and heterogeneous OH aging to enable a complete description of SOA aging mechanisms.²¹⁰ As these uncertainties are addressed, it will also allow for a greater understanding of the connection between SOA composition and aerosol optical properties. We conclude that in order to make the link between measured m_r values and SOA from different precursors and formation pathways, it is necessary to conduct comprehensive chemical analysis simultaneously, as is possible with AMS, together with simultaneous volatility measurements. This will enable an understanding of the chemical processes and aerosol chemical state that correspond to the derived m_r values and will allow comparisons between different measurements that may represent highly differing chemical states. Currently, the paucity of combined comprehensive chemical and optical measurements precludes clear conclusions as to the link between the real part of the refractive index and the chemical evolution of SOA.

3.5. Similarities between Ambient and Smog Chamber Secondary Organic Aerosol Composition

Extensive chemical analysis has been used to compare the molecular composition of smog chamber SOA and ambient SOA. Nanoelectrospray ultra-high-resolution mass spectrometry (ESI-UHR-MS),⁴⁴ scanning transmission X-ray microscopy (STXM) with near-edge X-ray absorption fine structure (NEXAFS) spectroscopy,⁴⁹ and Fourier transform infrared spectroscopy (FTIR)²¹³ have provided spectroscopic evidence of similarity between the molecular composition and functionality of SOA products from anthropogenic and biogenic VOC precursors and those of ambient particles, supporting the choice of precursors used in chamber experiments.

AMS analysis, already widely used in aerosol studies to provide bulk chemical characterization in real time, can, by use of f_{44} versus f_{43} and van Krevelen diagrams, help assess how close the laboratory-generated SOA used in the optical studies are to ambient samples. The van Krevelen diagram in Figure 9 compares H:C to O:C ratios measured for laboratory-generated SOA and ratios derived for aerosol sampled in field campaigns. We note that most SOA from the laboratory measurements are not oxidized enough compared to the atmosphere and have lower O:C and higher H:C ratios. The aged aerosol composition of BVOC and mixed ABVOC SOAs in the study of Flores et al.⁶¹ lie within the triangular space representative of ambient samples (see Figure 7), albeit showing them to be not very aged.

Continued efforts to relate laboratory optical measurements to elemental composition and molecular fragments of the SOA will enable comparison of optical measurement results between different aerosol formation and reaction systems and also evaluation of laboratory results to particular stages in the life cycle of ambient SOA. The aspiration is that the additional chemical information will aid in prediction of SOA RI values for

specific conditions, beyond the broad m_r range ($m_r = 1.45 \pm 0.1$) currently presented in Figure 6.

3.6. Predictive Tools for Refractive Index of Secondary Organic Aerosol

The Lorentz–Lorenz relationship relates the refractive index of a substance to the mean polarizability (α) and molecular volume [or equivalently, density (ρ) divided by molecular weight (MW) of the compound]:

$$\frac{(n^2 - 1)}{(n^2 + 2)} = \frac{\alpha\rho}{3\text{MW}} \quad (10)$$

Cappa et al.²³ formulated a model to calculate m_r from the Lorentz–Lorenz relationship in which mean polarizabilities for organic aerosol are calculated from a weighted linear combination of absolute C, O, and H elemental abundances, and atom-specific molecular volume is a component of the weighting procedure. This formulation does not account for differences that may result from atoms existing in different local environments (e.g., bonding configurations or functional groups). For SOA formed from α -pinene ozonolysis, they calculated the real part of RI at $\lambda = 532$ nm to be $m_r = 1.543$ for O:C = 0.3 and H:C = 1.51 and $m_r = 1.556$ for O:C = 0.45 and H:C = 1.38. These values are larger than the m_r at $\lambda = 532$ nm for this reaction measured in previous studies, which are in the range 1.41–1.53, as shown in Table 2 and Figure 4. They attribute the difference to higher mass loadings in the experiments that lead to higher H:C and lower O:C ratios than those used as input into the calculations, and consequently, a lower m_r than the calculated value.

A different approach using a quantitative structure–property relationship (QSPR) approach was developed by Redmond and Thompson¹⁸⁷ to calculate the mid-visible ($\lambda = 589$ nm) RI of nonabsorbing organic aerosol particles based on three parameters in the Lorentz–Lorenz equation linked to the refractive index: molecular polarizability, ratio of density to molecular weight, and degree of unsaturation. A set of over 100 organic compounds known to be present in SOA from chamber experiments was used to establish a quantitative relationship between these calculated parameters and the accepted values of refractive index for these compounds. Predicted refractive indices of SOA formed following toluene photo-oxidation and α -pinene ozonolysis were within the range of measurements. For α -pinene SOA, $\text{RI}_{\text{QSPR}} = 1.476$, within the measured range of 1.41–1.51, and for toluene SOA, $\text{RI}_{\text{QSPR}} = 1.493$, close to the $\text{RI} = 1.483$ measured by Nakayama et al.⁹⁹ Some RI values for the same SOA are slightly higher than the predicted QSPR values (see Table 2). Redmond and Thompson¹⁸⁷ suggest that higher molecular weight products that form during α -pinene ozonolysis, which are not accounted for in theoretical calculations, could increase the refractive index of the product aerosol relative to RI_{QSPR} due to higher projected polarizability of the oligomeric components.¹⁸⁷ In general, when it is averaged across classes of compounds, the QSPR predictive refractive index model based on molecular formula predicts RI that agree well with known RI values. The QSPR model consistently underestimates the RI for SOA containing alcohol groups.

4. OPTICAL ABSORPTION BY SECONDARY ORGANIC AEROSOL

As noted in the Introduction, both primary organic particulate emissions and SOA contribute to brown carbon (BrC).

Secondary brown carbon may be high molecular weight and multifunctional species, such as humic-like substances,⁷⁶ organonitrates,^{15,55,214} and nitrogen- and sulfate-containing organic material^{24,105,215} and can be formed from multiple precursors and a variety of reaction pathways. Some of the reaction pathways proposed for secondary brown carbon formation are described in brief in section 4.1, and we then continue to present results from recent studies that focus on a number of these pathways.

4.1. Reaction Pathways for Formation of Secondary Brown Carbon

Some of the reaction pathways proposed for secondary brown carbon formation are as follows.

(1) Nitration of aromatic compounds (oxidation via NO_2 , NO_3 , N_2O_5): Early theoretical studies and later experimental validation show that nitration of polycyclic aromatic hydrocarbons (PAH) leads to light-absorbing nitro-PAH and their derivatives such as nitrophenols.^{15,67,216} The nitro substituent on the aromatic ring in compounds such as phenols both enhances and shifts the absorption to longer wavelengths (>350 nm). Field studies report that nitrogen-containing mono- and polyaromatic SOA constituents absorb light at short (near-UV and visible) wavelengths.^{15,21,123}

(2) Reaction of ammonia (NH_3) or amino acids with SOA that contain carbonyl products: (a) Optical absorption studies have been conducted following the reduction reactions of NH_4^+ , NH_3 , and amino acids with terpene SOA.^{22,24,25,105,217} These reactions yield light-absorbing/colored products only in the aqueous phase or if water-facilitated.²² (b) Optical absorption studies have been conducted for aqueous-phase reactions and gas-to-particle uptake of the α -dicarbonyls glyoxal and methylglyoxal with ammonium sulfate and amino acids.^{65,95,218–220}

(3) Bond-forming reactions between SOA constituents generating dimers and larger oligomers: for example, the common oligomerization process of acid-catalyzed aldol condensation of volatile aldehydes.^{20,22,221,222}

(4) Reactions of biomass burning products, mostly lignin pyrolysis products: Upon combustion, lignin (primarily *p*-coumaryl, coniferyl, and sinapyl alcohols) degrades to yield phenols, aldehydes, acids, ketones, or alcohols, often retaining the original substituents on the aromatic ring.^{43,223} Aqueous photo-oxidation of aromatic hydroxy acids, phenols, catechols, guaiacols, and syringols^{223–225} and aqueous photonitration of guaiacol⁴³ result in light-absorbing products in the UV and short-visible light range (wavelengths up to 500 nm).

(5) Other proposed mechanisms: heterogeneous reactions of gas-phase isoprene on acidic aerosol particles²²⁶ and aqueous photochemistry of pyruvic acid in the presence of common atmospheric electrolytes (e.g., SO_4^{2-} , NH_4^+).^{227,228}

Except for pathway 1, the pathways listed proceed when water is present either as solvent or in humidified air, and the majority of the reactions were studied in bulk-phase reactions to simulate aerosol aging mechanisms. Optical absorption measurements are commonly conducted with UV–vis spectrometry and characterized by the compounds' mass absorption cross section (MAC). SOA formation and aging reactions occur either in bulk solution^{219,229} or as aerosol in flow reactors and smog chambers, which are then collected onto filters and directly analyzed²¹⁷ or extracted into a solvent and analyzed in bulk²⁵ or collected via a particle-into-liquid sampler (PILS).²³⁰ Recently, CRD and BBCES measurements have been

Table 3. Comparison of Absorbance Parameters for Fresh and Aged Organic Particles in Laboratory Studies and Field Measurements of Ambient Particles^a

Reaction	References	$\lambda(\text{nm})$	m_r	k	MAC ($\text{m}^2 \text{ g}^{-1}$)	SSA _(λ)
Laboratory Reacted Organic Compounds						
Biogenic SOA						
α -pinene/ Limonene ozonolysis	Liu et al. ⁵⁹	220		0.0088/ 0.005		
α -pinene OH oxidation	Lambe et al. ⁶³	405	1.51(± 0.02)-1.45(± 0.04)	~ 0.0002 -0.001	0.001-0.025	
α -pinene/ Limonene (UV/NO _x)	Zhong and Jang ¹¹⁶	350		0.0009/0.0014 ^a	0.029 / 0.038	
Limonene ozonolysis	Zhong and Jang ¹¹⁶	350		0.0009	0.025	
α -pinene/ Limonene (UV/NO _x +NH ₄ ⁺ seed)	Zhong and Jang ¹¹⁶	350		0.0015/0.0037 ^a	0.05/0.11	
Anthropogenic SOA						
Toluene (UV/NO _x)	Zhong and Jang ¹¹⁶	350		0.0214 ^a	0.57	
Naphthalene	Lambe et al. ⁶³ Updyke et al. ²⁵	405	1.66(± 0.04)-1.58(± 0.06)	0.0008-0.0037	0.02-0.08 0.10	0.96
Toluene 109 \rightarrow 571 ppbv NO _x	Nakayama et al. ⁶⁴	405 532	1.449(± 0.030)- 1.567(± 0.042) 1.431(± 0.025)-1.498(± 0.024)	0.0018(± 0.013)-(0.0072 (± 0.001)) (0.001 ± 0.001)	0.08-0.52 ^b	
Toluene 500 ppbv NO _x	Nakayama et al. ⁹⁹	355 532	1.632(± 0.038) 1.483(± 0.032)	(0.047 ± 0.041) (0.007 ± 0.039)		~ 0.83
Toluene 0 \rightarrow 10 ppm NO _x ; HC/NO _x = 2	Liu et al. ⁵⁵	320 405	1.567(± 0.008)- 1.591(± 0.009) 1.546(± 0.004)-1.571(± 0.005)	0.011(± 0.004)- 0.033(± 0.001) 0.0017(± 0.0002)- 0.015(± 0.002)	0.32-0.97 ^c 0.04-0.35 ^c	0.941-0.853 0.990-0.924
<i>m</i> -Xylene 0 \rightarrow 10 ppm NO _x ; HC/NO _x = 2	Liu et al. ⁵⁵	320 405	1.554(± 0.011)- 1.589(± 0.008) 1.531(± 0.006)- 1.565(± 0.007)	0.007(± 0.001)- 0.015(± 0.001) 0.0008(± 0.0001)- 0.003(± 0.0003)		0.062-0.926 0.995-0.984
HULIS Proxies						
Humic and fulvic acid standards	Lambe et al. ⁶³	405		-	0.18 to 1.5	
Suwannee River Fulvic Acid (SRFA) 1R101F IHSS	Dinar et al. ⁷⁶	390 532	1.602 (± 0.005) 1.634(± 0.004)	0.098(± 0.005) 0.021(± 0.005)	2.15 ⁱ 0.34 ⁱ	
Suwannee River Fulvic Acid (SRFA) 1S101F IHSS	Flores et al. ¹⁰⁵	360-420 405, 500	- -	0.046 (± 0.010)	-	0.5, 0.25
Biomass Combustion						
Wood combustion (low temperature)	Chen and Bond ²³¹	500	-	-	0.1-0.5 ^d	
Smoldering biomass combustion (low temperature)	Chakrabarty et al. ¹⁷	532	1.72-1.87	0.0006-0.003	0.01-0.07 ^e	
Guaiacol (surrogate for BB)	Lambe et al. ⁶³	405	1.55(± 0.01)- 1.53(± 0.01)	0.0005-0.001	0.02	
Biomass combustion (spruce, ponderosa pine, rice straw; organic hay, saw grass; wire grass)	Saleh et al. ²³²	550		0.013 (BC:OA of 0.011) ^f 0.21 (BC:OA of 0.037)		
BB (Pear tree leaves, Afghanistan pine needles)	Ma and Thompson ⁸³	355				0.84 \pm 0.01
NH₄⁺/NH₃ mediated aging of SOA						
glyoxal-glycine	Zarzana et al. ⁶⁵	532	1.64 \pm 0.02	0.044 \pm 0.017		0.85
glyoxal-methylamine			1.65 \pm 0.02	0.035 \pm 0.017		0.85
methylglyoxal- glycine			1.64 \pm 0.01	0.037 \pm 0.007		0.85
methylglyoxal-methylamine			1.55 \pm 0.04	0.114 \pm 0.037		0.65
Glyoxal uptake on AS core	Trainic et al. ²²⁰	355	1.68 \pm 0.010 ^g	0.01 \pm 0.02		
NH ₃ -aged (~1 ppm) Limonene + O ₃ SOA	Flores et al. ¹⁰⁵	360-420		0.007(± 0.007) ^h	< 0.2	
NH ₃ -aged (~1 .9 ppm) α -humulene + O ₃ SOA		360-420		0.029 (± 0.021) ^h		
NH ₃ -aged (~1 .9 ppm) Limonene + O ₃ SOA		360-420		0.031(± 0.019) ^h		
Limonene + O ₃ + SOA + NH ₄ ⁺	Bones et al. ²²	500	-		0.07	
Limonene + O ₃ SOA + NH ₄ ⁺	Updyke et al. ²⁵	500	-	-	0.12	
KLA/NH ₄ ⁺ + and KLA/GLY	Nguyen et al. ²⁴	500	-	-	0.2-0.5	
Ambient Aerosol						
Pollution HULIS		532 390	1.595 \pm 0.004 1.638 \pm 0.006	0.049 \pm 0.006 0.098 \pm 0.006	1 ⁱ	
Smoke HULIS (Middle East)	Dinar et al. ⁷⁶	532 390	1.622 \pm 0.003 1.640 \pm 0.003	0.048 \pm 0.009 0.116 \pm 0.005		
Rural HULIS (mixed forest, Hungary)		532 390	1.561 \pm 0.002 1.616 \pm 0.002	0.003 \pm 0.004 0.023 \pm 0.002		

Table 3. continued

Reaction	References	λ (nm)	m_r	k	MAC ($m^2 \cdot g^{-1}$)	SSA(λ)
Biomass Burning HULIS (Amazonia) daytime	Hoffer et al. ²³³	532 300	1.653	0.0019	0.031 2 - 3	
Mixed forest HULIS (PM<1) (Central Europe)	Utry et al. ¹⁹	532 355 266	-	-	0.030 0.319 4.925	
Biomass burning (Colorado)	Lack et al. ⁶⁹	404	-	0.007 ± 0.005	0.82 ± 0.43	0.85
Dry biomass burning, 3 biomes, fresh and aged (savannah, tropical, boreal)	Reid et al. ²³⁴	550	-	-	-	0.84 to 0.93
Biomass burning, SAFARI-2000	Kirchstetter et al. ⁸ Magi et al. ²³⁵	400 450 550	-	0.112 0.063 0.03	0.7±0.2	0.85±0.05
Amorphous carbon spheres (ACE Asia)	Alexander et al. ¹⁶	550	-	0.27	3.6 to 4.1	
Urban WSOC dominated by anthropogenic SOA, CalNex	Zhang et al. ²¹ Zhang et al. ²³⁶	365	-	-	0.77 0.71	
Urban primary BrC dominated by vehicular emissions, CalNex	Zhang et al. ²¹	365	-	-	2.45	
Urban insoluble OC, primary BrC, dominated by incomplete combustion, CalNex	Zhang et al. ²³⁶	365	-	-	2.45	
CalNex	Thompson et al. ⁸⁹	532	-	-	-	0.92 ± 0.08
California, urban (CalNex, CARES)	Cappa et al. ¹¹⁸	405	-	0.004	0.12; 0.14	
WSOC – Sth.East. USA, Urban Winter (BB dominance) Summer (SOA dominance)	Hecobian et al. ¹⁴	365	-	-	0.70±0.07 0.31±0.07	
WSOC – Beijing, China Winter (higher BB fraction of OC) Summer	Cheng et al. ²³⁷	365	-	-	1.79±0.24 0.71±0.20	
Aged pollution plume (BrC attributed to mixture of absorbing OC and nitrated-OC)	Flowers et al. ¹²³	405 532 781	1.590±0.01 1.547±0.01 1.668±0.01	0.017±0.001 0.013±0.001 0.011±0.001	2.1±0.1 – 2.6±0.1 0.0±0.1 – 0.8±0.1	
High OC/SO ₄ ²⁻ , forest fire contribution		405 532 781	1.492±0.01 1.426±0.01 1.524±0.02	0.029±0.001 0.017±0.001 0.015±0.001	3.4±1 0.0±0.2	

^a k was calculated in Zhong and Jang¹¹⁶ from the measured MAC. ^bMAC was evaluated for ambient toluene SOA for typical urban $[NO_2]/[O_3]$ range and particle sizes of 200–600 nm, by use of the laboratory-measured dependence of k on the $[NO_2]_{\text{eff}}/[O_3]_{\text{eff}}$ ratio. ^cMAC was calculated from values of k with the assumption $\rho = 1.34 \text{ g} \cdot \text{cm}^{-3}$ (density for toluene SOA taken from Zhong and Jang¹¹⁶). ^dEstimated from graphs in paper (quoted from Updyke et al.²⁵). ^eCalculated from k . ^fExamples of increasing k_{OA} values as the BC:OA ratio increases. ^gRetrieved for outer layer of particle with the assumption of a core–shell model. ^hAverage k values for measured range. ⁱMAC was calculated from values of k , with $\rho = 1.47 \text{ g} \cdot \text{cm}^{-3}$ taken from Dinar et al.²³⁸ Note that size-dependent SSA is for the particle size distribution stated in the referenced study.

conducted on NH₄⁺-mediated SOA samples in situ and the refractive index has been derived.^{61,65,105,220}

4.2. Optical Absorption of Secondary Organic Aerosol Formed via In Situ Oxidation Studies

Nitration of aromatic compounds following photo-oxidation of VOC in the presence of NO_x has been shown already in early studies to form light-absorbing chromophores in the UV wavelengths.¹⁵ Optical measurements of SOA formed by homogeneous nucleation and condensation following additional oxidation pathways (OH oxidation and ozonolysis) of biogenic and nonaromatic anthropogenic compounds for the most part display no absorption, as detailed earlier in section 3. The few measurements of biogenic SOA that display a non-negligible but still small absorption component are listed at the head of Table 3. Ellipsometry measurements of thin films of SOA formed from α -pinene and limonene ozonolysis yield values of the imaginary part of RI (k) of 0.0088 and 0.005, respectively, at the short wavelength of 220 nm.⁵⁹ However, for the atmospherically relevant wavelength region ($\lambda > 300 \text{ nm}$), the absorption is insignificant. Lambe et al.⁶³ used CRD-PAS to measure the complex refractive index and MAC at $\lambda = 405$ and 532 nm of α -pinene SOA formed from OH oxidation with no

NO_x. For increasing [OH] exposures that yield O:C ratios ranging from 0.42 to 0.93, k has values between ~0.0002 and 0.001. The absorption is very weak but corroborated also by analysis of SOA filter extracts analyzed by UV-vis spectrometry between 300 and 600 nm. The MAC_{extracts} and MAC_{PAS} are within 25% of each other. The MAC_{extracts} at $\lambda = 405 \text{ nm}$ range between 0.001 and 0.025 $\text{m}^2 \cdot \text{g}^{-1}$ for O:C ratios ranging from 0.42 to 0.68.⁶³

Zhong and Jang¹¹⁶ measured the MAC of SOA filter samples for SOA formed from photo-oxidation of α -pinene, limonene, and toluene in the presence of NO_x (with [NO_x] between 62 and 72 ppb and HC/NO_x = 2.1), using a UV-vis spectrometer with an integrating sphere. With densities (ρ) of 1.27, 1.07, and 1.34 $\text{g} \cdot \text{cm}^{-3}$ assumed for limonene, α -pinene, and toluene SOA, respectively, they obtained MAC values (corrected for multiple scattering within filter fibers) of 0.038, 0.029, and 0.574 $\text{m}^2 \cdot \text{g}^{-1}$ at $\lambda = 350 \text{ nm}$, corresponding to values for k of 0.0014, 0.0009, and 0.0214, respectively. Absorption at $\lambda = 450 \text{ nm}$ is around an order of magnitude lower for the three SOA types. No absorption is observed above 580 nm.

It is noted that absorption measurements in other studies of biogenic terpene SOA have not observed any detectable

absorption also at lower wavelengths. These include α -pinene SOA from photo-oxidation at $\lambda = 405$ nm and $\lambda = 355$ nm^{99,121} and from ozonolysis at $\lambda = 405$ nm,¹²¹ mixtures of α -pinene + limonene SOA from ozonolysis and OH oxidation at $\lambda = 360$ –420 nm,⁶¹ and α -pinene, limonene, and α -humulene SOA from ozonolysis at $\lambda = 360$ –420 nm.¹⁰⁵

In Table 3 we list the absorption measured also in studies of anthropogenic SOA surrogates. Measurable absorption for aromatic and phenolic SOA have been reported by Nakayama et al.,⁹⁹ Lambe et al.,⁶³ and Liu et al.⁵⁵ Nakayama et al.,⁹⁹ using both CRD and a three-wavelength nephelometer, observe absorption for toluene SOA at $\lambda = 355$ nm, retrieving an RI_{355} of $1.632^{(+0.038)}_{(-0.035)} + i0.047^{(+0.041)}_{(-0.036)}$. At 532 nm, there is no evidence of light absorption by toluene SOA and the derived $\text{RI}_{532} = 1.483^{(+0.032)}_{(-0.036)} + i0.007^{(+0.030)}_{(-0.007)}$. A different study of SOA produced from ozonolysis of toluene in the presence of NO_2 and water vapor shows little absorption at $\lambda = 355$ nm and yields a SSA of 0.95 ± 0.03 ,⁸³ in contrast to a SSA of ~ 0.83 that is derived from the RI data at $\lambda = 355$ nm in the study of Nakayama et al.⁹⁹ It was suggested that the difference arose from different NO_2 concentrations in the two studies (<150 ppbv in the former vs 500 ppbv in the latter). A later study by Nakayama et al.⁶⁴ looked at the same reaction but measured the absorption directly, on a three-wavelength PASS (rather than via extinction minus scattering) which is preferable for accurate determination of small values of k . In this study, the dependence of absorbance on NO_x concentration was substantiated, and at $\lambda = 405$ nm, k increased from $0.0018^{(+0.0013)}_{(-0.0014)}$ to $0.0072^{(\pm 0.01)}$ as NO_x increased from 109 to 571 ppbv. Nakayama et al.⁶⁴ evaluated MAC values for ambient toluene SOA by extrapolating the laboratory-measured dependence of k on $[\text{NO}_2]/[\text{O}_3]$ ratio to typical daytime urban conditions, in which $[\text{NO}_2]/[\text{O}_3]$ ranges between 0.1 and 10. The calculated MAC for ambient particles in the size range 200–600 nm ranged from 0.08 to $0.52 \text{ m}^2\cdot\text{g}^{-1}$ at $\lambda = 405$ nm. Comparable values for k of toluene SOA, ranging from 0.0018 to 0.015, for increasing initial NO concentrations ($[\text{NO}] = 0$ –10 ppm) also at $\lambda = 405$ nm were measured by Liu et al.⁵⁵ The *m*-xylene SOA displayed lower absorption, with values for k at $\lambda = 405$ nm ranging from 0.0008 to 0.003.⁵⁵

Lambe et al.⁶³ showed that anthropogenic aliphatic compounds such as tricyclo[5.2.1.0^{2,6}]decane also display very weak absorption following OH oxidation. At shorter wavelengths, 300–400 nm, its absorption is similar to that of α -pinene, whereas at wavelengths >400 nm, the anthropogenic aliphatic SOA has slightly higher absorbance than α -pinene SOA. In that same study,⁶³ the anthropogenic naphthalene, also aromatic, displays the highest absorption among the SOA that were studied (tricyclo[5.2.1.0^{2,6}]decane, α -pinene, guaiacol, and naphthalene). The wavelength dependence observed via UV-vis spectrometry shows that the MAC monotonically decreases with increasing wavelength, with maximal absorption at wavelengths <300 nm. The three studied SOAs have increasing absorption at higher O:C ratios. The SSA measured by CRD-PAS at $\lambda = 405$ nm ranged from 0.98 to 1.0 for toluene and tricyclo[5.2.1.0^{2,6}]decane SOA and was 0.96 for the highly oxidized naphthalene (O:C = 1.29). These SSA values for the three types of SOA reflect the very small k values (~0.001 up to 0.004) measured at $\lambda = 405$ nm. The maximal MAC at the same wavelength (for the respective highest O:C) ranges from 0.02 to $0.08 \text{ m}^2\cdot\text{g}^{-1}$. Updyke et al.²⁵ also show that naphthalene SOA (OH-initiated) had significant MAC at visible wavelengths, $0.1 \text{ m}^2\cdot\text{g}^{-1}$ at $\lambda = 405$ nm. Toluene SOA from

photooxidation in the presence of high NO_x concentrations displays the highest k values among anthropogenic aromatic precursors.^{55,64} The k values for toluene from photo-oxidation in the absence of NO_x (<70 ppt) are in the same range as those of naphthalene following OH oxidation.^{55,63}

We see that although photooxidation of biogenic SOA precursors can lead to optical absorption, the absorbance is much lower than for aromatic SOA precursors derived from photooxidation in the presence of NO_x . Comparisons of MAC and k values show that these are 10–20 times greater for toluene SOA than for limonene and α -pinene SOA^{55,116} (see also Figure 4 in Liu et al.⁵⁵). The MAC values for OH-oxidized α -pinene SOA at $\lambda = 405$ nm in the study of Lambe et al.⁶³ study (MAC = 0.001 – $0.025 \text{ m}^2\cdot\text{g}^{-1}$ for increasing OH exposures) are in the same range as those measured by Zhong and Jang¹¹⁶ for α -pinene SOA formed by photo-oxidation in the presence of NO_x (MAC = $0.029 \text{ m}^2\cdot\text{g}^{-1}$ at $\lambda = 350$ nm and $0.006 \text{ m}^2\cdot\text{g}^{-1}$ at $\lambda = 450$ nm) and for limonene SOA formed by ozonolysis (MAC = $0.025 \text{ m}^2\cdot\text{g}^{-1}$ at $\lambda = 350$ nm).¹¹⁶ Limonene SOA from photo-oxidation yielded slightly higher MAC (MAC at $\lambda = 350$ nm is $0.038 \text{ m}^2\cdot\text{g}^{-1}$).¹¹⁶

Anthropogenic aromatic SOAs, naphthalene formed via OH oxidation and toluene and *m*-xylene formed via photo-oxidation, display MAC and k values in the same range. MAC at $\lambda = 405$ nm for naphthalene was $\sim 0.1 \text{ m}^2\cdot\text{g}^{-1}$ ^{125,63} and the values of k for high- NO_x toluene SOA were 0.007 and 0.015 at $\lambda = 405$ nm in the studies of Nakayama et al.⁶⁴ and Liu et al.,⁵⁵ respectively, and for *m*-xylene SOA, a k value of 0.003 at $\lambda = 405$ nm was obtained. The k values for toluene, calculated from measured MAC in the study of Zhong et al.,¹¹⁶ were $k = 0.0214$ at $\lambda = 350$ nm and $k \approx 0.004$ at $\lambda = 450$ nm (MAC = 0.57 and $\sim 0.083 \text{ m}^2\cdot\text{g}^{-1}$ at $\lambda = 350$ and 450 nm, respectively) when a density of $1.34 \text{ g}\cdot\text{cm}^{-3}$ was assumed. They can be compared to values of k of 0.0263 and ~ 0.0098 at $\lambda = 350$ and 450 nm, respectively, measured by Liu et al.⁵⁵ for the same high- NO_x SOA. In contrast, the aliphatic anthropogenic precursor SOA, tricyclo[5.2.1.0^{2,6}]decane, is only weakly absorbing, with absorbance values similar to those measured for α -pinene SOA, with both SOA being formed via OH oxidation.⁶³

4.2.1. Influence of Chemical Structure. Molecules that absorb in the UVA/visible range may either have a few fused aromatic rings (PAHs) or have additional heteroatoms, O or N, attached to a single aromatic ring such as a carbonyl or nitro group. Heteroatoms allow for an $n-\pi^*$ transition, which reduces the electronic transition energy to a range corresponding to the energy of photons in the shorter visible wavelength range.²³⁹ The broad absorption spectra observed in the spectrally resolved measurements, in which individual electronic transitions are not distinguished, indicate that numerous types of conjugated bonds exist in these SOA and that SOA exist as complex mixtures of organic compounds as observed in many studies.^{240,241}

The increase of k for high NO_x can in part be explained by the production of light-absorbing nitrogen-containing organic compounds, mostly nitroaromatic compounds such as nitrophenols, nitrocatechols, and dinitrophenols.⁵⁵ An increase in both - NO_2 and - ONO_2 functionalities⁵⁵ and the nitrate to organic ratio⁶⁴ were observed for increasing NO_x concentrations during toluene SOA formation. The - NO_2 group is generated from reactions of the intermediate methyl phenoxy radical products with NO_2 ⁶⁴ as shown in Scheme 1a. 4-Nitro-*o*-cresol, identified as a major SOA component following toluene

Scheme 1. (a) Reaction Scheme of Nitrophenol Formation from Photo-oxidation of Toluene [reprinted with permission from ref 64, copyright 2013 Copernicus Publications]. (b) Corresponding Routes from Photo-oxidation of 1,3,5-Trimethylbenzene [reprinted with permission from ref 242, copyright 2012 Copernicus Publications].

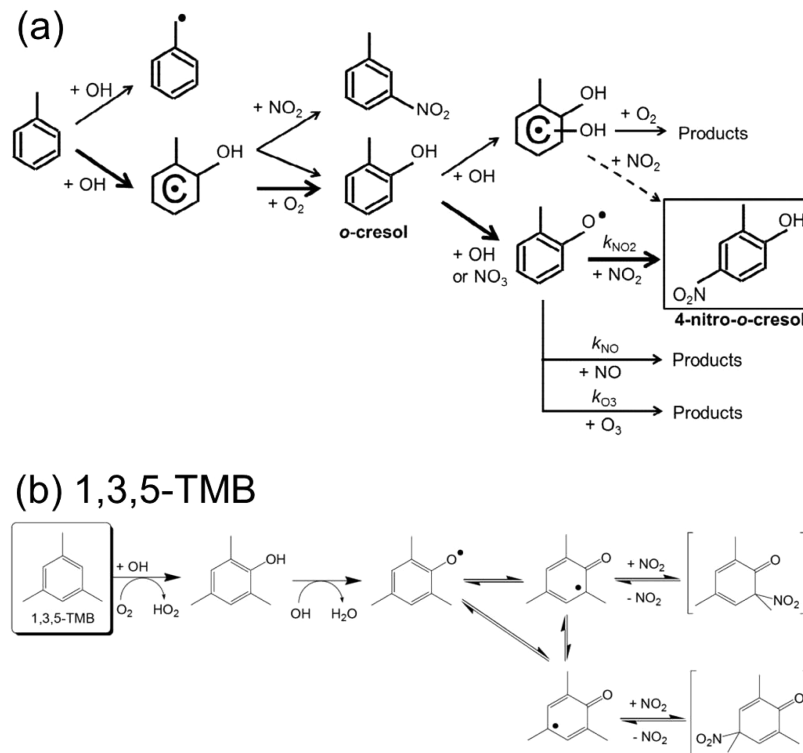


photo-oxidation,⁴⁸ has a strong absorption with a maximum k value of 0.54 at $\lambda = 319$ nm, while *o*-cresol (2-methylphenol) has a weak absorption with a maximum absorption k value of 0.096 at $\lambda = 273$ nm.¹⁵ SOA from methylbenzene rings such as 1,3,5-trimethylbenzene do not form stable NO_2 adducts (see Scheme 1b), and the lack of nitrocresol is the reason for the negligible absorbance of these SOA as compared to toluene.⁶⁴ Similarly, the methyl group at the meta site of *m*-xylene likely inhibits the production of stable -NO_2 adducts of phenoxy radicals, which is manifested in the smaller fraction (35–50% lower) of -NO_2 groups in the *m*-xylene-derived SOA as compared to the toluene-derived SOA for a fixed initial NO_x concentration, and hence the lower k values. Similarly, absorbance by benzo[*a*]pyrene (BaP) following nitration with NO_2 and NO_3 stems from the main reaction product identified, nitro-BaP, following addition of NO_3 to the aromatic ring.⁶⁷

Aromatic SOA absorb also in the absence of NO_x . Oxygenated functional groups identified by FTIR are alcoholic hydroxyls (O—H), carboxylic hydroxyls (O—H), carboxylic carbonyls (C=O), mixed ketones/aldehydes (C=O), and a feature proposed as an ether group (C—O—C) of acetals and hemiacetals produced via particle-phase reactions.⁵⁵ The hemiacetal/acetal production reactions can produce oligomers having conjugated structures that contribute to the light absorption even in the absence of nitrogen moieties.²⁴³ The absorbance of toluene and *m*-xylene at high- NO_x SOA were similar after normalization to the baseline absorbance ($\text{NO}_x = 0$) of each and accounting for the different -NO_2 mass fractions (see Figure 3 in Liu et al.⁵⁵), indicating that the difference stems from the extent of conjugation of the oxygenated products.

Both α -pinene and D-limonene SOA contain nonconjugated oxygenated compounds. α -pinene includes pinonaldehyde, norpinonic acid, hydroxyl pinonaldehydes, pinonic acid, and pinic acid, and D-limonene include keto-limononaldehyde, keto-limononic acid, and keto-limonalic acid. The $n \rightarrow \pi^*$ transitions absorption of such nonconjugated carbonyl and carboxylic acid products typically appear between 280 and 300 nm,¹¹⁶ shorter wavelengths than those at which absorption was observed in the studies of Lambe et al.⁶³ and Zhong and Jang.¹¹⁶ The UV-vis absorption spectra of some carboxylic acids (citric acid, 1,3,5-cyclohexanetricarboxylic acid, *cis*-pinonic acid, 4-oxohexanoic acid, 2-oxopentanedioic acid, and pyruvic acid) measured by Lambe et al.⁶³ do not exhibit any significant absorption above 400 nm, in contrast to all the SOA in that study at higher O:C ratios, for which absorption was measured up to 600 nm. As absorption shifts to longer wavelengths when the amount of delocalization in the molecule increases, the observed absorption up to 600 nm may suggest either more extensive conjugation in SOA relative to these individual compounds or the formation of additional chromophores that are not identified by the mass spectra.⁶³

Extensive conjugation could result from increased functionalization that increases as second-generation oxidation compounds form, such as the tricarboxylic acid (3-methyl-1,2,3-butanetricarboxylic acid) following pinonic acid oxidation^{210,244} and peroxy acids following pinonaldehyde oxidation.²⁴⁵ The ELVOCs produced from both ozonolysis and also OH oxidation of pinene are thought to contain multiple hydroperoxide moieties, in accordance with their high O:C and H:C ratios.¹⁸⁰ Additionally, the rate of autoxidation has been shown to accelerate as organic compounds gain oxygen-containing moieties (and thus partition more strongly to the condensed

phase), transforming carbonyls into highly functionalized dicarbonyl hydroperoxide compounds.²⁴⁶ It is possible that experiments that use very high radical abundances and therefore very short RO₂ lifetimes, such as PAM experiments, favor autoxidation due to fewer competing radical–radical RO₂ reactions. Possibly, these highly functionalized products extend the absorption to longer wavelengths.

4.3. Aging of Secondary Organic Aerosols with Reduced Nitrogen Compounds [NH_{3(g)}, NH₄⁺, and Amino Acids]

The discussion in section 4.2 relates to the spectral properties of secondary organic aerosol generated via primary oxidation pathways in the gas phase. In addition, heterogeneous and aqueous-phase reactions can lead to changes in the optical properties of an aerosol. Following bulk reactions of SOA with nitrogen reducing agents such as amino acids, nitrate, ammonia, and ammonium salts, browning of the organic species is visually observed, indicating light absorption in the visible spectrum.^{22,24,25,61,215,217,221} Recent optical studies have focused on these aqueous and multiphase reactions with two main groups of organic condensates: dicarbonyl compounds and terpene SOA. The studies examine aqueous-phase reactions,^{20,219,221,247,248} simulations of evaporating cloud droplets,^{218,221,249} and heterogeneous uptake at the surface of humidified aerosol.^{105,220,250} The extent and spectra of absorption and chromophore identification are detailed in the following sections.

4.3.1. Aqueous and Heterogeneous Reactions with Dicarbonyls: Glyoxal and Methylglyoxal. Glyoxal and methylglyoxal are the smallest tropospheric α -dicarbonyls. Both are generated from atmospheric oxidation of aromatics, acetylene, and biogenic hydrocarbons, dominantly isoprene, and due to their high volatility, they do not condense into the particle phase through traditional gas–particle partitioning. Glyoxal, however, is water-soluble and readily partitions to the aqueous phase, even at low RH ($\sim 30\%$) when a thin water layer is present.⁹⁵ Conclusions as to methylglyoxal uptake to aqueous aerosol are less conclusive,²¹⁸ yet they adsorb readily to the aerosol surface and can augment droplet formation.²⁵¹ Both glyoxal and methylglyoxal react rapidly in the aqueous phase, and are considered potential sources of highly oxidized and nitrogen-containing oligomeric compounds in SOA formed through aqueous chemistry pathways.^{20,41,49,218,219,252–254} Model estimates attribute as much as a third of global SOA production to aerosol formation by α -dicarbonyl compounds such as methylglyoxal and glyoxal if the uptake of these compounds by clouds and aerosol is irreversible.²¹⁸

Many studies have shown that reactions between α -dicarbonyls, such as glyoxal^{20,219,221,247–249} and methylglyoxal^{47,218} and amino acids, methylamine, dimethylamine, and ammonium salts produce brown particle-phase products that absorb UV and visible light. Studies in which the absorption spectra following glyoxal reactions with ammonium salts were probed display similar UV–vis absorption spectra, both for products of bulk solution reactions^{20,219,247} and for filter samples of evaporated droplets²⁴⁹ (see Figure 10). The UV–vis spectra show absorption at three major wavelengths, ~ 207 and ~ 277 nm and a broadband absorption that extends from 350 nm, which causes the brown appearance.^{20,219,247,249} Time evolution of the spectra differs somewhat between studies, depending on the specific experimental conditions, and for greater reaction duration and increasing glyoxal concentrations, the spectrum consists of a single broad absorption band that

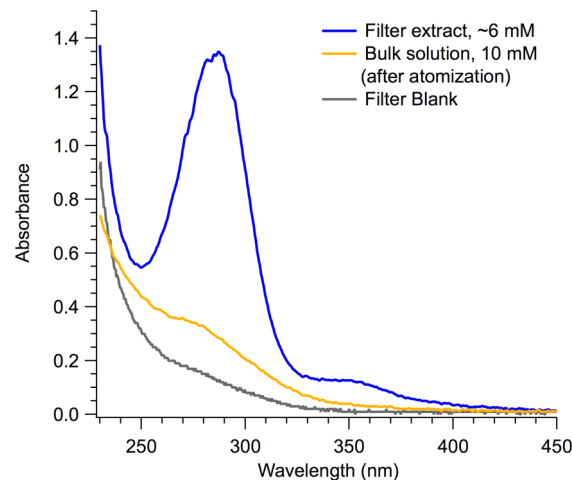


Figure 10. Absorption spectra measured in glyoxal–(NH₄)₂SO₄ solution experiments including aerosol filter extract (blue), filter blank (gray), and bulk solution after atomization (orange). Reprinted with permission from ref 249. Copyright 2013 American Chemical Society.

shifts to include longer wavelengths, extending to 550 nm and beyond.²⁰ The UV–vis spectrum for the methylglyoxal reaction with ammonium salts is analogous to that of the glyoxal reactions.⁴⁷

The UV spectra evolve with reaction duration, suggesting that the chemical identity, not just the quantity, of the light-absorbing products changes over time, consistent with multiple generations of products.²⁰ Reaction products, pathways, and kinetics have been investigated for bulk-phase reactions of glyoxal^{20,219,221,229,247–249,255} and methylglyoxal^{47,218} with amines and ammonium salts and for gas-phase glyoxal uptake on hydrated or aqueous ammonium sulfate seed particles^{220,250,255} by nuclear magnetic resonance (NMR), aerosol mass spectrometry (AMS), high-performance liquid chromatography (HPLC), and electrospray ionization mass spectrometry (ESI-MS). In brief, for the glyoxal reactions, carbon–nitrogen (C–N)-containing compounds such as imines and diamines are identified as intermediate products, and the light-absorbing imidazole and its derivatives (such as imidazole-2-carboxaldehyde and N¹-glyoxal-substituted imidazole) as well as formic and acetic acids are identified as later-generation products.^{219,229,247,249,250} Yu et al.²¹⁹ showed that imidazole (IM) and its derivative, imidazole-2-carboxaldehyde (IC), likely contribute to the 207 nm absorption band and IC to the 277 nm absorption band but that additional unknown absorbing species, not identified by the NMR studies, exist. Kampf et al.²²⁹ combine HPLC and ESI-MS analysis to detect the formation of 2-(1*H*-imidazol-2-yl)-1*H*-imidazole (or 2,2'-bisimidazole, 2,2'-biimidazole, BI) from further reactions of IC with ammonia and show BI to be an additional major contributor to the 277 nm absorbance band. A number of C–N-containing products with lower polarity than the mono- and bicyclic imidazole products were observed to absorb at wavelengths between 350 and 400 nm and were tentatively identified as formamides and formic acid ester imidazole derivatives. The proposed reaction pathway for the major products identified by Kampf et al.²²⁹ and Hamilton et al.²⁵⁵ is shown in Figure 11. A number of the light-absorbing organic nitrogen species, including 1*H*-imidazole, 1*H*-imidazole-2-carboxaldehyde, 2,2'-bisimidazole, and a glyoxal-substituted

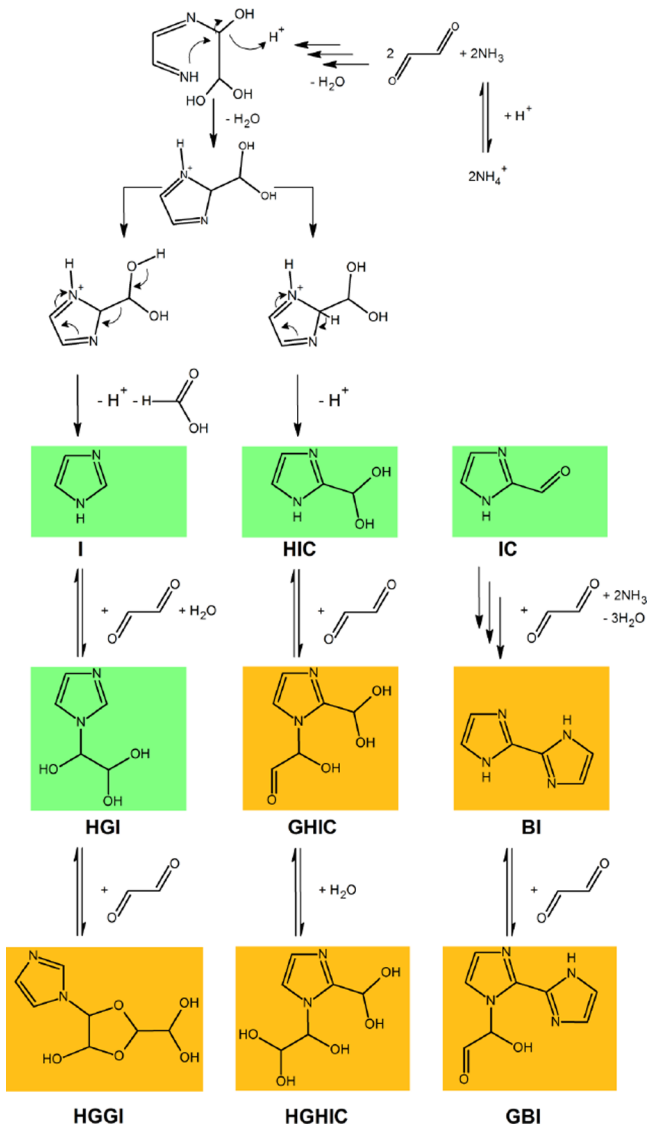


Figure 11. Proposed reaction pathways for imidazole formation in the glyoxal/ammonium sulfate system. Compounds shaded in green were described by Galloway et al.²⁵⁰ and Yu et al.²¹⁹ Compounds shaded in orange were identified in the study of Kampf et al.²²⁹ IG is *N*-glyoxal-substituted 1*H*-imidazole and HGI is its hydrated form; IC is 1*H*-imidazole-2-carbaldehyde and HIC is its hydrated form; BI is 2,2'-biimidazole and GBI is its glyoxal-substituted analogue; GHIC is *N*-glyoxal-substituted hydrated 1*H*-imidazole-2-carbaldehyde and HGGI is hydrated glyoxal-dimer-substituted imidazole. Reprinted with permission from ref 229. Copyright 2012 Copernicus Publications.

2,2'-bisimidazole, identified in aqueous laboratory solutions, were also identified in chamber-generated aerosol and were formed on atmospherically relevant time scales.²⁵⁵

De Haan et al.²²¹ and Lee et al.²⁴⁹ showed that evaporating glyoxal (NH_4HSO_4) droplets produced light-absorbing species on time scales that are orders of magnitude faster than observed in bulk solutions. This probably results from a combination of drying-induced conversion of glyoxal dihydrate to its reactive monohydrate form²²¹ and increasing reactant concentrations.^{229,249} In another study on the heterogeneous uptake of glyoxal on hydrated ammonium sulfate seed aerosol, increasing RH increased the relative contribution of imidazole and absorbing C–N compounds compared to the dominant glyoxal oligomer products, also suggesting that higher water content in

concentrated aerosol enhances the imidazole formation pathway.²²⁰

A number of studies have shown that light absorption is pH-dependent^{219,229,247,249} as the reaction proceeds via $\text{NH}_3\text{(aq)}$ in equilibrium with NH_4^+ and the equilibrium shifts toward NH_4^+ at lower pH. Although Shapiro et al.²⁰ report similar absorption spectra for both ammonium sulfate and ammonium nitrate reactions with glyoxal, Lee et al.²⁴⁹ observed much higher absorption and higher N:C ratios for ammonium sulfate as compared to ammonium nitrate and ammonium chloride and concluded that the sulfate ions play a critical role in controlling the formation of imidazole.

Bulk solution and bulk filter particle studies that identify the absorbance bands and absorbing chromophores in UV and visible wavelengths do not quantify the absorption in terms of MAC or RI but rather in terms of molar absorptivity (ϵ , with units of $\text{M}^{-1}\cdot\text{cm}^{-1}$). Following the approach of Noziere et al.²⁴⁷ and taking the lower-bound estimate of $\epsilon \geq 1 \text{ M}^{-1}\cdot\text{cm}^{-1}$, Shapiro et al.²⁰ calculate the extinction coefficient of the glyoxal and ammonium sulfate solution at 550 nm as $\beta_{\text{ext}} \geq 0.71 \text{ cm}^{-1}$ and the imaginary part of the refraction index, k , as $\geq 3.1 \times 10^{-6}$. Molar absorptivity values of major reaction products were calculated by Yu et al.²¹⁹ and Kampf et al.²²⁹ and are similar within uncertainties. Values from the two studies^{219,229} are as follows, with an equivalent value of k (which we calculate from the reported molar absorptivities with the assumption of density $1.4 \text{ g}\cdot\text{cm}^{-3}$) shown in parentheses. Imidazole (IM) at 207 nm, $4571 \pm 186 \text{ M}^{-1}\cdot\text{cm}^{-1}$ ($k = 0.0054$) and $4462 \pm 245 \text{ M}^{-1}\cdot\text{cm}^{-1}$ ($k = 0.0053$); IC at 213 nm, $6119 \pm 302 \text{ M}^{-1}\cdot\text{cm}^{-1}$ ($k = 0.0074$) and $6004 \pm 638 \text{ M}^{-1}\cdot\text{cm}^{-1}$ ($k = 0.0073$) and at 273 nm $229.9 \pm 3.0 \text{ M}^{-1}\cdot\text{cm}^{-1}$ ($k = 0.0004$) and $273 \pm 28 \text{ M}^{-1}\cdot\text{cm}^{-1}$ ($k = 0.0004$). Kampf et al.²²⁹ also report molar absorptivity at 300 nm for IM of $18 \pm 2 \text{ M}^{-1}\cdot\text{cm}^{-1}$ ($k = 0.3 \times 10^{-4}$) and for BI (2,2'-biimidazole) of $36\,690 \pm 998 \text{ M}^{-1}\cdot\text{cm}^{-1}$ ($k = 0.0626$). Although the production rates of 2,2'-biimidazole are approximately 2 orders of magnitude lower than for the major monoimidazole reaction products, its high molar absorptivity at 280 nm means that its contribution to the overall absorbance of the reacted solution is comparable to that of the monoimidazole reaction products.

The complex refractive index for glyoxal reactions with amines or ammonium sulfate has been measured in two aerosol flow tube studies.^{65,220} Zarzana et al.⁶⁵ examined dried and atomized aerosol formed from aqueous-phase reactions between α -dicarbonyls glyoxal and methylglyoxal and primary amines glycine and methylamine. The reaction products from all reactions exhibit significant absorption in the visible range. For glyoxal–glycine, methylglyoxal–glycine, and glyoxal–methylamine systems, the difference between RI values of each is less than the uncertainty within each system and the average $\text{RI} = 1.64 (\pm 0.02) + i0.039 (\pm 0.017)$ at $\lambda = 532 \text{ nm}$. RI for the methylglyoxal–methylamine system has a value for the imaginary part that is significantly higher than the imaginary part of the other three systems, $\text{RI} = 1.55 (\pm 0.04) + i0.114 (\pm 0.037)$. RI values for aerosol of each reaction system are shown in Table 3. Reactions of methylglyoxal have been observed to form light-absorbing material more rapidly than analogous glyoxal reactions,⁴⁷ and nitrogen-containing oligomers have been observed for all methylglyoxal reactions with amines but not for most glyoxal reactions.²¹⁸ In the visible wavelengths, the size-dependent SSA for methylglyoxal–methylamine is at most 0.65 and for the other systems

(glyoxal–glycine, glyoxal–methylamine, and methylglyoxal–glycine) is at most 0.85.⁶⁵

The complex refractive index has also been derived for aerosol reaction products following the heterogeneous reaction between gas-phase glyoxal and hydrated ammonium sulfate aerosol. RI is calculated with the assumption that reaction products are a shell of material around the ammonium sulfate core and was derived by fitting the CRD measured extinction efficiency at $\lambda = 532$ nm to a core–shell model.²²⁰ The RI at $\lambda = 355$ nm is $1.68 (\pm 0.10) + i0.01 (\pm 0.02)$ at 50% RH and $1.65 (\pm 0.06) + i0.02 (\pm 0.01)$ at 75% RH (see Table 3). Aerosol mass spectrometric analysis showed that the main reaction products are glyoxal oligomers, with a minor contribution from imidazoles, and that there is an increase in the ratio of absorbing C–N compounds (including imidazoles) to glyoxal oligomers when RH of the reaction is increased from 50% to 75%. However, this increase does not lead to a measurable change in the imaginary part of RI, probably because the changes in absorbance are smaller than the sensitivity of CRD for absorption retrievals and the small changes in absorption over the reaction time scales.²²⁰ In a follow-up study, optical extinction was also measured for mixed glycine–ammonium sulfate particles (1:100 mixing ratio as a realistic atmospheric proxy) for which the extinction efficiency was greater than for the reaction with ammonium sulfate or glycine alone, suggesting a synergistic effect.⁹⁵ The fraction of absorbing C–N compounds again increases when RH of the reaction is increased from 50% to 90%, and the extinction efficiency increases above a threshold RH, below which no reaction occurred and the extinction was as for the dry ammonia particle. The extinction efficiency is greatest at around 50% RH and then decreases as RH is increased. As the absorbing species comprise less than 0.1% by mass of the reaction products, the increased extinction was attributed to enhanced scattering by the dominant glyoxal oligomer reaction products, which may peak due to enhanced reactions and enrichment at the interfacial water layer at intermediate RH, well before deliquescence.⁹⁵

Low reaction rates for the major products of these reactions make it unlikely that the reactions contribute significantly to ambient SOA mass.^{219,229,256} However, the faster reaction rates of glyoxal with amino acids and ammonium sulfate under droplet drying conditions may suggest that bulk laboratory studies cannot be used unequivocally to assess aerosol reactions. Both Galloway et al.²⁵⁰ and Trainic et al.²²⁰ have shown in their studies of heterogeneous glyoxal reaction with ammonium sulfate seed aerosol that imidazoles constitute only a small fraction of total observed organic aerosol, at least on the time scales of their experiments. Even so, the influence of multiphase and aqueous-phase reactions on the atmospheric radiative budget cannot be neglected. Reactions between other dicarbonyls and aldehydes could increase imidazole formation,²⁵⁰ and due to the high absorption coefficients of some of the nitrogen-containing reaction products, even small concentrations could have an effect on the radiative properties of SOA.^{20,229} Regions with high pH and high ammonium concentrations could favor imidazole formation, and examples of such conditions were suggested by Kampf et al.²²⁹ to be regions with alkaline mineral soils and areas under the influence of livestock waste and heavy agricultural activity. For heterogeneous reactions, the fraction of absorbing substances in the reacted aerosol increases with increasing RH, suggesting

that the absorption component may become more substantial in cloud or fog droplets and after longer reaction times.²²⁰

4.3.2. Aqueous and Heterogeneous Reactions with Mono- and Sesquiterpenes.

A number of studies have been conducted to elucidate the chemistry of SOA aging by ammonium ions, amino acids, and NH₃ vapor and to identify the chromophores that absorb visible radiation and fluoresce at UV and visible wavelengths.^{22,24,25,105,215,217} We will refer to the reactions as “NH₄⁺/NH₃ mediated” because absorption spectra and trends are similar whether the reactions are with vapor-phase NH₃ or dissolved NH₄⁺ and because, in contrast to the glyoxal/methylglyoxal reactions described in section 4.2.1, replacing sulfate anions of ammonium sulfate in control experiments with (NH₄)₂SO₄, NH₄NO₃, or NH₄Cl has small-to-negligible effects on the browning reactions.²⁴

The greatest absorption for the NH₄⁺/NH₃-aged SOA, from among a large group of biogenic and anthropogenic VOC precursors studied, is observed for limonene, α -cedrene, and α -humulene SOA,^{22,25} which have a distinctive absorption band at around 500 nm superimposed on a broad absorption that smoothly increases toward the UV (down to 300 nm). NH₄⁺/NH₃-aged SOA from β -myrcene, isoprene, α -pinene, and β -pinene exhibit little absorption in the visible region, but absorption in the UV region increased.^{22,25} Chromophore formation at 500 nm was greatly accelerated for evaporative aging (drying of aqueous aerosol) relative to solution-phase aging or aging with NH₃ vapor, suggesting that browning involves condensation reactions, in which water is generated as a reaction product, and is thus accelerated by active removal of water by evaporation.^{25,215} In the aqueous phase, an additional peak observed at ~ 430 nm is thought to form through ammonium sulfate catalysis and may be nitrogen-free, whereas the 500 nm feature, which becomes more dominant at high ammonium sulfate concentrations, is formed through a two-stage mechanism to produce a nitrogen organic compound with at least one nitrogen atom.²¹⁵ Absorption spectra of the evaporative aged aerosol do not contain the 430 nm chromophore, reflecting possible differences in the reaction mechanisms.²¹⁵ Reactions with amino acids (glycine, alanine, arginine, and cysteine) produced similar absorption peaks, red-shifted to different extents, relative to the SOA + NH₄⁺ absorption peaks.^{22,25}

SOA formation through O₃ oxidation leads to higher Δ MAC (the difference between MAC of fresh and NH₄⁺/NH₃-aged SOA) than via OH oxidation,²⁵ suggesting that carbonyl compounds play a role in the browning process. Carbonyls are the dominant products of O₃-initiated oxidation of alkenes due to opening of the C=C bond. In contrast, carbonyl yields in the OH-initiated oxidation of terpenes are lower.²⁵

In contrast to the strong change in absorption and fluorescence spectra between fresh and NH₄⁺/NH₃-aged SOA, changes in chemical composition as measured by ESI-MS, FTIR, and NMR spectra are nonsignificant for NH₄⁺/NH₃-mediated terpene SOA, suggesting that the chromophores are minor species in aged SOA.²² Changes following NH₄⁺/NH₃ aging of SOA are observed, however, in nano DESI (desorption electrospray ionization–mass spectrometry) mass spectra that show that all newly formed peaks in NH₄⁺/NH₃-aged limonene SOA samples contain one or two N atoms.^{24,105,215,217} The yield of nitrogen-containing chromophores following NH₄⁺/NH₃ aging of limonene SOA is very small, less than 2% of SOA mass.²¹⁵

Assignment of elemental formulas to DESI-MS m/z ions through Kendrick analysis allows elucidation of product species.²¹⁷ The key aging reactions leading to absorbance by $\text{NH}_4^+/\text{NH}_3$ -aged limonene SOA were identified as the transformation of carbonyls to imines (Figure 12a), intra-

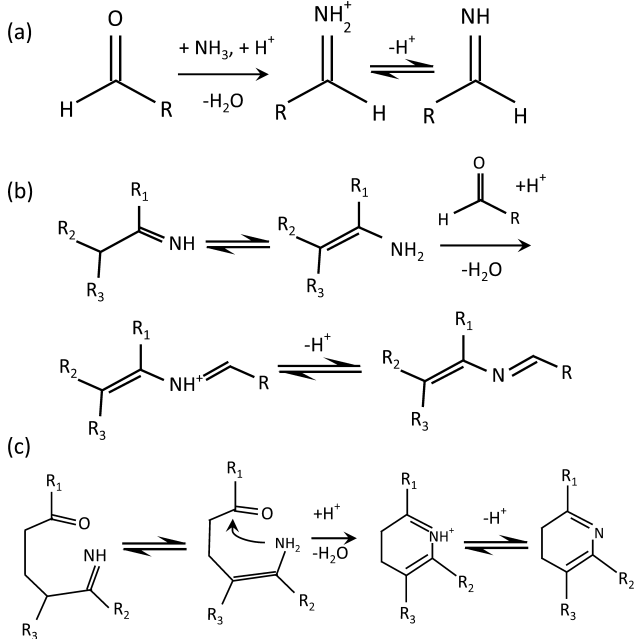


Figure 12. Reaction pathway for $\text{NH}_4^+/\text{NH}_3$ aging of terpene SOA. (a) Reaction between ammonia and carbonyl groups in the SOA molecules leading to hemiaminals, which then dehydrate into primary imines. (b) The imines may react further via with another carbonyl group, resulting in a more stable secondary imine/Schiff base. (c) If the carbonyl is present in the skeleton of the same molecule, nitrogen-containing heterocyclic compounds may be formed. Reprinted with permission from ref 217. Copyright 2010 American Chemical Society.

molecular dimerization of imines with other carbonyl compounds in SOA (Figure 12b), and intermolecular cyclization of imines and subsequent oligomerization processes (Figure 12c).^{24,25,217}

The carbonyl-to-imine transformation most probably does not generate light-absorbing chromophores,²¹⁷ whereas the cyclization and Schiff base formation reactions (see Figure 12) may produce light-absorbing products if they result in sufficient π -conjugation in the final product.²⁵ The conjugated nitrogen-containing organic species are measured as increased double-bond-equivalent (DBE) values of neutral molecules. This reflects the number of π bonds and ring structures in the compound and is calculated as

$$\text{DBE} = \text{C} - (\text{H}/2) + (\text{N}/2) + 1 \quad (11)$$

where C, H, and N are the numbers of carbon, hydrogen and halogen, and nitrogen atoms, respectively. $\text{NH}_4^+/\text{NH}_3$ -aged limonene SOA results in formation of a number of nitrogen-containing dimers and trimers with fairly high DBE values (up to $\text{DBE} \approx 11$) that are absent in the spectrum of fresh (white) limonene SOA samples^{105,217} and most likely are the light-absorbing products. These would be formed following oligomerization reactions in which imines generate higher-molecular-weight products through reactions with unreacted carbonyl groups of other molecules present, forming new C—N bonds that link together the ozonolysis products of limonene.

Ketolimononaldehyde (KLA, $\text{C}_9\text{H}_{14}\text{O}_3$), a second-generation ozonolysis product of limonene ($\text{C}_{10}\text{H}_{16}$), has been specifically identified²⁴ as the effective brown carbon precursor in $\text{NH}_4^+/\text{NH}_3$ -mediated reactions with limonene SOA.²⁴ Limononaldehyde (LA, $\text{C}_{10}\text{H}_{16}\text{O}_2$) and pinonaldehyde (PA, $\text{C}_{10}\text{H}_{16}\text{O}_2$), the first-generation ozonolysis products of limonene and α -pinene, respectively, are reactive toward ammonia and amino acids yet do not exhibit the light-absorption properties of brown carbon. All three, LA, PA, and KLA, are 1,6-ketoaldehydes, yet only KLA, the second-generation oxidation product, has an additional ketone group, providing 1,5-diketone and 1,4-ketoaldehyde moieties. The study shows that a high degree of selectivity of organic compound structures dictates the light-absorbing properties of SOA.²⁴ $\text{NH}_4^+/\text{NH}_3$ aging of cyclic sesquiterpenes, cedrene, and α -humulene leads to SOA browning, whereas aging of the open-chain sesquiterpene farnesene does not,²⁵ again suggesting the need to characterize detailed molecular structures of aerosol constituents in order to predict SOA aging chemistry and optical properties. Although the colored products represented only a small fraction of the SOA mass, their large molar absorptivity (e.g., $\epsilon > 10^5 \text{ L}\cdot\text{mol}^{-1}\cdot\text{cm}^{-1}$ at 500 nm for limonene SOA) increased the effective mass absorption coefficient of the NH_4^+ -aged organics in excess of $0.1 \text{ m}^2\cdot\text{g}^{-1}$.^{25,215} As the absorbing chromophores constitute $\sim 2\%$ of the residual organics, this implies a MAC of $\sim 5 \text{ m}^2\cdot\text{g}^{-1}$ at 500 nm for the absorbing fraction. The MAC values were dependent on SOA precursor concentration, and the above value should be treated as an upper limit to the MAC expected for atmospherically relevant limonene concentrations. The amount of nitrogen organic compounds, and thus the value of MAC, detected with DESI-MS for the gaseous reaction with NH_3 ²⁵ was about 2 times larger than for aqueous reactions or evaporative aging.²¹⁵

At shorter wavelengths in the near-UV (360–420 nm), Flores et al.¹⁰⁵ measured in situ the optical characteristics of terpene SOA aged with NH_3 by use of BBCES. The retrieved imaginary values of RI indicate minor to no detectable absorption at $[\text{NH}_3] < 1.0 \text{ ppm}$ for the three terpenes measured (α -pinene, α -humulene, and limonene), and absorption at higher ammonia concentrations ($> 1 \text{ ppm}$) for α -humulene and limonene SOA in the 360–420 nm range.¹⁰⁵ Collected filter samples analyzed by UV-vis spectrometry corroborated that, at low exposure concentrations ($\leq 1 \text{ ppm}$ for 1.5 h), absorption was extremely low. The imaginary component of RI increased from $k = 0.0$ to an average $k = 0.029 (\pm 0.021)$ for $[\text{NH}_3] = 1.3 \text{ ppm}$ for α -humulene SOA and to an average $k = 0.032 (\pm 0.019)$ for limonene SOA after 1.5 h exposure to 1.3 and 1.9 ppm NH_3 , respectively. If $\rho = 1.4 \text{ g}\cdot\text{cm}^{-3}$ is assumed, k values at $[\text{NH}_3] < 1 \text{ ppm}$ of all substances measured were $k < 0.01$, corresponding to a MAC of $< 0.25 \text{ m}^2\cdot\text{g}^{-1}$.¹⁰⁵

4.4. Acid-Catalyzed Aldol Condensation

A number of studies have shown the role of sulfuric acid in formation of light-absorbing organic compounds via acid-catalyzed aldol condensation of volatile aldehydes,^{222,257–260} which is expected to be important under H_2SO_4 concentrations characteristic of stratospheric aerosol or volcanic eruptions.

Browning was observed during evaporation of terpene SOA + H_2SO_4 solutions at low pH (<2), with no addition of reduced nitrogen species, which likely corresponds to an acid-catalyzed aldol condensation reaction.²¹⁵ However, absorption peaks at 390, 410, and 500 nm were specifically associated with sulfuric

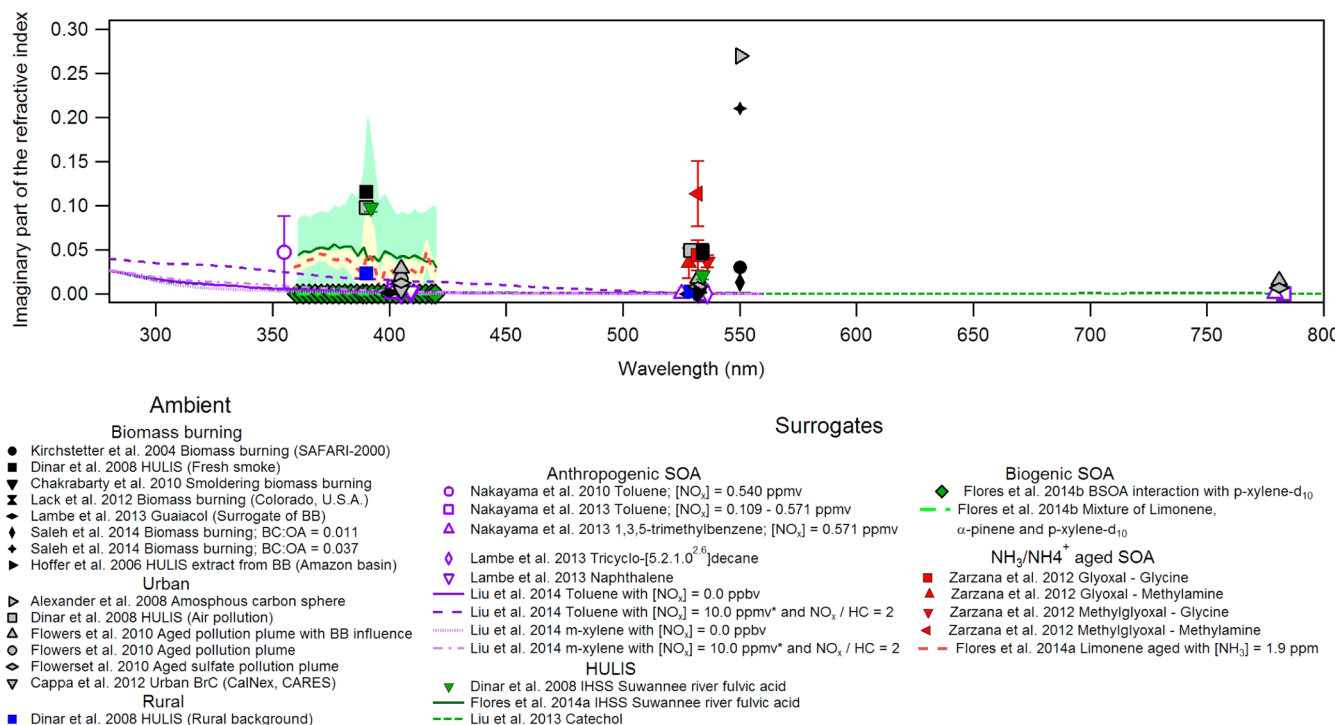


Figure 13. Compilation of the imaginary part of RI (k) for ambient BrC aerosol and for SOA surrogate aerosol as measured in various studies. Shaded yellow and green areas represent respective uncertainties for SRFA and NH_3 -aged limonene SOA in the study of Flores et al.¹⁰⁵ The overall uncertainty in Liu et al.⁵⁵ is $k \pm 15\%$ for $\lambda < 420$ nm.

rather than nitric or phosphoric acid, implying that these chromophores are sulfur-containing organic compounds and not just acid-catalyzed products. Sulfur-containing organic compounds (SOC) were identified by ESI, and while an organosulfate group is not chromophoric by itself, the study concluded that adding a sulfate group to a light-absorbing molecule may change its optical properties significantly.²¹⁵ The study demonstrated how increased reactant concentrations and acidity produced by evaporation of water droplets can greatly accelerate some otherwise slow processes and lead to changes in the composition and optical properties of the dissolved organics, rendering the acid-catalyzed aldol condensation reaction and organosulfate formation an atmospherically relevant pathway.²¹⁵

Light absorption was observed for the α -pinene + O_3 + NO_3 system in the presence of highly acidic sulfate seed aerosol under dry conditions.¹⁶¹ Organic nitrates, formed in the presence of neutral sulfate seed aerosol, are important constituents in the SOA from NO_3 oxidation of α -pinene but were found to be nonabsorbing. The average MAC values for α -pinene + O_3 + NO_3 oxidation in the presence of acidic seed at 355 and 405 nm, were 1.12 and $0.80 \text{ m}^2 \cdot \text{g}^{-1}$, respectively, while the values for O_3 oxidation only were 0.24 and $0.15 \text{ m}^2 \cdot \text{g}^{-1}$, respectively, demonstrating that light-absorbing oligomers are associated with the nitrate reaction and not only a result of acid-catalyzed aldol condensation reactions. The difference in MAC was attributed to nitrooxy organosulfate, a compound that can be produced during NO_3 oxidation, and the hypothesis proposed that aldol condensation oligomers with nitrate and sulfate groups have much stronger absorption at UV and near-UV spectral regions than those with just an organosulfate group.¹⁶¹

4.5. Comparison of Mass Absorption Cross Section and Imaginary Part of Refractive Index between Studies, Compounds, and Laboratory and Ambient Measurements

The laboratory studies detailed above present a complex picture in which the dependence of optical properties and chemical composition of early-generation and aged SOA depend dominantly on specific molecular signatures but also on precursor and reactant concentrations, reaction duration, pH, and RH. Nevertheless, we conduct a comparison between MAC and k values measured in various laboratory systems and between those measured in the field or for ambient samples, in an attempt to discern conclusions as to observed trends and regimes. In general, ambient measurements of brown carbon can include components of both primary sources as well as secondary sources of organic aerosol, and the same applies to laboratory measurements of biofuel and biomass burning aerosols, which can also have contributions from both primary and secondary particulates.^{5,261,262} The measurements we discuss here for ambient samples (BB, urban, rural, and aged pollution aerosol) and SOA surrogates (fulvic acids, anthropogenic SOA, and $\text{NH}_3/\text{NH}_4^+$ -aged SOA) are all tabulated in Table 3.

The highest BrC MAC values are measured in ambient samples with vehicular emission sources^{21,236} ($\text{MAC} \approx 2.5 \text{ m}^2 \cdot \text{g}^{-1}$ at $\lambda = 365$ nm) and aged pollution plumes having a component of biomass burning¹²³ (MAC up to $3.4 \text{ m}^2 \cdot \text{g}^{-1}$ at $\lambda = 405$ nm) rather than BrC associated with only SOA or water-soluble OC. MAC values from humic-like substances (HULIS) with a pollution or smoke source are similarly high⁷⁶ ($\text{MAC}_{532} \approx 1 \text{ m}^2 \cdot \text{g}^{-1}$), whereas HULIS from a mixed forest source display much lower MAC values (MAC_{532} and $\text{MAC}_{355} = 0.03$ and $0.32 \text{ m}^2 \cdot \text{g}^{-1}$, respectively).¹⁹ The higher MAC values of ambient HULIS extracts are in the same range as MAC measured for large multifunctional compounds, such as humic

and fulvic acids, that are used as surrogates for atmospheric HULIS (MAC_{405} between 0.18 and $1.5 \text{ m}^2 \cdot \text{g}^{-1}$),^{63,76,105} as well as biomass burning particles from U.S. forests (MAC_{404} of $0.82 \text{ m}^2 \cdot \text{g}^{-1}$)⁶⁹ and South African SAFARI-2000 campaigns (MAC_{550} of 0.6^8 and $0.7 \text{ m}^2 \cdot \text{g}^{-1}$)^{235,263}). Much higher MAC values ($\text{MAC}_{\sim 450}$ of $\sim 4 \text{ m}^2 \cdot \text{g}^{-1}$) were observed for BrC carbon sphere “tarballs” over Asia.¹⁶

Ambient aerosol from biomass burning sources displays slightly higher or comparable MAC values to those measured for biomass combustion aerosol in the laboratory. Low-temperature combustion (such that BC is not emitted) of biomass combustion samples yields MAC_{532} up to $0.07 \text{ m}^2 \cdot \text{g}^{-1}$ ¹⁷ and MAC_{500} up to $0.5 \text{ m}^2 \cdot \text{g}^{-1}$.²³¹ Guaiacol, a methoxyphenol present in wood smoke following pyrolysis of lignin and used as a single-component laboratory surrogate for biomass burning BrC, yields a much lower MAC (MAC_{405} up to $0.02 \text{ m}^2 \cdot \text{g}^{-1}$ when highly oxidized).⁶³ It was found that MAC for wood combustion smoke particles formed in the University of Florida Atmospheric Photochemical Outdoor Reactor (UF-APHOR) is lower in the afternoon hours than MAC measured in the early morning hours. This was explained by bleaching, in which the exposure to high-energy photons in sunlight can excite electrons in colored molecules and disrupt the conjugated structure of chromophores, resulting in gradual fading of wood smoke color and lower MAC as compared to early morning hours.²⁶⁴ Saleh et al.²⁶¹ conducted a study to differentiate between primary and secondary organic aerosol produced from fresh pine and oak burning emissions. Their measured absorbance is evaluated with limiting cases in which the SOA absorbance is defined by the biomass absorption values of studies by Chakrabarty et al.,¹⁷ Chen and Bond,²³¹ and Kirchstetter et al.⁸, and they demonstrate SOA to specifically be a contributing BrC component of the emissions following biomass burning. A recent study by Saleh et al.²³² correlates absorption by organic aerosol from a biomass burning source with the BC:OA ratio (black carbon to organic aerosol) of the emissions, which is a measure of combustion conditions. Absorption and k values of the organic component increased with increasing BC:OA ratio. The same relationship was not upheld for diesel engine emissions. Almost all of the OA absorption was associated with ELVOCs, which were shown to have k values (termed k_{OA}) an order of magnitude higher than SVOCs (semivolatile organic compounds) and LVOCs (low-volatility organic compounds). Moreover, the same study suggests that the high values of absorbance seen for amorphous carbon spheres in Asia measured by Alexander et al.¹⁶ are due to vaporization of organics other than ELVOCs in the TEM (transmission electron microscopy) beam, leading to comparable k values of carbon spheres (0.27 at $\lambda = 550 \text{ nm}$) and ELVOCs (see Figure 13 and Table 3). The SOA component of biomass burning OA would lead to a similar trend in absorbance: that is, lower k_{OA} values as the fraction of SOAs increases, which is expected to occur in the lower BC:OA ratio regime. Indeed, fresh and aged (with a greater SOA component) emissions displayed similar k values for a given BC:OA ratio.²³² Should the relationship between k values and BC:OA ratio for biomass burning aerosol be found to be consistent in further studies, the parametrization proposed by Saleh et al.²³² linking biomass k_{OA} to BC:OA ratio can be implemented in chemical transport and climate models as the BC:OA ratio is tracked in emission inventories.²³²

Ambient samples of urban water-soluble organic carbon (WSOC) aerosol from the Los Angeles basin that were

measured in the CalNex campaign by Zhang et al.,^{21,236} and are dominated by anthropogenic SOA, have MAC_{365} values of 0.77 and $0.71 \text{ m}^2 \cdot \text{g}^{-1}$. Although measured at a shorter wavelength ($\lambda = 365 \text{ nm}$) than most of the aforementioned biomass burning and laboratory wood combustion aerosol, the MAC values are in a similar range. The presence of light-absorbing WSOC in these urban samples correlated with the campaign-averaged MAC,⁸⁹ although the MAC values of identified individual nitroaromatics that contributed to the total absorbance of WSOC were around an order of magnitude larger than the ambient BrC MAC, indicating that these species compose only a small mass fraction of the WSOC.²³⁶ The MAC measured for urban BrC in Atlanta, GA, was $\text{MAC}_{405} = 0.19 \text{ m}^2 \cdot \text{g}^{-1}$, around 4 times lower than the MAC value of $0.77 \text{ m}^2 \cdot \text{g}^{-1}$ measured in Los Angeles.²¹ This was attributed to the source SOA being a mix of both anthropogenic and biogenic (isoprene) VOCs in Atlanta, in contrast to the SOA formed in the anthropogenic (aromatics)-dominated environment of the Los Angeles basin. Cappa et al.¹¹⁸ also measured lower MAC values at $\lambda = 405 \text{ nm}$ for urban BrC from the CalNex and CARES campaigns with $\text{MAC}_{405} = 0.12$ and $0.14 \text{ m}^2 \cdot \text{g}^{-1}$, respectively. These measurements were made in the marine boundary layer along the Los Angeles coast (CalNex) and an urban ground site in Sacramento, CA (CARES).

The more absorbing compounds of anthropogenic OH oxidized SOA precursors, such as naphthalene,^{25,63} have MAC values at the lower end of the range measured for laboratory wood combustion particles and are similar to the low MAC of NH_4^+ -mediated terpene SOA ranging from 0.001 to $\sim 0.1 \text{ m}^2 \cdot \text{g}^{-1}$.^{22,25,105} However, the MAC for toluene SOA formed from photo-oxidation ($\text{HC}/\text{NO}_x = 7$, $\text{NO}_x = 570 \text{ ppbv}$), extrapolated from laboratory values and dependencies to atmospheric conditions,⁶⁴ yields values of $0.08\text{--}0.52 \text{ m}^2 \cdot \text{g}^{-1}$ at $\lambda = 405 \text{ nm}$, comparable to the MAC of the Suwannee River fulvic acid (SRFA) and biomass combustion samples.

We see that BrC absorbance, evaluated by MAC, is highest for urban aerosol dominated by vehicular emissions and transported pollution plume aerosol. Slightly lower and comparable values are observed for HULIS from International Humic Substance Society (IHSS) standards, smoke and polluted samples, laboratory wood combustion, ambient biomass burning (excluding the study of Alexander et al.¹⁶ that measured very high absorbance), and urban (WSOC or nonspecific) aerosol. Direct measurements of MAC for surrogate anthropogenic SOA yield values in the lower range of ambient urban samples. In Figure 13 we show the imaginary part of the refractive index versus wavelength for some of the aforementioned studies and additional laboratory SOA surrogates (see also Table 3). Values for the imaginary part of the refractive index for glyoxal and methylglyoxal reactions⁶⁵ are in the same range of those measured for high-absorbing HULIS samples from both polluted and fresh smoke sources.⁷⁶ HULIS samples with lower k values are observed for rural forest samples from Dinar et al.⁷⁶ and Utry et al.,¹⁹ and Amazonia biomass burning samples from the study of Hoffer et al.²³³ The highly spectrally resolved k values measured by Liu et al.⁵⁵ for anthropogenic SOA precursors in the high- NO_x regime, are within the range reported for ambient urban and biomass burning samples (somewhat lower than HULIS samples). $\text{NH}_3/\text{NH}_4^+$ -aged limonene SOA has comparably high k values only at high $[\text{NH}_3]$ concentration. Increased absorption by BrC at shorter wavelengths is clearly seen in Figure 13 for the studies of Liu et al.,⁵⁵ Kirchstetter et al.,⁸ and Dinar et al.⁷⁶

5. ABSORPTION BY INTERNALLY MIXED ORGANIC MATTER/BLACK CARBON AEROSOL

One of the complexities in characterizing aerosol in ambient air is that the aerosol has a mixed composition and many different chemical species. Laboratory optical measurements of ambient aerosol collected on filters (in contrast to satellite optical measurements) are often applied to separated chemical fractions of the aerosol (often distinguished by fractions soluble in water or organic solvent or by elution times), thus distinguishing between groups of compounds on the basis of their water or solvent solubility, polarity, and mass.^{25,76,231,236} The spectral dependence observed for BrC in ambient aerosol can also be a distinguishing tool to differentiate between types of aerosol^{265–267} and for partitioning (remotely) measured absorption aerosol optical depths (AAOD) and single scattering albedo (SSA) among BC and BrC constituents. In this section we present studies that use different approaches to deconvolute the measured atmospheric absorption of carbonaceous aerosol to its BC, BrC, and mixed BrC/BC components. This necessitates an understanding also of BC and mixed BrC/BC absorption features as detailed within.

The aerosol absorption coefficient (β_{abs}) generally decreases monotonically with wavelength, and the spectral dependence can be approximated by a power-law expression, $\beta_{\text{abs}} \approx \lambda^{-\text{AAE}}$, where AAE is the absorption Ångström exponent, defined as

$$\text{AAE}(\lambda_1, \lambda_2) = -\frac{\ln[\beta_{\text{abs}}(\lambda_1)] - \ln[\beta_{\text{abs}}(\lambda_2)]}{\ln(\lambda_1) - \ln(\lambda_2)} \quad (12)$$

where AAE depends on the wavelength pair, particle size, and particle composition.^{122,123,268} Small spherical particles ($x \ll 1$) with constant refractive indices have a λ^{-1} dependence, or a wavelength-independent AAE of 1.²⁶⁸ BC appears to have a relatively constant RI independent of wavelength, and thus should have an AAE of 1,^{268,269} though soot morphology, size, and mixing state lead to deviations from this canonical value of unity. A compilation of measured AAE values from the literature provides ranges of AAE values for specific compositions: for dust, 1–4; for total carbon, 1–1.3; for OC, 1.8–7 (Bahadur et al.²⁷⁰ and references within); and for nonorganic carbon (BC/EC/soot), 0.6–1.1.^{8,12,270,271}

A confounding factor for attribution of the aerosol composition to a non-BC source when $\text{AAE} > 1$ is the optical behavior of mixed-composition aerosol, as aged soot can typically exist as internally well-mixed particles and as encapsulated cores,^{272–276} which modifies its optical properties.²⁷⁷ A model treatment for mixed particles with a black-carbon core surrounded by a well-mixed shell shows a lensing effect in which absorption is enhanced and MAC increases. Additional light is intercepted by the larger particle, with the shell acting as a lens that focuses more photons onto the absorbing core than would otherwise reach it.^{278,279} An approximate absorption enhancement (E_{abs}) of 1.5–2²⁷⁸ and an AAE, valid for the wavelength range between 380 and 750 nm, of 1.6²⁸⁰ has been modeled for an absorbing BC core and both nonabsorbing (clear) and weakly absorbing coatings for core and shell sizes typical of the atmosphere.

5.1. Absorption Amplification in Core–Shell Aerosol

Model results of absorption amplification for coated BC aerosol have been substantiated by laboratory studies for aerosol with core–shell configurations that suggest absorption enhancements of 1–2-fold are plausible.^{70,159,160,281} Single scattering

properties for a core–shell configuration can be calculated from a Mie scattering subroutine adapted for a coated sphere model rather than for a homogeneous sphere [e.g., “DMiLay”,²⁸² “bhcoat” (appendix B in Bohren and Huffman⁷²), and <http://www.wave-scattering.com/codes.html>²⁸³]. Studies that compare calculated extinction and absorption enhancement, predicted from core–shell Mie codes, with laboratory-measured extinction and absorption enhancements show that, generally, measured amplification is reproduced well. For an absorbing substance coated by a nonabsorbing substance, the measured absorption (by PAS) and extinction (by CRD) enhancements agreed with modeled enhancements to within an average of 5%,¹⁶⁰ and somewhat larger discrepancies (up to 10%) were observed for extinction efficiencies as the coating thickness increases.^{66,68} Amplification increased as core size was reduced (for a fixed coating thickness)¹⁵⁹ or as coating thickness was increased.⁷⁰

The absorption enhancement of coated BC will affect the aerosol AAE. However, as enhancement is highly dependent on core size, thickness coating, and internal state of mixing, it is complex to invert from AAE to the fractional contribution of BC, BrC, and mixed BC–BrC aerosol to ambient light absorption, though such knowledge is necessary for radiative forcing estimates of different aerosol constituents over the full solar spectrum.

5.2. Deriving Absorption Contributions of Black Carbon, Brown Carbon, and Internally Mixed Brown–Black Carbon Aerosol Fractions via Multispectral Analysis

Field measurements of the last years have utilized in situ multiwavelength absorption measurements with PAS to measure MAC values at given discrete wavelength pairs and to determine the absorption Ångström exponent (AAE). Multispectral absorption measurements combined with complementary chemical measurements can be utilized to assess the effects of morphology (e.g., coatings), to provide field evidence for laboratory and theoretical findings of enhancement and lensing effect, and as a distinguishing tool between BC and BrC aerosol components.^{69,120,122,123,268}

There are some examples of multispectral absorption measurements that were used to deconvolute the mixing state of ambient carbonaceous aerosol and contributions of non-BC absorbers to measured light absorption. Lack et al.⁶⁹ combine multiwavelength extinction (CRD) and absorption (PAS) measurements of dry and thermal-denuded ambient aerosol to develop an attribution method for absorption and mixing state of organic particulates and black carbon in biomass burning events. The attribution is based on measured enhancement in absorption measured at different wavelengths (532 and 404 nm) between dry and thermodenuded (200 °C) aerosol, where most of the nonrefractory carbon is expected to volatilize at 200 °C and the organic material is considered to be nonabsorbing at $\lambda = 532$ nm. Complementary chemical analysis of nonrefractory particulate matter (by AMS) and BC (by use of SP2, single-particle soot photometer) are used to quantify mass and size distributions of these components. If a BC core size is assumed (constrained by SP2 measurements) and Mie theory is used, a coating thickness is optimized until measured and modeled absorption enhancements match. The amounts of internally and externally mixed BrC can then be determined. The study demonstrates that up to ~80% of particulate organic matter is externally mixed and that BC internally mixed with organic matter and ammonium nitrate has a lens-driven

absorption enhancement of up to 70%. Knowledge of the mixing state and wavelength-dependent absorption allows the evaluation of specific absorptive properties of the organic material, such as RI and MAC. In this study, the imaginary part of the refractive index and MAC for particulate organic matter from biomass burning were determined at $\lambda = 404$ nm as 0.007 (± 0.005) and $0.82 \pm (0.43)$ $\text{m}^2 \cdot \text{g}^{-1}$, respectively (see Table 3). Were the increased absorption at 404 nm vs 532 nm to be attributed to organic matter (OM) alone, without determination of the contribution from internal mixing of BC and OM, the MAC for the BrC would be biased high by up to 50%. In a follow-up study, Lack et al.¹⁶² show that the derived MAC for externally mixed organic matter alone is well-correlated with the AMS measured f_{60}/f_{44} ratio, which appears to be a good proxy for BrC absorption for a forest burning event, close to the source and prior to extensive atmospheric processing.

Similar in situ multiwavelength PAS measurements of dry and thermodenuded samples were conducted around urban sites in California [part of the Carbonaceous Aerosols and Radiative Effects Study (CARES) and CalNex campaigns] to determine aerosol E_{abs} and mixing state. It was shown that photochemical aging produced nonrefractory particulate material and that BC-containing particles grew through condensation of oxygenated organic aerosol and SO_4^{2-} . However, the enhancement factor and thus the lensing effect of coated BC particles by organic matter was determined to be very small,^{118,284,285} and it was suggested that BC may not be embedded as a core within a core–shell structure but rather lie at the edge of mixed particles.¹¹⁸ In a parallel study from the CalNex campaign, TEM analysis of aged particles showed soot to be frequently mixed with organic matter and sulfates or adhering to other particles, but the particles often do not exhibit classic core–shell morphology.⁸⁹ Albedometer measurements at $\lambda = 532$ nm do not indicate a significant enhancement of light absorption due to BC and sulfate or organic mixed composition. On the other hand, increases in MAC values at $\lambda = 532$ nm were linked to higher concentrations of light-absorbing WSOC (measured at $\lambda = 365$ nm), suggesting that also at 532 nm, absorption by soluble brown carbon contributes to the total absorption.⁸⁹ These two studies suggest that, in contrast to BC coatings from biomass events, BC emitted in urban centers dominated by fossil fuel emissions does not exhibit substantial absorption enhancement when internally mixed with non-BC material. This is in contrast to results from laboratory experiments and model calculations for core–shell structures. Models may need to treat BC from fossil-fuel combustion differently than BC from biomass burning.¹¹⁸ Lower absorption enhancements for vehicular-related aerosol in contrast to biomass burning aerosol were also observed by Gyawali et al.,¹²² who suggest that the smaller BC core size for wood smoke than for vehicular emissions may contribute to this difference.

The studies cited utilize multispectral analysis and volatilization to identify coatings as well as direct TEM imaging, together with total EC or BC quantification, aerosol size distribution measurements, and mass fraction analysis of organics and additional ions with AMS. The particles studied were sampled close to the source and not yet aged.

A comprehensive study combining multispectral CRD and PAS measurements with chemical filter analysis was conducted by Flowers et al.¹²³ to quantify the effects of coatings on light absorption for aerosol in Asian aerosol pollution plumes. Chemical composition and $\beta_{\text{abs}}(\lambda)$ data are used to separate

brown carbon, elemental carbon, and coating (morphological) contributions to total aerosol mass absorption cross sections at each wavelength by use of an empirical model. The polluted air masses entrain regional anthropogenic and natural emissions and have varying amounts of particle carbon, sulfate, organics, and nitrate. Absorption enhancement, SSA, and the imaginary part of the refractive index are defined for specific source regions, based on chemical analysis, size and optical data, and the transport trajectory of the plumes. Episodes with higher organic carbon (OC)/sulfate (SO_4^{2-}) and nitrate (NO_3^-)/sulfate (SO_4^{2-}) composition ratios were identified as having a greater biomass burning component and exhibit lower single scattering albedo at shorter wavelengths ($\lambda = 405$ nm) and greater k values at all wavelengths (Table 3). The analysis shows that coatings and processing during transport may enhance light absorption by black carbon by factors of greater than 3 and that MAC_{Br} comprised a substantial part of total MAC for carbonaceous aerosol (50% of light absorption at 405 nm in high OC/ SO_4^{2-} events).

Different results from ambient measurements from biomass events, urban pollution, and aged pollution plumes as to the degree of absorption enhancement of BC coatings indicate that more work is needed to elucidate the effect of coatings on BC absorption and to attribute the effect of lensing and enhancement to different SOA components and sources.

6. SUMMARY AND PROSPECTS

Assessment of radiative forcing of aerosol in models still lacks sufficient input data for spectrally resolved light scattering and absorption by fresh and aged SOA. SOA from anthropogenic precursors displays greater scattering than biogenic SOA, yet the range of SOA RI scattering coefficients, between 1.36 and 1.66 (Table 2), is large and has a significant effect on radiative forcing. For example, the associated change in asymmetry parameter between a real refractive index of 1.4 and 1.5 is estimated to increase radiative forcing for nonabsorbing particles by 12% and likewise to decrease surface-level irradiation.¹¹⁰ Current laboratory measurements are conducted with higher accuracy instrumentation than in the past. They directly measure in situ absorption and can spectrally resolve optical measurements, thus leading current research to new frontiers. Even so, there is variability in recently retrieved m_r values between different experimental procedures for SOA generation and different optical measurements. Different chemical pathways for SOA formation lead to variance in generated oxidation products and SOA composition that affect the aerosol scattering coefficient. The O:C and H:C ratios are not a good enough metric, when used alone, to explain and predict RI. Together with this, concurrent measurements of optical and chemical data indicative of specific functionalities and fragments and density and volatility measurements seem to be the pathway to better interpret the laboratory simulations. Such methodology in future studies could enable a broad and comprehensive optical and chemical database to be compiled, from which the retrieved optical data could be linked to a quantitative chemical state for varied types of precursors and SOA and could better enable application of the data to ambient aerosol and conditions.

Additional uncertainties arise not only from chemical variance of the laboratory SOA (a factor common also to ambient SOA) but also experimental uncertainties in optical systems, length of interaction between particle and laser beam, particle counting efficiency, and particle diameter. In

accumulation mode, where extinction efficiency varies steeply with particle size,^{84,86,286} these issues can be overcome by improved calibration procedures,⁸⁶ improved instrumentation,¹²⁹ and alternative methodologies, such as single-particle analysis, that can reduce the uncertainties significantly.^{175,286}

Spectrally resolved measurements explicitly show the major impact of light absorption by SOA at wavelengths that drive photochemical reactions. The value of spectrally resolved data is apparent in Figure 14, which displays an example from Liu et

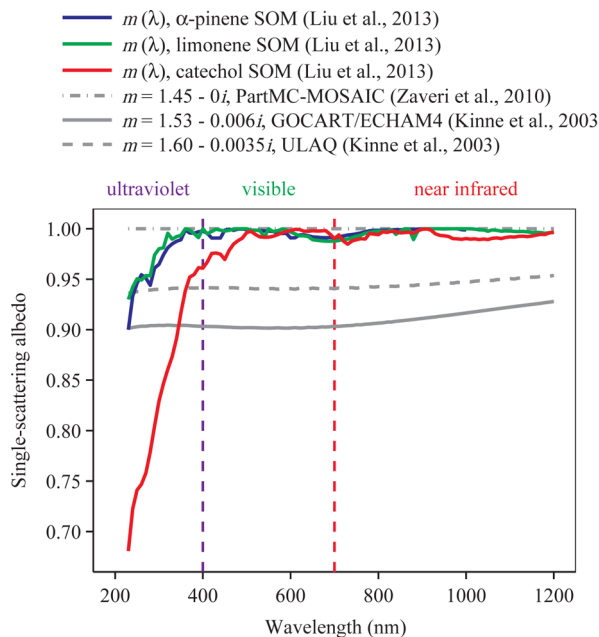


Figure 14. Modeled effective single-scattering albedo, ω_{eff} , based on the results of Liu et al.⁵⁹ for $m_r(\lambda)$ and a typical atmospheric particle number-diameter distribution measured during the Amazonian Aerosol Characterization Experiment (AMAZE-08).²⁹ Results based on optical constants reported in the literature are shown for comparison. Adapted with permission from ref 59. Copyright 2013 American Chemical Society.

al.⁵⁹ in which optical properties of ambient biogenic SOA were calculated by applying the measured laboratory RI for biogenic (terpene and humic-like proxy) SOA to a representative particle population of the central Amazon basin in the wet season, which is dominated by secondary organic material. In Figure 14, SSA values are shown for the full solar spectrum modeled both with spectrally resolved optical constants from Liu et al.⁵⁹ and with optical constants reported in the literature (for which SSA is uniform along the spectrum). The modeled SSA demonstrates how the spectral data resolve for threshold wavelengths, below which SSA becomes <1 . It appears that, in visible wavelengths, fresh biogenic SOA do not absorb light and do not contribute to BrC.

With regard to light-absorbing properties of aqueous SOA, some studies suggest that the structure of organic precursor and product chromophore compounds is crucial rather than a particular combination of functional groups. However, for many of the complex organics, such as HULIS, the dominating chromophore(s) have not been identified yet, and the absorption may be due to charge-transfer complexes or interactions between chromophores. It is possible that the source of absorption in complex organics such as HULIS does not originate from specific chromophores but rather from

charge-transfer interactions that are responsible for the broad absorption that extends to long wavelengths.^{240,241}

Significant changes in relative humidity should favor brown carbon production via the NH₄-mediated SOA aging pathway, suggesting that browning reactions are accelerated by cloud and fog processing of aerosol.²¹⁵ Conditions with frequent changes in humidity, high concentration of reduced nitrogen compounds, and high photochemical activity may exist in predominantly agricultural and forested areas. In such areas, NH₃/NH₄ SOA brown carbon may potentially become a dominant contributor to aerosol absorption.²⁵

The MAC value for products of NH₃(g) reaction with limonene SOA were about 2 times larger than for the aqueous reactions or evaporative aging.²¹⁵ Bulk-phase reactions of dissolved SOA with NH₃/NH₄ can identify the chemical changes that lead to absorbing components, but particle-size-resolved information is lost. Additionally, the rates of transport of reactants and products in and out of the condensed phase differ between in situ aerosol reactions and bulk solution reactions. Retrieval of refractive indices via in situ reactions of ammonia with biogenic SOA enables quantitative assessment of the climatic impact of these reactions. The observed change in refractive index due to terpene SOA aging by NH₃ (from $k \approx 0$ to $k \approx 0.05$) can lead to a decrease in the cooling effect of aerosol by a factor of 3 (from -28 to $-9.6 \text{ W}\cdot\text{g}^{-1}$), as calculated¹⁰⁵ with a wavelength-dependent version of the simple forcing efficiency proposed by Bond and Bergstrom.³ However, this drastic change may only occur where NH₃ concentrations reach very high levels, >1 ppm, as has been observed in forest fire plumes.²⁸⁷

SOA has been shown to comprise a significant fraction of BrC. BrC absorption by anthropogenic SOA lies in the lower range of BrC absorption by biomass burning organic aerosol (BBOA), but as the global production rate of SOA is thought to be significantly larger than the production rate of BBOA,²⁸ absorption by SOA could be potentially significant. Even so, MAC values of anthropogenic SOA and NH₃/NH₄-aged SOA are much lower (upper limit of $\sim 0.5 \text{ m}^2\cdot\text{g}^{-1}$) than those of ambient BrC samples, even those thought to be explicitly composed of SOA (such as WSOC extracts). As discussed, the NH₃/NH₄-aged SOA would most probably be atmospherically relevant only at very specific localities. Yet dramatic changes in composition and optical properties of dissolved dicarbonyls and terpene SOA organics in the presence of NH₃/NH₄ during evaporation of water droplets^{218,249} would support further studies on additional reactive organic pathways in the aqueous phase as additional sources of light-absorbing SOA.

Field studies that directly deconvolute measured absorption into its absorbing carbonaceous constituents (BC, mixed BC particles, and BrC) enable derivation of MAC and RI for each constituent of the ambient absorbing aerosol and provide in situ data on absorption amplification for aged and coated BC aerosol. As seen from the radiative forcing assessment by Wang et al.,⁵ this enables more accurate radiative forcing assessments for both BrC aerosol and BC aerosol components.

6.1. Recommendations for Future Directions

This review discussed the current state of knowledge in laboratory measurements on optical properties of SOA in the near-UV and visible wavelength range and highlighted some remaining gaps. Occurrence, sources, and properties of brown carbon in the atmosphere remain major topics to understand. From the compilation of refractive indices that we presented, it

is clear that there are important gaps in measuring scattering and absorption by SOA. Understanding the spread of RI values for different SOA, and a good assessment of the implications of these values, should be undertaken in order to direct further research.

Only a few studies have tried to untangle the connection between complex refractive indices of SOA and specific molecular constituents. We suggest that more studies should further explore how scattering and absorbing properties are related to chemical composition, existence of specific chromophores, or other forms of absorbing species in complex matrices, such as charge-transfer complexes.

Most of the laboratory- and ambient-derived RI discussed in this review assume that organic aerosols are spherical and homogeneous. Some derive the RI based on a mixed composition, by use of a core–shell model for aerosol morphology. Sphericity and homogeneity are, however, not always the case. Although many theoretical studies relate to the effects of mixed composition, nonsphericity, phase separation, surface roughness, and porosity of particles on the measured optical parameter (scattering, extinction, and absorption) (see Adler et al.¹⁴⁸), additional experimental work needs to be conducted to support the theoretical approaches and elucidate the importance of these parameters to derived RI values.

Recent findings that link the extent of absorbance to the BC:OA ratio for aged and fresh biomass burning aerosol²³² is a potentially strong predictive tool for light-absorbing properties of biomass burning aerosol and should be validated in further studies.

Spectral dependence of both scattering and absorbing coefficients of SOA implicates the need to develop further spectrally resolved optical measurements, both for inclusion into optical databases of aerosol particles used for direct radiative forcing assessments and to improve aerosol data retrieved from spectral satellite retrievals. It is also clear that RI values of SOA in the thermal and IR spectral ranges are needed. Broadband instruments, together with instruments that measure absorption and or scattering together with total extinction, should continue to be developed. For deployment also for field measurements, simple, portable (and inexpensive) systems such as CAPS can be advantageous.

The large regions where biogenic and anthropogenic precursor VOCs coexist support additional studies on the optical properties of such mixed SOA. To date, only one study on mixed AVOC and BVOC SOA has been conducted,⁶¹ in which it was demonstrated that mixed-composition AVOC + BVOC have a somewhat lower real part of RI than the RI measured for AVOC alone ($\Delta n = -0.05$ to -0.10 at $\lambda = 405$ nm). Also, optical absorption seems to be lower in regions influenced by mixed-composition SOA precursors.²¹ This is especially relevant as there is evidence of enhanced SOA formation from biogenic precursors following reactions with regional anthropogenic emissions.^{37,288}

In urban areas, one would expect a contribution to SOA also from nonaromatic anthropogenic compounds, such as aliphatic compounds from diesel exhaust,²⁸⁹ and for these, optical measurements are lacking and there are no representative optical values. The single RI measurement of aliphatic tricyclo[5.2.1.0^{2,6}]decane presents RI values (both m_r and k) more similar to biogenic α -pinene than anthropogenic toluene or naphthalene.⁶³ We suggest that more studies on mixtures of anthropogenic and biogenic SOA should be conducted.

Further work is needed to link the properties of laboratory-generated SOA to atmospheric observations. In the atmosphere, a wide range of precursors contributes to SOA formation, resulting in a more complex SOA composition compared to the single-precursor laboratory systems.⁴⁴ Recently, laboratory and chamber studies pertaining to SOA formation pathways and yields have been conducted with real plant emissions.^{180,183,184} Optical measurements can be conducted with similar type experiments, with real plants,¹⁷⁶ groups of plants, and background pollutants and additional urban SOA precursors to learn about the products of these more realistic interactions. Similarly, additional optical measurements could be conducted for realistic anthropogenic organic complex mixtures, such as those conducted by Adler et al.⁹⁸ for water-soluble organics from tailpipe emissions.

Updyke et al.²⁵ previously suggested conducting experiments with field samples collected from different locations: for example, aerosol from Amazon forest dominated by isoprene SOA versus boreal forests dominated by α -pinene SOA versus urban environments, to test whether the browning chemistry described in laboratory experiments occurs also in the ambient aerosol. Focused field campaigns that include optical and chemical measurements of fresh and aged SOA samples from biogenic, anthropogenic, and mixed-source regions could contribute to the application of controlled experimental results to predictive models.

Additional pathways for generation of light-absorbing SOA that contribute to atmospheric BrC need to be elucidated. Nitration of PAH has been shown to lead to optical absorption.^{15,67} In addition, the study of Rollins et al.²⁹⁰ suggests that NO_x can control light absorption by aerosol formed during the night. Thus, additional studies on NO_3 reactions with BSOA could contribute information on nighttime reaction pathways that form BrC in forested regions.

Properties of aqueous SOA, especially from biomass burning, are not well-constrained. Aqueous-phase photolysis and oxidation by H_2O_2 , OH, and triplet excited states of organic compounds (3C*) of phenolic compounds (e.g., phenol, guaiacol, and syringol) can form secondary organic aerosol at high yields^{223,225,291} and have been shown to be light-absorbing.²²³ Further studies on aqueous SOA and specifically phenols should be studied to better identify and quantify their light-absorbing properties. When the liquid water content of a wet aerosol with a mixed highly oxidized organic/inorganic salt composition decreases upon drying, liquid–liquid phase separation may occur.²⁹² It is important to understand if and how this may affect aerosol absorption and scattering.

Inconsistent results from field campaigns with regard to absorption enhancement of BC aerosol clearly indicate that more work is needed to elucidate the effect of coatings on absorption and to attribute the effect of lensing and enhancement to different SOA components.

This review focused on optical properties of organic aerosol in the near-UV and visible range. Black carbon, dust, and mineral particles also absorb light in the atmosphere, and further work should be conducted also on mineral dust to better resolve the optical properties of these aerosols and their contribution to radiative forcing when in a mixed state with organic aerosol.

Finally, recent studies point to decreased absorption following reactions and photobleaching of absorbing organics. Hence, additional studies should focus on the fate of absorbing species in aerosol under atmospheric conditions and how they

evolve with time, and determination of dominant bleaching factors and the resulting species.

AUTHOR INFORMATION

Corresponding Author

*E-mail yinon.rudich@weizmann.ac.il.

Notes

The authors declare no competing financial interest.

Biographies



Yinon Rudich received his B.Sc. degree from Ben Gurion University and M.Sc. and Ph.D. degrees in chemical physics from the Weizmann Institute. Following postdoctoral work at the National Oceanic and Atmospheric Administration, he joined the Weizmann Institute of Science, where he is presently a professor in the Department of Earth and Planetary Sciences. His research interests include the chemistry and physical properties of organic aerosols, ice nucleation, bioaerosols, and the health effects of atmospheric aerosols. Other interests include heterogeneous atmospheric chemistry and development of new analytical techniques for characterization of atmospheric particles and bio aerosols. He was editor of the *Journal of Geophysical Research: Atmospheres*.

Tamar Moise received her B.Sc. and M.Sc. degrees from the Hebrew University and continued to a Ph.D. degree and postdoctoral research at the Department of Earth and Planetary Sciences at the Weizmann Institute. She has continued to research in the Atmospheric Chemistry group of Y. Rudich while, in parallel, utilizing her broad earth science background for scientific consultancy in other related fields. Her interests include the chemistry of organic aerosols, phase transformations of organic aerosol, aerosol optics, and aerosol–climate interactions.



J. Michel Flores received his B.Sc. degrees in physics and mathematics from The Pennsylvania State University, his M.Sc. in atmospheric physics from the Universidad Nacional Autónoma de México, and his Ph.D. degree in atmospheric physics from the Institute for Atmospheric Physics at the Johannes Gutenberg University. He is currently a postdoctoral fellow at the Department of Earth and Planetary Sciences in the Weizmann Institute of Science. His research interests include the physicochemistry of organic aerosols, cloud–aerosol interactions, and ocean–atmosphere interactions. Other interests include the development of new instrumentation for characterization of atmospheric particles.

ACKNOWLEDGMENTS

We acknowledge continuous support from the Israel Science Foundation (Grant 913/12), USA–Israel Binational Science Foundation (BSF, Grant 2012013) and by the German–Israel Science Foundation (Grant 1136-26.8/2011).

ABBREVIATIONS

β_{ext} , β_{abs} , β_{sca}	extinction, absorption, and scattering coefficients (Mm^{-1})
σ_{ext} , σ_{abs} , σ_{sca}	extinction, absorption, and scattering cross sections (m^2)
ω	ratio of the scattering and extinction cross sections (also termed SSA)
AAE	absorption Ångström exponent
ABSOA	mixed anthropogenic and biogenic secondary organic aerosol
AMS	aerosol mass spectrometry
AS	ammonium sulfate
ASOA	anthropogenic secondary organic aerosol
AVOC	anthropogenic volatile organic compounds
BC	black carbon
BrC	brown carbon
BSOA	biogenic secondary organic aerosol
BVOC	biogenic volatile organic compounds
CRDS	cavity ring-down spectroscopy
DESI-UHR-MS	desorption electrospray ionization ultra-high-resolution mass spectrometry
DBE	double-bond-equivalent
E_{abs}	absorption enhancement
ELVOC	extremely low volatility organic compounds
IPCC	Intergovernmental Panel on Climate Change
k	imaginary part of refractive index
LVOC	low-volatility organic compounds
MAC	mass absorption cross section or mass absorption coefficient ($\text{m}^2 \cdot \text{g}^{-1}$)

m_r	real part of refractive index
OA	organic aerosol
OOA	oxygenated organic aerosol
OC	organic carbon
PAH	polycyclic aromatic hydrocarbons
PAS	photoacoustic spectrometry
PM	particulate matter
Q_{ext} , Q_{abs} , Q_{sca}	extinction, absorption, and scattering efficiencies
RH	relative humidity
RI	refractive index
RF	radiative forcing
SOA	secondary organic aerosol
SRFA	Suwannee River fulvic acid
SSA	single scattering albedo, ω
SVOC	semivolatile organic compounds
TEM	transmission electron microscopy
VOC	volatile organic compounds

REFERENCES

- (1) Boucher, O.; Randall, D.; Artaxo, P.; Bretherton, C.; Feingold, G.; Forster, P.; Kärninen, V.-M.; Kondo, Y.; Liao, H.; Lohmann, U.; Rasch, P.; Satheesh, S. K.; Sherwood, S.; Stevens, B.; Zhang, X. Y. Clouds and Aerosols. In *Climate Change 2013: The Physical Science Basis*. Contribution of Working Group I to the Fifth Assessment Report of the Intergovernmental Panel on Climate Change, 2013.
- (2) Andreae, M. O.; Ramanathan, V. *Science* **2013**, *340*, 280.
- (3) Bond, T. C.; Bergstrom, R. W. *Aerosol Sci. Technol.* **2006**, *40*, 27.
- (4) Bond, T. C.; Doherty, S. J.; Fahey, D. W.; Forster, P. M.; Berntsen, T.; DeAngelo, B. J.; Flanner, M. G.; Ghan, S.; Kärcher, B.; Koch, D.; Kinne, S.; Kondo, Y.; Quinn, P. K.; Sarofim, M. C.; Schultz, M. G.; Schulz, M.; Venkataraman, C.; Zhang, H.; Zhang, S.; Bellouin, N.; Guttikunda, S. K.; Hopke, P. K.; Jacobson, M. Z.; Kaiser, J. W.; Klimont, Z.; Lohmann, U.; Schwarz, J. P.; Shindell, D.; Storelvmo, T.; Warren, S. G.; Zender, C. S. *J. Geophys. Res.: Atmos.* **2013**, *118*, 5380.
- (5) Wang, X.; Heald, C. L.; Ridley, D. A.; Schwarz, J. P.; Spackman, J. R.; Perring, A. E.; Coe, H.; Liu, D.; Clarke, A. D. *Atmos. Chem. Phys.* **2014**, *10*, 10989.
- (6) Myhre, G.; Samset, B. H.; Schulz, M.; Balkanski, Y.; Bauer, S.; Berntsen, T. K.; Bian, H.; Bellouin, N.; Chin, M.; Diehl, T.; Easter, R. C.; Feichter, J.; Ghan, S. J.; Hauglustaine, D.; Iversen, T.; Kinne, S.; Kirkevag, A.; Lamarque, J. F.; Lin, G.; Liu, X.; Lund, M. T.; Luo, G.; Ma, X.; van Noije, T.; Penner, J. E.; Rasch, P. J.; Ruiz, A.; Selard, O.; Skeie, R. B.; Stier, P.; Takemura, T.; Tsigaridis, K.; Wang, P.; Wang, Z.; Xu, L.; Yu, H.; Yoo, F.; Yoon, J. H.; Zhang, K.; Zhang, H.; Zhou, C. *Atmos. Chem. Phys.* **2013**, *13*, 1853.
- (7) Andreae, M. O.; Gelencser, A. *Atmos. Chem. Phys.* **2006**, *6*, 3131.
- (8) Kirchstetter, T. W.; Novakov, T.; Hobbs, P. V. *J. Geophys. Res.: Atmos.* **2004**, *109*, No. D21208.
- (9) Liu, J.; Scheuer, E.; Dibb, J.; Ziembka, L. D.; Thornhill, K. L.; Anderson, B. E.; Wisthaler, A.; Mikoviny, T.; Devi, J. J.; Bergin, M.; Weber, R. J. *Geophys. Res. Lett.* **2014**, *41*, 2191 DOI: 10.1002/2013GL058976.
- (10) Sun, H.; Biedermann, L.; Bond, T. C. *Geophys. Res. Lett.* **2007**, *34*, No. L17813.
- (11) Chung, C. E.; Ramanathan, V.; Decremer, D. *Proc. Natl. Acad. Sci. U.S.A.* **2012**, *109*, 11624.
- (12) Kirchstetter, T. W.; Thatcher, T. L. *Atmos. Chem. Phys.* **2012**, *12*, 6067.
- (13) Lin, G.; Penner, J. E.; Flanner, M. G.; Sillman, S.; Xu, L.; Zhou, C. *J. Geophys. Res.: Atmos.* **2014**, *119*, 7453 DOI: 10.1002/2013JD021186.
- (14) Hecobian, A.; Zhang, X.; Zheng, M.; Frank, N.; Edgerton, E. S.; Weber, R. J. *Atmos. Chem. Phys.* **2010**, *10*, 5965.
- (15) Jacobson, M. Z. *J. Geophys. Res.: Atmos.* **1999**, *104*, 3527.
- (16) Alexander, D. T. L.; Crozier, P. A.; Anderson, J. R. *Science* **2008**, *321*, 833.
- (17) Chakrabarty, R. K.; Moosmüller, H.; Chen, L. W. A.; Lewis, K.; Arnott, W. P.; Mazzoleni, C.; Dubey, M. K.; Wold, C. E.; Hao, W. M.; Kreidenweis, S. M. *Atmos. Chem. Phys.* **2010**, *10*, 6363.
- (18) Lukács, H.; Gelencsér, A.; Hammer, S.; Puxbaum, H.; Pio, C.; Legrand, M.; Kasper-Giebl, A.; Handler, M.; Limbeck, A.; Simpson, D.; Preunkert, S. *J. Geophys. Res.: Atmos.* **2007**, *112*, No. D23S18.
- (19) Utry, N.; Ajtai, T.; Filep, A.; Pinter, M. D.; Hoffer, A.; Bozoki, Z.; Szabo, G. *Atmos. Environ.* **2013**, *69*, 321.
- (20) Shapiro, E. L.; Szprengiel, J.; Sareen, N.; Jen, C. N.; Giordano, M. R.; McNeill, V. F. *Atmos. Chem. Phys.* **2009**, *9*, 2289.
- (21) Zhang, X.; Lin, Y.-H.; Surratt, J. D.; Zotter, P.; Prévôt, A. S. H.; Weber, R. J. *Geophys. Res. Lett.* **2011**, *38*, L21810.
- (22) Bones, D. L.; Henricksen, D. K.; Mang, S. A.; Gonsior, M.; Bateman, A. P.; Nguyen, T. B.; Cooper, W. J.; Nizkorodov, S. A. *J. Geophys. Res.: Atmos.* **2010**, *115*, No. D05203.
- (23) Cappa, C. D.; Che, D. L.; Kessler, S. H.; Kroll, J. H.; Wilson, K. R. *J. Geophys. Res.: Atmos.* **2011**, *116*, D15204.
- (24) Nguyen, T. B.; Laskin, A.; Laskin, J.; Nizkorodov, S. A. *Faraday Discuss.* **2013**, *165*, 473.
- (25) Updyke, K. M.; Nguyen, T. B.; Nizkorodov, S. A. *Atmos. Environ.* **2012**, *63*, 22.
- (26) Stocker, T. F.; Qin, D.; Plattner, G.-K.; Alexander, L.V.; Allen, S. K.; Bindoff, N. L.; Bréon, F.-M.; Church, J. A.; Cubasch, U.; Emori, S.; Forster, P.; Friedlingstein, P.; Gillett, N.; Gregory, J. M.; Hartmann, D. L.; Jansen, E.; Kirtman, B.; Knutti, R.; Krishna Kumar, K.; Lemke, P.; Marotzke, J.; Masson-Delmotte, V.; Meehl, G.A.; Mokhov, I. I.; Piao, S.; Ramaswamy, V.; Randall, D.; Rhein, M.; Rojas, M.; Sabine, C.; Shindell, D.; Talley, L. D.; Vaughan, D. G.; Xie, S.-P. Technical Summary. In *Climate Change 2013: The Physical Science Basis*. Contribution of Working Group I to the Fifth Assessment Report of the Intergovernmental Panel on Climate Change, 2013.
- (27) Goldstein, A. H.; Galbally, I. E. *Environ. Sci. Technol.* **2007**, *41*, 1514.
- (28) Hallquist, M.; Wenger, J. C.; Baltensperger, U.; Rudich, Y.; Simpson, D.; Claeys, M.; Dommen, J.; Donahue, N. M.; George, C.; Goldstein, A. H.; Hamilton, J. F.; Herrmann, H.; Hoffmann, T.; Iinuma, Y.; Jang, M.; Jenkin, M. E.; Jimenez, J. L.; Kiendler-Scharr, A.; Maenhaut, W.; McFiggans, G.; Mentel, T. F.; Monod, A.; Prevot, A. S. H.; Seinfeld, J. H.; Surratt, J. D.; Szmigielski, R.; Wildt, J. *Atmos. Chem. Phys.* **2009**, *9*, 5155.
- (29) Heald, C. L.; Kroll, J. H.; Jimenez, J. L.; Docherty, K. S.; DeCarlo, P. F.; Aiken, A. C.; Chen, Q.; Martin, S. T.; Farmer, D. K.; Artaxo, P. *Geophys. Res. Lett.* **2010**, *37*, No. L08803.
- (30) Kanakidou, M.; Seinfeld, J. H.; Pandis, S. N.; Barnes, I.; Dentener, F. J.; Facchini, M. C.; Van Dingenen, R.; Ervens, B.; Nenes, A.; Nielsen, C. J.; Swietlicki, E.; Putaud, J. P.; Balkanski, Y.; Fuzzi, S.; Horth, J.; Moortgat, G. K.; Winterhalter, R.; Myhre, C. E. L.; Tsigaridis, K.; Vignati, E.; Stephanou, E. G.; Wilson, J. *Atmos. Chem. Phys.* **2005**, *5*, 1053.
- (31) Spracklen, D. V.; Jimenez, J. L.; Carslaw, K. S.; Worsnop, D. R.; Evans, M. J.; Mann, G. W.; Zhang, Q.; Canagaratna, M. R.; Allan, J.; Coe, H.; McFiggans, G.; Rap, A.; Forster, P. *Atmos. Chem. Phys.* **2011**, *11*, 12109.
- (32) De Gouw, J.; Jimenez, J. L. *Environ. Sci. Technol.* **2009**, *43*, 7614.
- (33) Weber, R. J.; Sullivan, A. P.; Peltier, R. E.; Russell, A.; Yan, B.; Zheng, M.; de Gouw, J.; Warneke, C.; Brock, C.; Holloway, J. S.; Atlas, E. L.; Edgerton, E. J. *Geophys. Res.: Atmos.* **2007**, *112*, D13302.
- (34) Setyan, A.; Song, C.; Merkel, M.; Knighton, W. B.; Onasch, T. B.; Canagaratna, M. R.; Worsnop, D. R.; Wiedensohler, A.; Shilling, J. E.; Zhang, Q. *Atmos. Chem. Phys.* **2014**, *14*, 6477.
- (35) Emanuelsson, E. U.; Hallquist, M.; Kristensen, K.; Glasius, M.; Bohn, B.; Fuchs, H.; Kammer, B.; Kiendler-Scharr, A.; Nehr, S.; Rubach, F.; Tillmann, R.; Wahner, A.; Wu, H. C.; Mentel, T. F. *Atmos. Chem. Phys.* **2013**, *13*, 2837.
- (36) Glasius, M.; la Cour, A.; Lohse, C. *J. Geophys. Res.: Atmos.* **2011**, *116*, D11302.
- (37) Hoyle, C. R.; Boy, M.; Donahue, N. M.; Fry, J. L.; Glasius, M.; Guenther, A.; Hallar, A. G.; Huff Hartz, K.; Petters, M. D.; Petäjä, T.; Rosenoern, T.; Sullivan, A. P. *Atmos. Chem. Phys.* **2011**, *11*, 321.

- (38) Kautzman, K. E.; Surratt, J. D.; Chan, M. N.; Chan, A. W. H.; Hersey, S. P.; Chhabra, P. S.; Daleska, N. F.; Wennberg, P. O.; Flagan, R. C.; Seinfeld, J. H. *J. Phys. Chem. A* **2010**, *114*, 913.
- (39) Hildebrandt, L.; Henry, K. M.; Kroll, J. H.; Worsnop, D. R.; Pandis, S. N.; Donahue, N. M. *Environ. Sci. Technol.* **2011**, *45*, 6329.
- (40) Chen, J. J.; Griffin, R. J. *Atmos. Environ.* **2005**, *39*, 7731.
- (41) Ervens, B.; Turpin, B. J.; Weber, R. J. *Atmos. Chem. Phys.* **2011**, *11*, 11069.
- (42) Kalberer, M.; Paulsen, D.; Sax, M.; Steinbacher, M.; Dommen, J.; Prevot, A. S. H.; Fisseha, R.; Weingartner, E.; Frankevich, V.; Zenobi, R.; Baltensperger, U. *Science* **2004**, *303*, 1659.
- (43) Kitanovski, Z.; Čusak, A.; Grgić, I.; Claeys, M. *Atmos. Meas. Tech.* **2014**, *7*, 2457.
- (44) Kourtchev, I.; Fuller, S. J.; Giorio, C.; Healy, R. M.; Wilson, E.; O'Connor, I. P.; Wenger, J. C.; McLeod, M.; Aalto, J.; Ruuskanen, T. M.; Maenhaut, W.; Jones, R.; Venables, D. S.; Sodeau, J. R.; Kulmala, M.; Kalberer, M. *Atmos. Chem. Phys.* **2013**, *13*, 2155.
- (45) Lee, H. J.; Laskin, A.; Laskin, J.; Nizkorodov, S. A. *Environ. Sci. Technol.* **2013**, *47*, 5763.
- (46) Lin, G.; Sillman, S.; Penner, J. E.; Ito, A. *Atmos. Chem. Phys.* **2014**, *14*, 5451.
- (47) Sareen, N.; Schwier, A. N.; Shapiro, E. L.; Mitroo, D.; McNeill, V. F. *Atmos. Chem. Phys.* **2010**, *10*, 997.
- (48) Sato, K.; Hatakeyama, S.; Imamura, T. *J. Phys. Chem. A* **2007**, *111*, 9796.
- (49) Shakya, K. M.; Liu, S.; Takahama, S.; Russell, L. M.; Keutsch, F. N.; Galloway, M. M.; Shilling, J. E.; Hirunuma, N.; Song, C.; Kim, H.; Paulson, S. E.; Pfaffenberger, L.; Barmet, P.; Slowik, J.; Prévôt, A. S. H.; Dommen, J.; Baltensperger, U. *Aerosol Sci. Technol.* **2013**, *47*, 543.
- (50) Shilling, J. E.; Zaveri, R. A.; Fast, J. D.; Kleinman, L.; Alexander, M. L.; Canagaratna, M. R.; Fortner, E.; Hubbe, J. M.; Jayne, J. T.; Sedlacek, A.; Setyan, A.; Springston, S.; Worsnop, D. R.; Zhang, Q. *Atmos. Chem. Phys.* **2013**, *13*, 2091.
- (51) Rudich, Y.; Donahue, N. M.; Mentel, T. F. *Annu. Rev. Phys. Chem.* **2007**, *58*, 321.
- (52) Pye, H. O. T.; Seinfeld, J. H. *Atmos. Chem. Phys.* **2010**, *10*, 4377.
- (53) Tsigaridis, K.; Daskalakis, N.; Kanakidou, M.; Adams, P. J.; Artaxo, P.; Bahadur, R.; Balkanski, Y.; Bauer, S. E.; Bellouin, N.; Benedetti, A.; Bergman, T.; Berntsen, T. K.; Beukes, J. P.; Bian, H.; Carslaw, K. S.; Chin, M.; Curci, G.; Diehl, T.; Easter, R. C.; Ghan, S. J.; Gong, S. L.; Hodzic, A.; Hoyle, C. R.; Iversen, T.; Jathar, S.; Jimenez, J. L.; Kaiser, J. W.; Kirkevåg, A.; Koch, D.; Kokkola, H.; Lee, Y. H.; Lin, G.; Liu, X.; Luo, G.; Ma, X.; Mann, G. W.; Mihalopoulos, N.; Morcrette, J. J.; Müller, J. F.; Myhre, G.; Myriokefalitakis, S.; Ng, S.; O'Donnell, D.; Penner, J. E.; Pozzoli, L.; Pringle, K. J.; Russell, L. M.; Schulz, M.; Sciaire, J.; Seland, Ø.; Shindell, D. T.; Sillman, S.; Skeie, R. B.; Spracklen, D.; Stavrakou, T.; Steenrod, S. D.; Takemura, T.; Tiitta, P.; Tilmes, S.; Tost, H.; van Noije, T.; van Zyl, P. G.; von Salzen, K.; Yu, F.; Wang, Z.; Wang, Z.; Zaveri, R. A.; Zhang, H.; Zhang, K.; Zhang, Q.; Zhang, X. *Atmos. Chem. Phys.* **2014**, *14*, 6027.
- (54) Corr, C. A.; Krotkov, N.; Madronich, S.; Slusser, J. R.; Holben, B.; Gao, W.; Flynn, J.; Lefer, B.; Kreidenweis, S. M. *Atmos. Chem. Phys.* **2009**, *9*, 5813.
- (55) Liu, P. F.; Abdelmalki, N.; Hung, H. M.; Wang, Y.; Brune, W. H.; Martin, S. T. *Atmos. Chem. Phys.* **2015**, *15*, 1435.
- (56) Shindell, D. T.; Faluvegi, G.; Koch, D. M.; Schmidt, G. A.; Unger, N.; Bauer, S. E. *Science* **2009**, *326*, 716.
- (57) Shindell, D. T.; Lamarque, J. F.; Schulz, M.; Flanner, M.; Jiao, C.; Chin, M.; Young, P. J.; Lee, Y. H.; Rotstain, L.; Mahowald, N.; Milly, G.; Faluvegi, G.; Balkanski, Y.; Collins, W. J.; Conley, A. J.; Dalsoren, S.; Easter, R.; Ghan, S.; Horowitz, L.; Liu, X.; Myhre, G.; Nagashima, T.; Naik, V.; Rumbold, S. T.; Skeie, R.; Sudo, K.; Szopa, S.; Takemura, T.; Voulgarakis, A.; Yoon, J. H.; Lo, F. *Atmos. Chem. Phys.* **2013**, *13*, 2939.
- (58) Moosmüller, H.; Chakrabarty, R. K.; Arnott, W. P. *J. Quant. Spectrosc. Radiat. Transfer* **2009**, *110*, 844.
- (59) Liu, P.; Zhang, Y.; Martin, S. T. *Environ. Sci. Technol.* **2013**, *47*, 13594.
- (60) Kim, H.; Liu, S.; Russell, L. M.; Paulson, S. E. *Aerosol Sci. Technol.* **2014**, *48*, 498.
- (61) Flores, J. M.; Zhao, D. F.; Segev, L.; Schlag, P.; Kiendler-Scharr, A.; Fuchs, H.; Watne, Å. K.; Bluvshtein, N.; Mentel, T. F.; Hallquist, M.; Rudich, Y. *Atmos. Chem. Phys.* **2014**, *14*, 5793.
- (62) Kim, H.; Paulson, S. E. *Atmos. Chem. Phys.* **2013**, *13*, 7711.
- (63) Lambe, A. T.; Cappa, C. D.; Massoli, P.; Onasch, T. B.; Forestieri, S. D.; Martin, A. T.; Cummings, M. J.; Croasdale, D. R.; Brune, W. H.; Worsnop, D. R.; Davidovits, P. *Environ. Sci. Technol.* **2013**, *47*, 6349.
- (64) Nakayama, T.; Sato, K.; Matsumi, Y.; Imamura, T.; Yamazaki, A.; Uchiyama, A. *Atmos. Chem. Phys.* **2013**, *13*, 531.
- (65) Zarzana, K. J.; De Haan, D. O.; Freedman, M. A.; Hasenkopf, C. A.; Tolbert, M. A. *Environ. Sci. Technol.* **2012**, *46*, 4845.
- (66) Lang-Yona, N.; Abo-Riziq, A.; Erlick, C.; Segre, E.; Trainic, M.; Rudich, Y. *Phys. Chem. Chem. Phys.* **2010**, *12*, 21.
- (67) Lu, J. W.; Flores, J. M.; Lavi, A.; Abo-Riziq, A.; Rudich, Y. *Phys. Chem. Chem. Phys.* **2011**, *13*, 6484.
- (68) Riziq, A. A.; Trainic, M.; Erlick, C.; Segre, E.; Rudich, Y. *Atmos. Chem. Phys.* **2008**, *8*, 1823.
- (69) Lack, D. A.; Langridge, J. M.; Bahreini, R.; Cappa, C. D.; Middlebrook, A. M.; Schwarz, J. P. *Proc. Natl. Acad. Sci. U.S.A.* **2012**, *109*, 14802.
- (70) Shiraiwa, M.; Kondo, Y.; Iwamoto, T.; Kita, K. *Aerosol Sci. Technol.* **2010**, *44*, 46.
- (71) Kerker, M. *The Scattering of Light and Other Electromagnetic Radiation*; Academic Press: New York, 1969.
- (72) Bohren, C. F.; Huffman, D. R. *Absorption and Scattering of Light by Small Particles*; Wiley: New York, 1983.
- (73) Hinds, W. H. *Aerosol Technology: Properties, Behavior, and Measurement of Airborne Particles*, 2nd ed.; John Wiley & Sons: New York, 1999.
- (74) Redmond, H. E.; Dial, K. D.; Thompson, J. E. *Aeolian Res.* **2010**, *2*, 5.
- (75) Bluvshtein, N.; Flores, J. M.; Riziq, A. A.; Rudich, Y. *Aerosol Sci. Technol.* **2012**, *46*, 1140.
- (76) Dinar, E.; Riziq, A. A.; Spindler, C.; Erlick, C.; Kiss, G.; Rudich, Y. *Faraday Discuss.* **2008**, *137*, 279.
- (77) Flores, J. M.; Bar-Or, R. Z.; Bluvshtein, N.; Abo-Riziq, A.; Kostinski, A.; Borrmann, S.; Koren, I.; Koren, I.; Rudich, Y. *Atmos. Chem. Phys.* **2012**, *12*, 5511.
- (78) Laj, P.; Klausen, J.; Bilde, M.; Plass-Duelmer, C.; Pappalardo, G.; Clerbaux, C.; Baltensperger, U.; Hjorth, J.; Simpson, D.; Reimann, S.; Coheur, P. F.; Richter, A.; De Maziere, M.; Rudich, Y.; McFiggans, G.; Torsæth, K.; Wiedensohler, A.; Morin, S.; Schulz, M.; Allan, J. D.; Attie, J. L.; Barnes, I.; Birmili, W.; Cammas, J. P.; Dommen, J.; Dorn, H. P.; Fowler, D.; Fuzzi, S.; Glasius, M.; Granier, C.; Hermann, M.; Isaksen, I. S. A.; Kinne, S.; Koren, I.; Madonna, F.; Maione, M.; Massling, A.; Moehler, O.; Mona, L.; Monks, P. S.; Muller, D.; Muller, T.; Orphal, J.; Peuch, V. H.; Stratmann, F.; Tanre, D.; Tyndall, G.; Riziq, A. A.; Van Roozendael, M.; Villani, P.; Wehner, B.; Wex, H.; Zardini, A. A. *Atmos. Environ.* **2009**, *43*, 5351.
- (79) Riziq, A. A.; Erlick, C.; Dinar, E.; Rudich, Y. *Atmos. Chem. Phys.* **2007**, *7*, 1523.
- (80) Lack, D. A.; Richardson, M. S.; Law, D.; Langridge, J. M.; Cappa, C. D.; McLaughlin, R. J.; Murphy, D. M. *Aerosol Sci. Technol.* **2012**, *46*, 555.
- (81) Langridge, J. M.; Richardson, M. S.; Lack, D. A.; Brock, C. A.; Murphy, D. M. *Aerosol Sci. Technol.* **2013**, *47*, 1163.
- (82) Freedman, M. A.; Hasenkopf, C. A.; Beaver, M. R.; Tolbert, M. A. *J. Phys. Chem. A* **2009**, *113*, 13584.
- (83) Ma, L. L.; Thompson, J. E. *Anal. Chem.* **2012**, *84*, 5611.
- (84) Miles, R. E. H.; Rudic, S.; Orr-Ewing, A. J.; Reid, J. P. *Aerosol Sci. Technol.* **2011**, *45*, 1360.
- (85) Pettersson, A.; Lovejoy, E. R.; Brock, C. A.; Brown, S. S.; Ravishankara, A. R. *J. Aerosol Sci.* **2004**, *35*, 995.
- (86) Toole, J. R.; Renbaum-Wolff, L.; Smith, G. D. *Aerosol Sci. Technol.* **2013**, *47*, 955.

- (87) Butler, T. J. A.; Mellon, D.; Kim, J.; Litman, J.; Orr-Ewing, A. J. *J. Phys. Chem. A* **2009**, *113*, 3963.
- (88) Strawa, A. W.; Castaneda, R.; Owano, T.; Baer, D. S.; Paldus, B. A. *J. Atmos. Oceanic Technol.* **2003**, *20*, 454.
- (89) Thompson, J. E.; Hayes, P. L.; Jimenez, J. L.; Adachi, K.; Zhang, X.; Liu, J.; Weber, R. J.; Buseck, P. R. *Atmos. Environ.* **2012**, *55*, 190.
- (90) Baynard, T.; Lovejoy, E. R.; Pettersson, A.; Brown, S. S.; Lack, D.; Osthoff, H.; Massoli, P.; Ciciora, S.; Dube, W. P.; Ravishankara, A. R. *Aerosol Sci. Technol.* **2007**, *41*, 447.
- (91) Dubé, W. P.; Brown, S. S.; Osthoff, H. D.; Nunley, M. R.; Ciciora, S. J.; Paris, M. W.; McLaughlin, R. J.; Ravishankara, A. R. *Rev. Sci. Instrum.* **2006**, *77*, No. 034101.
- (92) Langridge, J. M.; Richardson, M. S.; Lack, D.; Law, D.; Murphy, D. M. *Aerosol Sci. Technol.* **2011**, *45*, 1305.
- (93) Smith, J. D.; Atkinson, D. B. *Analyst* **2001**, *126*, 1216.
- (94) Miles, R. E. H.; Rudic, S.; Orr-Ewing, A. J.; Reid, J. P. *Phys. Chem. Chem. Phys.* **2010**, *12*, 3914.
- (95) Trainic, M.; Riziq, A. A.; Lavi, A.; Rudich, Y. *J. Phys. Chem. A* **2012**, *116*, 5948.
- (96) Lang-Yona, N.; Rudich, Y.; Segre, E.; Dinar, E.; Abo-Riziq, A. *Anal. Chem.* **2009**, *81*, 1762.
- (97) Mellon, D.; King, S. J.; Kim, J.; Reid, J. P.; Orr-Ewing, A. J. *J. Phys. Chem. A* **2011**, *115*, 774.
- (98) Adler, G.; Riziq, A. A.; Erlick, C.; Rudich, Y. *Proc. Natl. Acad. Sci. U.S.A.* **2010**, *107*, 6699.
- (99) Nakayama, T.; Matsumi, Y.; Sato, K.; Imamura, T.; Yamazaki, A.; Uchiyama, A. J. *Geophys. Res.: Atmos.* **2010**, *115*, No. D24204.
- (100) Kebabian, P. L.; Robinson, W. A.; Freedman, A. *Rev. Sci. Instrum.* **2007**, *78*, No. 063102.
- (101) Massoli, P.; Kebabian, P. L.; Onasch, T. B.; Hills, F. B.; Freedman, A. *Aerosol Sci. Technol.* **2010**, *44*, 428.
- (102) Yu, Z.; Ziomba, L. D.; Onasch, T. B.; Herndon, S. C.; Albo, S. E.; Miake-Lye, R.; Anderson, B. E.; Kebabian, P. L.; Freedman, A. *Aerosol Sci. Technol.* **2011**, *45*, 1319.
- (103) Petzold, A.; Onasch, T.; Kebabian, P.; Freedman, A. *Atmos. Meas. Tech.* **2013**, *6*, 1141.
- (104) Washenfelder, R. A.; Flores, J. M.; Brock, C. A.; Brown, S. S.; Rudich, Y. *Atmos. Meas. Tech.* **2013**, *6*, 861.
- (105) Flores, J. M.; Washenfelder, R. A.; Adler, G.; Lee, H. J.; Segev, L.; Laskin, J.; Laskin, A.; Nizkorodov, S. A.; Brown, S. S.; Rudich, Y. *Phys. Chem. Chem. Phys.* **2014**, *16*, 10629.
- (106) Wilson, E. M.; Chen, J.; Varma, R. M.; Wenger, J. C.; Venables, D. S. In *Radiation Processes in the Atmosphere and Ocean*; Cahalan, R. F., Fischer, J., Eds.; American Institute of Physics: Melville, NY, 2013; Vol. 1531.
- (107) Varma, R. M.; Ball, S. M.; Brauers, T.; Dorn, H. P.; Heitmann, U.; Jones, R. L.; Platt, U.; Pöhler, D.; Ruth, A. A.; Shillings, A. J. L.; Thieser, J.; Wahner, A.; Venables, D. S. *Atmos. Meas. Tech.* **2013**, *6*, 3115.
- (108) Chartier, R. T.; Greenslade, M. E. *Atmos. Meas. Tech.* **2012**, *5*, 709.
- (109) Barkey, B.; Kim, H.; Paulson, S. E. *Aerosol Sci. Technol.* **2010**, *44*, 1089.
- (110) Kim, H.; Barkey, B.; Paulson, S. E. *J. Geophys. Res.: Atmos.* **2010**, *115*, No. D24212.
- (111) Kim, H.; Barkey, B.; Paulson, S. E. *J. Phys. Chem. A* **2012**, *116*, 6059.
- (112) Schnaiter, M.; Linke, C.; Möhler, O.; Naumann, K. H.; Saathoff, H.; Wagner, R.; Schurath, U.; Wehner, B. *J. Geophys. Res.: Atmos.* **2005**, *110*, No. D19204.
- (113) Fischer, E. V.; Jaffe, D. A.; Marley, N. A.; Gaffney, J. S.; Marchany-Rivera, A. J. *Geophys. Res.: Atmos.* **2010**, *115*, No. D20209.
- (114) Arnott, W. P.; Moosmüller, H.; Rogers, C. F.; Jin, T. F.; Bruch, R. *Atmos. Environ.* **1999**, *33*, 2845.
- (115) Ajtai, T.; Filep, A.; Schnaiter, M.; Linke, C.; Vragel, M.; Bozoki, Z.; Szabo, G.; Leisner, T. *J. Aerosol Sci.* **2010**, *41*, 1020.
- (116) Zhong, M.; Jang, M. *Atmos. Environ.* **2011**, *45*, 4263.
- (117) Massoli, P.; Murphy, D. M.; Lack, D. A.; Baynard, T.; Brock, C. A.; Lovejoy, E. R. *Aerosol Sci. Technol.* **2009**, *43*, 1064.
- (118) Cappa, C. D.; Onasch, T. B.; Massoli, P.; Worsnop, D. R.; Bates, T. S.; Cross, E. S.; Davidovits, P.; Hakala, J.; Hayden, K. L.; Jobson, B. T.; Kolesar, K. R.; Lack, D. A.; Lerner, B. M.; Li, S. M.; Mellon, D.; Nuaman, I.; Olfert, J. S.; Petaja, T.; Quinn, P. K.; Song, C.; Subramanian, R.; Williams, E. J.; Zaveri, R. A. *Science* **2012**, *337*, 1078.
- (119) Lewis, K.; Arnott, W. P.; Moosmüller, H.; Wold, C. E. *J. Geophys. Res.: Atmos.* **2008**, *113*, No. D16203.
- (120) Gyawali, M.; Arnott, W. P.; Zaveri, R. A.; Song, C.; Moosmüller, H.; Liu, L.; Mishchenko, M. I.; Chen, L. W. A.; Green, M. C.; Watson, J. G.; Chow, J. C. *Atmos. Chem. Phys.* **2012**, *12*, 2587.
- (121) Nakayama, T.; Sato, K.; Matsumi, Y.; Imamura, T.; Yamazaki, A.; Uchiyama, A. *Sola* **2012**, *8*, 119.
- (122) Gyawali, M.; Arnott, W. P.; Lewis, K.; Moosmüller, H. *Atmos. Chem. Phys.* **2009**, *9*, 8007.
- (123) Flowers, B. A.; Dubey, M. K.; Mazzoleni, C.; Stone, E. A.; Schauer, J. J.; Kim, S. W.; Yoon, S. C. *Atmos. Chem. Phys.* **2010**, *10*, 10387.
- (124) Chan, T. W.; Brook, J. R.; Smallwood, G. J.; Lu, G. *Atmos. Chem. Phys.* **2011**, *11*, 10407.
- (125) Wang, Q.; Huang, R. J.; Cao, J.; Han, Y.; Wang, G.; Li, G.; Wang, Y.; Dai, W.; Zhang, R.; Zhou, Y. *Aerosol Sci. Technol.* **2014**, *48*, 689.
- (126) Sharma, N.; Arnold, I. J.; Moosmueller, H.; Arnott, W. P.; Mazzoleni, C. *Atmos. Meas. Tech.* **2013**, *6*, 3501.
- (127) Dial, K. D.; Hiemstra, S.; Thompson, J. E. *Anal. Chem.* **2010**, *82*, 7885.
- (128) Qian, F.; Ma, L.; Thompson, J. E. *Eur. Opt. Soc.* **2012**, *7*, No. 12021.
- (129) Zhao, W.; Xu, X.; Dong, M.; Chen, W.; Gu, X.; Hu, C.; Huang, Y.; Gao, X.; Huang, W.; Zhang, W. *Atmos. Meas. Tech.* **2014**, *7*, 2551.
- (130) Mazurenka, M.; Orr-Ewing, A. J.; Peverall, R.; Ritchie, G. A. D. *Annu. Rep. Prog. Chem., Sect. C: Phys. Chem.* **2005**, *101*, 100.
- (131) Scherer, J. J.; Paul, J. B.; O'Keefe, A.; Saykally, R. J. *Chem. Rev.* **1997**, *97*, 25.
- (132) Wheeler, M. D.; Newman, S. M.; Orr-Ewing, A. J.; Ashfold, M. N. R. *J. Chem. Soc., Faraday Trans.* **1998**, *94*, 337.
- (133) *Cavity-Ringdown Spectroscopy: An Ultratrace-Absorption Measurement Technique*; Busch, K. W., Busch, M. A., Eds.; American Chemical Society: Washington, DC, 1999.
- (134) Berden, G.; Peeters, R.; Meijer, G. *Int. Rev. Phys. Chem.* **2000**, *19*, 565.
- (135) Brown, S. S. *Chem. Rev.* **2003**, *103*, 5219.
- (136) Cross, E. S.; Onasch, T. B.; Aherne, A.; Wrobel, W.; Slowik, J. G.; Olfert, J.; Lack, D. A.; Massoli, P.; Cappa, C. D.; Schwarz, J. P.; Spackman, J. R.; Fahey, D. W.; Sedlacek, A.; Trimborn, A.; Jayne, J. T.; Freedman, A.; Williams, L. R.; Ng, N. L.; Mazzoleni, C.; Dubey, M.; Brem, B.; Kok, G.; Subramanian, R.; Freitag, S.; Clarke, A.; Thornhill, D.; Marr, L. C.; Kolb, C. E.; Worsnop, D. R.; Davidovits, P. *Aerosol Sci. Technol.* **2010**, *44*, 592.
- (137) Dallmann, T. R.; DeMartini, S. J.; Kirchstetter, T. W.; Herndon, S. C.; Onasch, T. B.; Wood, E. C.; Harley, R. A. *Environ. Sci. Technol.* **2012**, *46*, 8511.
- (138) Gilardoni, S.; Massoli, P.; Giulianelli, L.; Rinaldi, M.; Paglione, M.; Pollini, F.; Lanconelli, C.; Poluzzi, V.; Carbone, S.; Hillamo, R.; Russell, L. M.; Facchini, M. C.; Fuzzi, S. *Atmos. Chem. Phys.* **2014**, *14*, 6967.
- (139) Hayes, P. L.; Ortega, A. M.; Cubison, M. J.; Froyd, K. D.; Zhao, Y.; Cliff, S. S.; Hu, W. W.; Toohey, D. W.; Flynn, J. H.; Lefer, B. L.; Grossberg, N.; Alvarez, S.; Rappenglueck, B.; Taylor, J. W.; Allan, J. D.; Holloway, J. S.; Gilman, J. B.; Kuster, W. C.; De Gouw, J. A.; Massoli, P.; Zhang, X.; Liu, J.; Weber, R. J.; Corrigan, A. L.; Russell, L. M.; Isaacman, G.; Worton, D. R.; Kreisberg, N. M.; Goldstein, A. H.; Thalman, R.; Waxman, E. M.; Volkamer, R.; Lin, Y. H.; Surratt, J. D.; Kleindienst, T. E.; Offenberg, J. H.; Dusanter, S.; Griffith, S.; Stevens, P. S.; Brioude, J.; Angevine, W. M.; Jimenez, J. L. *J. Geophys. Res.: Atmos.* **2013**, *118*, 9233.
- (140) Massoli, P.; Fortner, E. C.; Canagaratna, M. R.; Williams, L. R.; Zhang, Q.; Sun, Y.; Schwab, J. J.; Trimborn, A.; Onasch, T. B.;

- Demerjian, K. L.; Kolb, C. E.; Worsnop, D. R.; Jayne, J. T. *Aerosol Sci. Technol.* **2012**, *46*, 1201.
- (141) Ryerson, T. B.; Andrews, A. E.; Angevine, W. M.; Bates, T. S.; Brock, C. A.; Cairns, B.; Cohen, R. C.; Cooper, O. R.; de Gouw, J. A.; Fehsenfeld, F. C.; Ferrare, R. A.; Fischer, M. L.; Flagan, R. C.; Goldstein, A. H.; Hair, J. W.; Hardesty, R. M.; Hostetler, C. A.; Jimenez, J. L.; Langford, A. O.; McCauley, E.; McKeen, S. A.; Molina, L. T.; Nenes, A.; Oltmans, S. J.; Parrish, D. D.; Pederson, J. R.; Pierce, R. B.; Prather, K.; Quinn, P. K.; Seinfeld, J. H.; Senff, C. J.; Sorooshian, A.; Stutz, J.; Surratt, J. D.; Trainer, M.; Volkamer, R.; Williams, E. J.; Wofsy, S. C. *J. Geophys. Res.: Atmos.* **2013**, *118*, 5830.
- (142) Platt, U.; Meinen, J.; Pöhler, D.; Leisner, T. *Atmos. Meas. Tech.* **2009**, *2*, 713.
- (143) Zhao, W. X.; Dong, M. L.; Chen, W. D.; Gu, X. J.; Hu, C. J.; Gao, X. M.; Huang, W.; Zhang, W. *J. Anal. Chem.* **2013**, *85*, 2260.
- (144) Fiedler, S. E.; Hese, A.; Ruth, A. A. *Chem. Phys. Lett.* **2003**, *371*, 284.
- (145) Spindler, C.; Riziq, A. A.; Rudich, Y. *Aerosol Sci. Technol.* **2007**, *41*, 1011.
- (146) Mason, B. J.; King, S. J.; Miles, R. E. H.; Manfred, K. M.; Rickards, A. M. J.; Kim, J.; Reid, J. P.; Orr-Ewing, A. J. *J. Phys. Chem. A* **2012**, *116*, 8547.
- (147) Zarzana, K. J.; Cappa, C. D.; Tolbert, M. A. *Aerosol Sci. Technol.* **2014**, *48*, 1133.
- (148) Adler, G.; Haspel, C.; Moise, T.; Rudich, Y. *J. Geophys. Res.: Atmos.* **2014**, *119*, 6768 DOI: 10.1002/2013JD021314.
- (149) Mishchenko, M. I.; Hovenier, J. W.; Travis, L. D. *Light Scattering by Nonspherical Particles: Theory, Measurements, and Applications*; Academic Press: San Diego, CA, 2000.
- (150) Mishchenko, M. I.; Travis, L. D.; Mackowski, D. W. *J. Quant. Spectrosc. Radiat. Transfer* **2010**, *111*, 1700.
- (151) Beuttell, R. G.; Brewer, A. W. *J. Sci. Instrum.* **1949**, *26*, 357.
- (152) Anderson, T. L.; Covert, D. S.; Marshall, S. F.; Laucks, M. L.; Charlson, R. J.; Waggoner, A. P.; Ogren, J. A.; Caldow, R.; Holm, R. L.; Quant, F. R.; Sem, G. J.; Wiedensohler, A.; Ahlquist, N. A.; Bates, T. S. *J. Atmos. Oceanic Technol.* **1996**, *13*, 967.
- (153) Müller, T.; Laborde, M.; Kassell, G.; Wiedensohler, A. *Atmos. Meas. Tech.* **2011**, *4*, 1291.
- (154) Barkey, B.; Paulson, S. E.; Chung, A. *Aerosol Sci. Technol.* **2007**, *41*, 751.
- (155) Bruce, C. W.; Pinnick, R. G. *Appl. Opt.* **1977**, *16*, 1762.
- (156) Japar, S. M.; Szkarlat, A. C. *Combust. Sci. Technol.* **1981**, *24*, 215.
- (157) Terhune, R. W.; Anderson, J. E. *Opt. Lett.* **1977**, *1*, 70.
- (158) Müller, T.; Henzing, J. S.; de Leeuw, G.; Wiedensohler, A.; Alastuey, A.; Angelov, H.; Bizjak, M.; Collaud Coen, M.; Engström, J. E.; Gruening, C.; Hillamo, R.; Hoffer, A.; Imre, K.; Ivanow, P.; Jennings, G.; Sun, J. Y.; Kalivitis, N.; Karlsson, H.; Komppula, M.; Laj, P.; Li, S. M.; Lunder, C.; Marinoni, A.; Martins dos Santos, S.; Moerman, M.; Nowak, A.; Ogren, J. A.; Petzold, A.; Pichon, J. M.; Rodriguez, S.; Sharma, S.; Sheridan, P. J.; Teinilä, K.; Tuch, T.; Viana, M.; Virkkula, A.; Weingartner, E.; Wilhelm, R.; Wang, Y. Q. *Atmos. Meas. Tech.* **2011**, *4*, 245.
- (159) Bueno, P. A.; Havey, D. K.; Mulholland, G. W.; Hodges, J. T.; Gillis, K. A.; Dickerson, R. R.; Zachariah, M. R. *Aerosol Sci. Technol.* **2011**, *45*, 1217.
- (160) Lack, D. A.; Cappa, C. D.; Cross, E. S.; Massoli, P.; Ahern, A. T.; Davidovits, P.; Onasch, T. B. *Aerosol Sci. Technol.* **2009**, *43*, 1006.
- (161) Song, C.; Gyawali, M.; Zaveri, R. A.; Shilling, J. E.; Arnott, W. P. *J. Geophys. Res.: Atmos.* **2013**, *118*, 11741.
- (162) Lack, D. A.; Bahreini, R.; Langridge, J. M.; Gilman, J. B.; Middlebrook, A. M. *Atmos. Chem. Phys.* **2013**, *13*, 2415.
- (163) Ajtai, T.; Filep, A.; Utry, N.; Schnaiter, M.; Linke, C.; Bozoki, Z.; Szabo, G.; Leisner, T. *J. Aerosol Sci.* **2011**, *42*, 859.
- (164) Meyer, P. L.; Sigrist, M. W. *Rev. Sci. Instrum.* **1990**, *61*, 1779.
- (165) Schäfer, S.; Miklós, A.; Hess, P. *Appl. Opt.* **1997**, *36*, 3202.
- (166) Miklós, A.; Hess, P.; Bozóki, Z. *Rev. Sci. Instrum.* **2001**, *72*, 1937.
- (167) Nakayama, T.; Kondo, Y.; Moteki, N.; Sahu, L. K.; Kinase, T.; Kita, K.; Matsumi, Y. *J. Aerosol Sci.* **2010**, *41*, 333.
- (168) Lack, D. A.; Quinn, P. K.; Massoli, P.; Bates, T. S.; Coffman, D.; Covert, D. S.; Sierau, B.; Tucker, S.; Baynard, T.; Lovejoy, E.; Murphy, D. M.; Ravishankara, A. R. *Geophys. Res. Lett.* **2009**, *36*, No. L24805.
- (169) Murphy, D. M. *Aerosol Sci. Technol.* **2009**, *43*, 356.
- (170) Onasch, T. B.; Massoli, P.; Kebabian, P. L.; Hills, F. B.; Bacon, F. W.; Freedman, A. Single Scattering Albedo Monitor for Airborne Particulates. *Aerosol Sci. Technol.* **2015**, DOI: 10.1080/02786826.2015.1022248.
- (171) Krieger, U. K.; Marcolli, C.; Reid, J. P. *Chem. Soc. Rev.* **2012**, *41*, 6631.
- (172) Lienhard, D. M.; Bones, D. L.; Zuend, A.; Krieger, U. K.; Reid, J. P.; Peter, T. *J. Phys. Chem. A* **2012**, *116*, 9954.
- (173) Miles, R. E. H.; Carruthers, A. E.; Reid, J. P. *Laser Photonics Rev.* **2011**, *5*, 534.
- (174) Miles, R. E. H.; Walker, J. S.; Burnham, D. R.; Reid, J. P. *Phys. Chem. Chem. Phys.* **2012**, *14*, 3037.
- (175) Walker, J. S.; Carruthers, A. E.; Orr-Ewing, A. J.; Reid, J. P. *J. Phys. Chem. Lett.* **2013**, *4*, 1748.
- (176) Lang-Yona, N.; Rudich, Y.; Mentel, T. F.; Bohne, A.; Buchholz, A.; Kiendler-Scharr, A.; Kleist, E.; Spindler, C.; Tillmann, R.; Wildt, J. *Atmos. Chem. Phys.* **2010**, *10*, 7253.
- (177) Wex, H.; Petters, M. D.; Carrico, C. M.; Hallbauer, E.; Massling, A.; McMeeking, G. R.; Poulain, L.; Wu, Z.; Kreidenweis, S. M.; Stratmann, F. *Atmos. Chem. Phys.* **2009**, *9*, 3987.
- (178) Yu, Y.; Ezell, M. J.; Zelenyuk, A.; Imre, D.; Alexander, L.; Ortega, J.; D'Anna, B.; Harmon, C. W.; Johnson, S. N.; Finlayson-Pitts, B. J. *Atmos. Environ.* **2008**, *42*, 5044.
- (179) Paulson, S. E.; Sen, A. D.; Liu, P.; Fenske, J. D.; Fox, M. J. *Geophys. Res. Lett.* **1997**, *24*, 3193.
- (180) Ehn, M.; Thornton, J. A.; Kleist, E.; Sipila, M.; Junninen, H.; Pullinen, I.; Springer, M.; Rubach, F.; Tillmann, R.; Lee, B.; Lopez-Hilfiker, F.; Andres, S.; Acir, I.-H.; Rissanen, M.; Jokinen, T.; Schobesberger, S.; Kangasluoma, J.; Kontkanen, J.; Nieminen, T.; Kurten, T.; Nielsen, L. B.; Jorgensen, S.; Kjaergaard, H. G.; Canagaratna, M.; Maso, M. D.; Berndt, T.; Petaja, T.; Wahner, A.; Kerminen, V.-M.; Kulmala, M.; Worsnop, D. R.; Wildt, J.; Mentel, T. F. *Nature* **2014**, *506*, 476.
- (181) Guenther, A. B.; Jiang, X.; Heald, C. L.; Sakulyanontvittaya, T.; Duhl, T.; Emmons, L. K.; Wang, X. *Geosci. Model Dev.* **2012**, *5*, 1471.
- (182) Kleist, E.; Mentel, T. F.; Andres, S.; Bohne, A.; Folkers, A.; Kiendler-Scharr, A.; Rudich, Y.; Springer, M.; Tillmann, R.; Wildt, J. *Biogeosciences* **2012**, *9*, 5111.
- (183) Mentel, T. F.; Kleist, E.; Andres, S.; Dal Maso, M.; Hohaus, T.; Kiendler-Scharr, A.; Rudich, Y.; Springer, M.; Tillmann, R.; Uerlings, R.; Wahner, A.; Wildt, J. *Atmos. Chem. Phys.* **2013**, *13*, 8755.
- (184) Mentel, T. F.; Wildt, J.; Kiendler-Scharr, A.; Kleist, E.; Tillmann, R.; Dal Maso, M.; Fisseha, R.; Hohaus, T.; Spahn, H.; Uerlings, R.; Wegener, R.; Griffiths, P. T.; Dinar, E.; Rudich, Y.; Wahner, A. *Atmos. Chem. Phys.* **2009**, *9*, 4387.
- (185) Wildt, J.; Mentel, T. F.; Kiendler-Scharr, A.; Hoffmann, T.; Andres, S.; Ehn, M.; Kleist, E.; Musgen, P.; Rohrer, F.; Rudich, Y.; Springer, M.; Tillmann, R.; Wahner, A. *Atmos. Chem. Phys.* **2014**, *14*, 2789.
- (186) Ng, N. L.; Kroll, J. H.; Chan, A. W. H.; Chhabra, P. S.; Flagan, R. C.; Seinfeld, J. H. *Atmos. Chem. Phys.* **2007**, *7*, 3909.
- (187) Redmond, H.; Thompson, J. E. *Phys. Chem. Chem. Phys.* **2011**, *13*, 6872.
- (188) Schnaiter, M.; Schmid, O.; Petzold, A.; Fritzsche, L.; Klein, K. F.; Andreae, M. O.; Helas, G.; Thielmann, A.; Gimmler, M.; Mohler, O.; Linke, C.; Schurath, U. *Aerosol Sci. Technol.* **2005**, *39*, 249.
- (189) Henze, D. K.; Seinfeld, J. H.; Ng, N. L.; Kroll, J. H.; Fu, T. M.; Jacob, D. J.; Heald, C. L. *Atmos. Chem. Phys.* **2008**, *8*, 2405.
- (190) Kroll, J. H.; Seinfeld, J. H. *Atmos. Environ.* **2008**, *42*, 3593.
- (191) Xu, L.; Kollman, M. S.; Song, C.; Shilling, J. E.; Ng, N. L. *Environ. Sci. Technol.* **2014**, *48*, 2253.

- (192) Varma, R. M.; Venables, D. S.; Ruth, A. A.; Heitmann, U.; Schlosser, E.; Dixneuf, S. *Appl. Opt.* **2009**, *48*, B159.
- (193) Jimenez, J. L.; Canagaratna, M. R.; Donahue, N. M.; Prevot, A. S. H.; Zhang, Q.; Kroll, J. H.; DeCarlo, P. F.; Allan, J. D.; Coe, H.; Ng, N. L.; Aiken, A. C.; Docherty, K. S.; Ulbrich, I. M.; Grieshop, A. P.; Robinson, A. L.; Duplissy, J.; Smith, J. D.; Wilson, K. R.; Lanz, V. A.; Hueglin, C.; Sun, Y. L.; Tian, J.; Laaksonen, A.; Raatikainen, T.; Rautiainen, J.; Vaattovaara, P.; Ehn, M.; Kulmala, M.; Tomlinson, J. M.; Collins, D. R.; Cubison, M. J.; Dunlea, E. J.; Huffman, J. A.; Onasch, T. B.; Alfarra, M. R.; Williams, P. I.; Bower, K.; Kondo, Y.; Schneider, J.; Drewnick, F.; Borrmann, S.; Weimer, S.; Demerjian, K.; Salcedo, D.; Cottrell, L.; Griffin, R.; Takami, A.; Miyoshi, T.; Hatakeyama, S.; Shimono, A.; Sun, J. Y.; Zhang, Y. M.; Dzepina, K.; Kimmel, J. R.; Sueper, D.; Jayne, J. T.; Herndon, S. C.; Trimborn, A. M.; Williams, L. R.; Wood, E. C.; Middlebrook, A. M.; Kolb, C. E.; Baltensperger, U.; Worsnop, D. R. *Science* **2009**, *326*, 1525.
- (194) Kroll, J. H.; Donahue, N. M.; Jimenez, J. L.; Kessler, S. H.; Canagaratna, M. R.; Wilson, K. R.; Altieri, K. E.; Mazzoleni, L. R.; Woziak, A. S.; Bluhm, H.; Mysak, E. R.; Smith, J. D.; Kolb, C. E.; Worsnop, D. R. *Nat. Chem.* **2011**, *3*, 133.
- (195) Kroll, J. H.; Smith, J. D.; Che, D. L.; Kessler, S. H.; Worsnop, D. R.; Wilson, K. R. *Phys. Chem. Chem. Phys.* **2009**, *11*, 8005.
- (196) Pankow, J. F. *Atmos. Environ.* **1994**, *28*, 189.
- (197) Odum, J. R.; Hoffmann, T.; Bowman, F.; Collins, D.; Flagan, R. C.; Seinfeld, J. H. *Environ. Sci. Technol.* **1996**, *30*, 2580.
- (198) Chan, A. W. H.; Kroll, J. H.; Ng, N. L.; Seinfeld, J. H. *Atmos. Chem. Phys.* **2007**, *7*, 4135.
- (199) Donahue, N. M.; Kroll, J. H.; Pandis, S. N.; Robinson, A. L. *Atmos. Chem. Phys.* **2012**, *12*, 615.
- (200) Kokkola, H.; Yli-Pirilä, P.; Vesterinen, M.; Korhonen, H.; Keskinen, H.; Romakkaniemi, S.; Hao, L.; Kortelainen, A.; Joutsensaari, J.; Worsnop, D. R.; Virtanen, A.; Lehtinen, K. E. *J. Atmos. Chem. Phys.* **2014**, *14*, 1689.
- (201) Moise, T.; Rudich, Y. *J. Phys. Chem. A* **2002**, *106*, 6469.
- (202) Molina, M. J.; Ivanov, A. V.; Trakhtenberg, S.; Molina, L. T. *Geophys. Res. Lett.* **2004**, *31*, No. L22104.
- (203) Kuwata, M.; Zorn, S. R.; Martin, S. T. *Environ. Sci. Technol.* **2012**, *46*, 787.
- (204) Chhabra, P. S.; Ng, N. L.; Canagaratna, M. R.; Corrigan, A. L.; Russell, L. M.; Worsnop, D. R.; Flagan, R. C.; Seinfeld, J. H. *Atmos. Chem. Phys.* **2011**, *11*, 8827.
- (205) Ng, N. L.; Canagaratna, M. R.; Jimenez, J. L.; Chhabra, P. S.; Seinfeld, J. H.; Worsnop, D. R. *Atmos. Chem. Phys.* **2011**, *11*, 6465.
- (206) Ng, N. L.; Canagaratna, M. R.; Zhang, Q.; Jimenez, J. L.; Tian, J.; Ulbrich, I. M.; Kroll, J. H.; Docherty, K. S.; Chhabra, P. S.; Bahreini, R.; Murphy, S. M.; Seinfeld, J. H.; Hildebrandt, L.; Donahue, N. M.; DeCarlo, P. F.; Lanz, V. A.; Prévôt, A. S. H.; Dinar, E.; Rudich, Y.; Worsnop, D. R. *Atmos. Chem. Phys.* **2010**, *10*, 4625.
- (207) Aiken, A. C.; DeCarlo, P. F.; Jimenez, J. L. *Anal. Chem.* **2007**, *79*, 8350.
- (208) Aiken, A. C.; Decarlo, P. F.; Kroll, J. H.; Worsnop, D. R.; Huffman, J. A.; Docherty, K. S.; Ulbrich, I. M.; Mohr, C.; Kimmel, J. R.; Sueper, D.; Sun, Y.; Zhang, Q.; Trimborn, A.; Northway, M.; Ziemann, P. J.; Canagaratna, M. R.; Onasch, T. B.; Alfarra, M. R.; Prevot, A. S. H.; Dommen, J.; Duplissy, J.; Metzger, A.; Baltensperger, U.; Jimenez, J. L. *Environ. Sci. Technol.* **2008**, *42*, 4478.
- (209) Alfarra, M. R.; Coe, H.; Allan, J. D.; Bower, K. N.; Boudries, H.; Canagaratna, M. R.; Jimenez, J. L.; Jayne, J. T.; Garforth, A. A.; Li, S. M.; Worsnop, D. R. *Atmos. Environ.* **2004**, *38*, 5745.
- (210) Donahue, N. M.; Henry, K. M.; Mentel, T. F.; Kiendler-Scharr, A.; Spindler, C.; Bohn, B.; Brauers, T.; Dorn, H. P.; Fuchs, H.; Tillmann, R.; Wahner, A.; Saathoff, H.; Naumann, K.-H.; Möhler, O.; Leisner, T.; Müller, L.; Reinnig, M.-C.; Hoffmann, T.; Salo, K.; Hallquist, M.; Frosch, M.; Bilde, M.; Tritscher, T.; Barmet, P.; Praplan, A. P.; DeCarlo, P. F.; Dommen, J.; Prévôt, A. S. H.; Baltensperger, U. *Proc. Natl. Acad. Sci. U.S.A.* **2012**, *109*, 13503.
- (211) Kessler, S. H.; Nah, T.; Daumit, K. E.; Smith, J. D.; Leone, S. R.; Kolb, C. E.; Worsnop, D. R.; Wilson, K. R.; Kroll, J. H. *J. Phys. Chem. A* **2012**, *116*, 6358.
- (212) Tkacik, D. S.; Lambe, A. T.; Jathar, S.; Li, X.; Presto, A. A.; Zhao, Y.; Blake, D.; Meinardi, S.; Jayne, J. T.; Croteau, P. L.; Robinson, A. L. *Environ. Sci. Technol.* **2014**, *48*, 11235.
- (213) Russell, L. M.; Bahadur, R.; Ziemann, P. J. *Proc. Natl. Acad. Sci. U.S.A.* **2011**, *108*, 3516.
- (214) Liu, S.; Shilling, J. E.; Song, C.; Hiranuma, N.; Zaveri, R. A.; Russell, L. M. *Aerosol Sci. Technol.* **2012**, *46*, 1359.
- (215) Nguyen, T. B.; Lee, P. B.; Updyke, K. M.; Bones, D. L.; Laskin, J.; Laskin, A.; Nizkorodov, S. A. *J. Geophys. Res.: Atmos.* **2012**, *117*, No. D01207.
- (216) Harrison, M. A. J.; Barra, S.; Borghesi, D.; Vione, D.; Arsene, C.; Iulian Olariu, R. *Atmos. Environ.* **2005**, *39*, 231.
- (217) Laskin, J.; Laskin, A.; Roach, P. J.; Slysz, G. W.; Anderson, G. A.; Nizkorodov, S. A.; Bones, D. L.; Nguyen, L. Q. *Anal. Chem.* **2010**, *82*, 2048.
- (218) De Haan, D. O.; Hawkins, L. N.; Kononenko, J. A.; Turley, J. J.; Corrigan, A. L.; Tolbert, M. A.; Jimenez, J. L. *Environ. Sci. Technol.* **2011**, *45*, 984.
- (219) Yu, G.; Bayer, A. R.; Galloway, M. M.; Korshavn, K. J.; Fry, C. G.; Keutsch, F. N. *Environ. Sci. Technol.* **2011**, *45*, 6336.
- (220) Trainic, M.; Riziq, A. A.; Lavi, A.; Flores, J. M.; Rudich, Y. *Atmos. Chem. Phys.* **2011**, *11*, 9697.
- (221) De Haan, D. O.; Corrigan, A. L.; Smith, K. W.; Stroik, D. R.; Turley, J. J.; Lee, F. E.; Tolbert, M. A.; Jimenez, J. L.; Cordova, K. E.; Ferrell, G. R. *Environ. Sci. Technol.* **2009**, *43*, 2818.
- (222) Noziere, B.; Esteve, W. *Atmos. Environ.* **2007**, *41*, 1150.
- (223) Chang, J. L.; Thompson, J. E. *Atmos. Environ.* **2010**, *44*, 541.
- (224) Gelencser, A.; Hoffer, A.; Kiss, G.; Tombacz, E.; Kurdi, R.; Bencze, L. J. *Atmos. Chem.* **2003**, *45*, 25.
- (225) Smith, J. D.; Sio, V.; Yu, L.; Zhang, Q.; Anastasio, C. *Environ. Sci. Technol.* **2013**, *48*, 1049.
- (226) Limbeck, A.; Kulmala, M.; Puxbaum, H. *Geophys. Res. Lett.* **2003**, *30*, 1996.
- (227) Rincon, A. G.; Guzman, M. I.; Hoffmann, M. R.; Colussi, A. J. *J. Phys. Chem. Lett.* **2010**, *1*, 368.
- (228) Rincón, A. G.; Guzmán, M. I.; Hoffmann, M. R.; Colussi, A. J. *J. Phys. Chem. A* **2009**, *113*, 10512.
- (229) Kampf, C. J.; Jakob, R.; Hoffmann, T. *Atmos. Chem. Phys.* **2012**, *12*, 6323.
- (230) Bateman, A. P.; Nizkorodov, S. A.; Laskin, J.; Laskin, A. *Phys. Chem. Chem. Phys.* **2011**, *13*, 12199.
- (231) Chen, Y.; Bond, T. C. *Atmos. Chem. Phys.* **2010**, *10*, 1773.
- (232) Saleh, R.; Robinson, E. S.; Tkacik, D. S.; Ahern, A. T.; Liu, S.; Aiken, A. C.; Sullivan, R. C.; Presto, A. A.; Dubey, M. K.; Yokelson, R. J.; Donahue, N. M.; Robinson, A. L. *Nat. Geosci.* **2014**, *7*, 647.
- (233) Hoffer, A.; Gelencser, A.; Guyon, P.; Kiss, G.; Schmid, O.; Frank, G. P.; Artaxo, P.; Andreae, M. O. *Atmos. Chem. Phys.* **2006**, *6*, 3563.
- (234) Reid, J. S.; Eck, T. F.; Christopher, S. A.; Koppmann, R.; Dubovik, O.; Eleuterio, D. P.; Holben, B. N.; Reid, E. A.; Zhang, J. *Atmos. Chem. Phys.* **2005**, *5*, 827.
- (235) Magi, B. I. *Atmos. Chem. Phys.* **2011**, *11*, 4777; **2009**, *9*, 7643.
- (236) Zhang, X. L.; Lin, Y. H.; Surratt, J. D.; Weber, R. J. *Environ. Sci. Technol.* **2013**, *47*, 3685.
- (237) Cheng, Y.; He, K. B.; Zheng, M.; Duan, F. K.; Du, Z. Y.; Ma, Y. L.; Tan, J. H.; Yang, F. M.; Liu, J. M.; Zhang, X. L.; Weber, R. J.; Bergin, M. H.; Russell, A. G. *Atmos. Chem. Phys.* **2011**, *11*, 11497.
- (238) Dinar, E.; Taraniuk, I.; Gruber, E. R.; Katsman, S.; Moise, T.; Anttila, T.; Mentel, T. F.; Rudich, Y. *Atmos. Chem. Phys.* **2006**, *6*, 2465.
- (239) Desyaterik, Y.; Sun, Y.; Shen, X.; Lee, T.; Wang, X.; Wang, T.; Collett, J. L. *J. Geophys. Res.: Atmos.* **2013**, *118*, 7389.
- (240) Phillips, S. M.; Smith, G. D. *J. Phys. Chem. A* **2014**, DOI: 10.1021/jp510709e.
- (241) Phillips, S. M.; Smith, G. D. *Environ. Sci. Technol. Lett.* **2014**, *1*, 382.
- (242) Sato, K.; Takami, A.; Kato, Y.; Seta, T.; Fujitani, Y.; Hikida, T.; Shimono, A.; Imamura, T. *Atmos. Chem. Phys.* **2012**, *12*, 4667.
- (243) Zhong, M.; Jang, M.; Oliferenko, A.; Pillai, G. G.; Katritzky, A. R. *Phys. Chem. Chem. Phys.* **2012**, *14*, 9058.

- (244) Müller, L.; Reinnig, M. C.; Naumann, K. H.; Saathoff, H.; Mentel, T. F.; Donahue, N. M.; Hoffmann, T. *Atmos. Chem. Phys.* **2012**, *12*, 1483.
- (245) Eddingsaas, N. C.; Loza, C. L.; Yee, L. D.; Chan, M.; Schilling, K. A.; Chhabra, P. S.; Seinfeld, J. H.; Wennberg, P. O. *Atmos. Chem. Phys.* **2012**, *12*, 7413.
- (246) Crounse, J. D.; Nielsen, L. B.; Jørgensen, S.; Kjaergaard, H. G.; Wennberg, P. O. *J. Phys. Chem. Lett.* **2013**, *4*, 3513.
- (247) Noziere, B.; Dziedzic, P.; Cordova, A. *J. Phys. Chem. A* **2009**, *113*, 231.
- (248) De Haan, D. O.; Tolbert, M. A.; Jimenez, J. L. *Geophys. Res. Lett.* **2009**, *36*, No. L11819.
- (249) Lee, A. K. Y.; Zhao, R.; Li, R.; Liggio, J.; Li, S. M.; Abbatt, J. P. D. *Environ. Sci. Technol.* **2013**, *47*, 12819.
- (250) Galloway, M. M.; Chhabra, P. S.; Chan, A. W. H.; Surratt, J. D.; Flagan, R. C.; Seinfeld, J. H.; Keutsch, F. N. *Atmos. Chem. Phys.* **2009**, *9*, 3331.
- (251) Sareen, N.; Schwier, A. N.; Lathem, T. L.; Nenes, A.; McNeill, V. F. *Proc. Natl. Acad. Sci. U.S.A.* **2013**, *110*, 2723.
- (252) Volkamer, R.; Ziemann, P. J.; Molina, M. J. *Atmos. Chem. Phys.* **2009**, *9*, 1907.
- (253) Kirkland, J. R.; Lim, Y. B.; Tan, Y.; Altieri, K. E.; Turpin, B. J. *Environ. Chem.* **2013**, *10*, 158.
- (254) Tan, Y.; Lim, Y. B.; Altieri, K. E.; Seitzinger, S. P.; Turpin, B. J. *Atmos. Chem. Phys.* **2012**, *12*, 801.
- (255) Hamilton, J. F.; Baeza-Romero, M. T.; Finessi, E.; Rickard, A. R.; Healy, R. M.; Peppe, S.; Adams, T. J.; Daniels, M. J. S.; Ball, S. M.; Goodall, I. C. A.; Monks, P. S.; Borras, E.; Munoz, A. *Faraday Discuss.* **2013**, *165*, 447.
- (256) Ervens, B.; Volkamer, R. *Atmos. Chem. Phys.* **2010**, *10*, 8219.
- (257) Casale, M. T.; Richman, A. R.; Elrod, M. J.; Garland, R. M.; Beaver, M. R.; Tolbert, M. A. *Atmos. Environ.* **2007**, *41*, 6212.
- (258) Zhao, J.; Levitt, N. P.; Zhang, R. Y. *Geophys. Res. Lett.* **2005**, *32*, No. L09802.
- (259) Garland, R. M.; Elrod, M. J.; Kincaid, K.; Beaver, M. R.; Jimenez, J. L.; Tolbert, M. A. *Atmos. Environ.* **2006**, *40*, 6863.
- (260) Nozière, B.; Esteve, W. *Geophys. Res. Lett.* **2005**, *32*, No. L03812.
- (261) Saleh, R.; Hennigan, C. J.; McMeeking, G. R.; Chuang, W. K.; Robinson, E. S.; Coe, H.; Donahue, N. M.; Robinson, A. L. *Atmos. Chem. Phys.* **2013**, *13*, 7683.
- (262) Yokelson, R. J.; Crounse, J. D.; DeCarlo, P. F.; Karl, T.; Urbanski, S.; Atlas, E.; Campos, T.; Shinozuka, Y.; Kapustin, V.; Clarke, A. D.; Weinheimer, A.; Knapp, D. J.; Montzka, D. D.; Holloway, J.; Weibring, P.; Flocke, F.; Zheng, W.; Toohey, D.; Wennberg, P. O.; Wiedinmyer, C.; Mauldin, L.; Fried, A.; Richter, D.; Walega, J.; Jimenez, J. L.; Adachi, K.; Buseck, P. R.; Hall, S. R.; Shetter, R. *Atmos. Chem. Phys.* **2009**, *9*, 5785.
- (263) Magi, B. I. *Atmos. Chem. Phys.* **2009**, *9*, 7643.
- (264) Zhong, M.; Jang, M. *Atmos. Chem. Phys.* **2014**, *14*, 1517.
- (265) Cazorla, A.; Bahadur, R.; Suski, K. J.; Cahill, J. F.; Chand, D.; Schmid, B.; Ramanathan, V.; Prather, K. A. *Atmos. Chem. Phys.* **2013**, *13*, 9337.
- (266) Giles, D. M.; Holben, B. N.; Eck, T. F.; Sinyuk, A.; Smirnov, A.; Slutsker, I.; Dickerson, R. R.; Thompson, A. M.; Schafer, J. S. *J. Geophys. Res.: Atmos.* **2012**, *117*, No. D17203.
- (267) Russell, P. B.; Bergstrom, R. W.; Shinozuka, Y.; Clarke, A. D.; DeCarlo, P. F.; Jimenez, J. L.; Livingston, J. M.; Redemann, J.; Dubovik, O.; Strawa, A. *Atmos. Chem. Phys.* **2010**, *10*, 1155.
- (268) Moosmuller, H.; Chakrabarty, R. K.; Ehlers, K. M.; Arnott, W. P. *Atmos. Chem. Phys.* **2011**, *11*, 1217.
- (269) Bergstrom, R. W.; Pilewskie, P.; Russell, P. B.; Redemann, J.; Bond, T. C.; Quinn, P. K.; Siera, B. *Atmos. Chem. Phys.* **2007**, *7*, 5937.
- (270) Bahadur, R.; Praveen, P. S.; Xu, Y. Y.; Ramanathan, V. *Proc. Natl. Acad. Sci. U.S.A.* **2012**, *109*, 17366.
- (271) Feng, Y.; Ramanathan, V.; Kotamarthi, V. R. *Atmos. Chem. Phys.* **2013**, *13*, 8607.
- (272) Shiraiwa, M.; Kondo, Y.; Moteki, N.; Takegawa, N.; Miyazaki, Y.; Blake, D. R. *Geophys. Res. Lett.* **2007**, *34*, No. L16803.
- (273) Shi, Z.; Zhang, D.; Ji, H.; Hasegawa, S.; Hayashi, M. *Sci. Total Environ.* **2008**, *389*, 195.
- (274) Jacobson, M. Z. *Geophys. Res. Lett.* **2000**, *27*, 217.
- (275) Adachi, K.; Buseck, P. R. *Atmos. Chem. Phys.* **2008**, *8*, 6469.
- (276) Khalizov, A. F.; Lin, Y.; Qiu, C.; Guo, S.; Collins, D.; Zhang, R. *Environ. Sci. Technol.* **2013**, *47*, 2254.
- (277) Zhang, R.; Khalizov, A. F.; Pagels, J.; Zhang, D.; Xue, H.; McMurry, P. H. *Proc. Natl. Acad. Sci. U.S.A.* **2008**, *105*, 10291.
- (278) Bond, T. C.; Habib, G.; Bergstrom, R. W. *J. Geophys. Res.: Atmos.* **2006**, *111*, D20211.
- (279) Jacobson, M. Z. *Nature* **2001**, *409*, 695.
- (280) Lack, D. A.; Cappa, C. D. *Atmos. Chem. Phys.* **2010**, *10*, 4207.
- (281) Schnaiter, M.; Linke, C.; Möhler, O.; Naumann, K. H.; Saathoff, H.; Wagner, R.; Schurath, U.; Wehner, B. *J. Geophys. Res.: Atmos.* **2005**, *110*, No. D19204.
- (282) Toon, O. B.; Ackerman, T. P. *Appl. Opt.* **1981**, *20*, 3657.
- (283) Moroz, A. *Ann. Phys.* **2005**, *315*, 352.
- (284) Cappa, C. D.; Onasch, T. B.; Massoli, P.; Worsnop, D. R.; Bates, T. S.; Cross, E. S.; Davidovits, P.; Hakala, J.; Hayden, K. L.; Jobson, B. T.; Kolesar, K. R.; Lack, D. A.; Lerner, B. M.; Li, S.-M.; Mellon, D.; Nuaaman, I.; Olfert, J. S.; Petäjä, T.; Quinn, P. K.; Song, C.; Subramanian, R.; Williams, E. J.; Zaveri, R. A. *Science* **2013**, *339*, 393.
- (285) Jacobson, M. Z. *Science* **2013**, *339*, 393.
- (286) Mason, B. J.; King, S.-J.; Miles, R. E. H.; Manfred, K. M.; Rickards, A. M. J.; Kim, J.; Reid, J. P.; Orr-Ewing, A. J. *J. Phys. Chem. A* **2012**, *116*, 8547.
- (287) Griffith, D. W. T.; Mankin, W. G.; Coffey, M. T.; Ward, D. E.; Riebau, A. In *Global Biomass Burning: Atmospheric, Climatic, and Biospheric Implications*; Levine, J. S., Ed.; MIT Press: Cambridge, MA, 1991.
- (288) Goldstein, A. H.; Koven, C. D.; Heald, C. L.; Fung, I. Y. *Proc. Natl. Acad. Sci. U.S.A.* **2009**, *106*, 8835.
- (289) Gentner, D. R.; Isaacman, G.; Worton, D. R.; Chan, A. W. H.; Dallmann, T. R.; Davis, L.; Liu, S.; Day, D. A.; Russell, L. M.; Wilson, K. R.; Weber, R.; Guha, A.; Harley, R. A.; Goldstein, A. H. *Proc. Natl. Acad. Sci. U.S.A.* **2012**, *109*, 18318.
- (290) Rollins, A. W.; Browne, E. C.; Min, K.-E.; Pusede, S. E.; Wooldridge, P. J.; Gentner, D. R.; Goldstein, A. H.; Liu, S.; Day, D. A.; Russell, L. M.; Cohen, R. C. *Science* **2012**, *337*, 1210.
- (291) Sun, Y. L.; Zhang, Q.; Anastasio, C.; Sun, J. *Atmos. Chem. Phys.* **2010**, *10*, 4809.
- (292) You, Y.; Renbaum-Wolff, L.; Carreras-Sospedra, M.; Hanna, S. J.; Hiranuma, N.; Kamal, S.; Smith, M. L.; Zhang, X.; Weber, R. J.; Shilling, J. E.; Dabdub, D.; Martin, S. T.; Bertram, A. K. *Proc. Natl. Acad. Sci. U.S.A.* **2012**, *109*, 13188.
- (293) Daumit, K. E.; Kessler, S. H.; Kroll, J. H. *Faraday Discuss.* **2013**, *165*, 181.